Annex 1

List of Completion Research Reports In Biomedical Engineering

(2010 - 2012)	* An inexpensive functional finger prosthesis with rebounded type progressive hinge lock
	* Diffusion Tensor MRI Predictors of Cognitive Impairment in Confluent White Matter Lesion
	* Lanthanide-impregnated molecularly imprinted polymer microspheres as antibody mimics on an optofluidic platform for the detection of disease biomarkers
(2009 – 2012)	* Signal Processing Strategies on Cochlear Implant Devices for Effective Speech Perception of Tonal Languages
	* Terahertz probe for in vivo imaging
(2009 – 2011)	* Development of A Robotic Endoscope Holder for Nasal Surgery
(2008 - 2010)	* Development of highly sensitive and large throughput surface enhanced Raman scattering (SERS) substrates for molecular diagnosis
	* Research on Language and Brain Waves
	* Development of an Efficient Locomotion Mechanism for Wireless Active Capsule Endoscope
(2007 – 2009)	* Bio-electromagnetic Modeling and Experiment Setup for Medical Electronics RF Safety Assessment
	* Medical Applications of Terahertz Imaging
	* Hybrid Assistive Knee Braces with Smart Actuators
(2006 - 2008)	* RF Radiation Effect and Efficiency of Wireless Medical Devices on Human Body
	* Photonic biosensor micro-arrays for screening of common cancers
(2005 - 2007)	* Cochlear Implants
	* Virtual Anatomy and Dexterous Simulators for Minimal Access Cardiothoracic and Neuro-endoscopic Surgeries
	* Systematic Synthesis of Nano-informatics Chips by Nano-Robotics Manipulation

AN INEXPENSIVE FUNCTIONAL FINGER PROSTHESIS WITH REBOUNDED TYPE PROGRESSIVE HINGE LOCK

Principal Investigator: Prof Fong Tik-Pui Daniel [1]
Co-Investigator (if any): Prof Liao Wei Hsin[2], Prof Hung Leung Kim[1], Dr Ho Pak Cheong[1], Dr Tse Wing Lim[1], Dr Wong Wing Yee Clara[1] ,Mr Au Yang Choi Kam[3], Mr Sin Sai Wing[3], Dr Yung Shu Hang Patrick[1], Prof Chan Kai Ming[1]

Research Team Members: Mr Yau Kai Ching Quentin, Physiotherapist II [1]
Miss Chu Wing Shan Vikki, Research Associate [1]
Miss Chung Man Ling, Research Assistant [1]
Miss Chan Yuk Wun, Research Assistant [1]

[1] Dept. of Orthopaedics and Traumatology
[2] Dept. of Mechanical and Automation Engineering
[3] Dept. of Prosthetics and Orthotics, Prince of Wales Hospital

Project Start Date: 1st July 2010
Completion Date: 30th Jun 2012

ABSTRACT

Hand function is very important to human's daily life. Finger loss leads to weakened hand function, medical burden, diminished working capability and inferior quality of life. The estimated incidence of hand injury is about 600 per 100,000 population annually in Hong Kong. Therefore we estimate that the total patients would be around 42,000 every year. Among, 65% are occupational related and 36.1% of these injuries are caused by heavy machinery and electric saw. Therefore we estimate the number of patients losing fingers annually would be about 10,000.

"X-finger", the world's first active-function artificial finger, has been invented for patients to regain the finger function. Such device allows users to perform flexion and extension actively. However, the device is expensive – each of such artificial finger costs USD 10,000. Therefore, it is often not affordable to most people, especially those low-income factory workers who lost their fingers due to occupational accidents.

The current proposal aims to design an inexpensive artificial finger. A ring like detachable structure is to be designed to attach the prosthesis to the remaining finger bone with the surrounding muscles and soft tissues. The ring is made with soft metal that allows easy adjustment with manual strength. The artificial finger joint is made with a rebounded type progressive hinge lock which is often used in chairs, seats and sofas for adjusting the back support angle. It locks for every 15 degrees, starting from full extension of the whole finger joint. Flexion is done by assistance of another hand. At each of the angles, the hinge gets locked to prevent extension, thus providing a rigid support for hand grip. To reset the device to full extension, just flex it to 90 degrees and it gets rebounded to the original position.

Such design provides simple passive flexion adjustment and serves as an inexpensive prosthesis for patient having finger amputation to regain basic hand function.

1. OBJECTIVES AND SIGNIFICANCE

The device allows user to regain flexion and extension movement of finger. This project aims to design an inexpensive artificial finger which is affordable to most people, especially those factory workers losing their fingers due to occupational injuries.

2. RESEARCH METHODOLOGY

2.1. Design of joint

The design (Figure 1) makes use of a rebounded type progressive hinge lock which is often used in chairs, seats and sofas for adjusting the back support angle. The "progressive hinge lock" allows the joint to be bent easily in one direction and locked against the opposite force. In this prosthesis, the joint starts working from zero flexion and then flexion is performed by assistance of another hand, with 15 degrees increment, until a 90-degree flexion is reached. At each of the interval, the joint is locked to prevent extension of finger. This makes possible the thumb opposition nature of human hand for amputee. When the flexion angle exceeds 90-degree, it rebounds and returns to starting position.

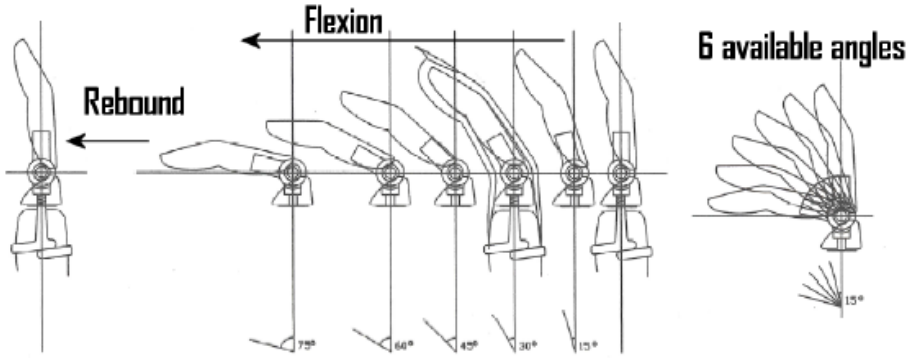

Figure 1. The design and the operation of the finger prosthesis

2.2. Prosthesis evaluation test

Clinical Jebsen hand function test involving daily activity will be conducted. Grip force and pinch force in 5 different positions will be evaluated on the uninjured hand, the injured hand without the prosthesis and the injured hand with the prosthesis. In addition, hand grip biomechanics test will be conducted for quantitative evaluation by using cylindrical mug. Force sensor will be applied to measure the force exerted by hand on the cylindrical surface. We expect a functional recovery rather than a maximum force exertion, so a series of functional trials will be conducted by means of mug that filling with different amount of water.

3. RESULTS ACHIEVED

3.1. Design of joint, ring and tip

The designs of joint, ring and tip structure were completed (Figure 2). Assembly method for different parts was also decided. Several versions of prototype were fabricated and tested. The joint thickness and weight was optimal. Also, the size and shape of ring was modified for better attachment to joint.

Figure 2. Several versions of prototype

The joint consists of two moving parts, including the rotating wheel and the shifting part to allow the joint to rotate at six lockable intervals as shown in figure 3.

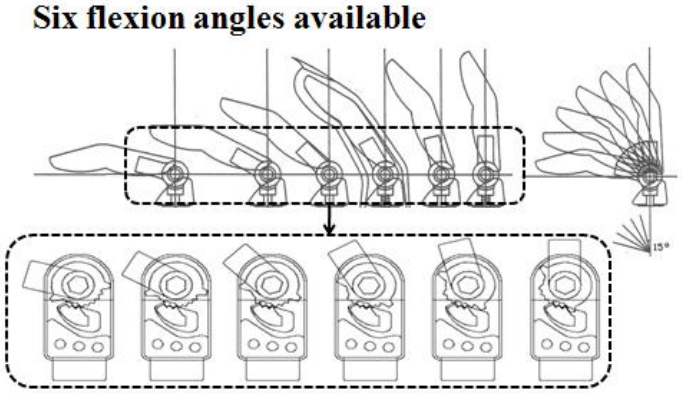

Figure 3. Illustration of six lockable intervals

The working principle is shown in figure 4, (a) The two parts are interlocked by gear at six intervals. (b) The other side of the shifting part is backed with a thin aluminum sheet, which provides a spring-like nature that allows little displacement of the shifting part. (c) and (d) At the end of the sixth interval, a larger gear tooth of the rotating wheel which exerts force on the end of the shifting part. The shifting part would be shifted to the other side of the capacity, allowing the rotating wheel to return to the start position smoothly. (e) Another larger gear tooth would push the shifting part back to the “locking” position. All moving parts were made of stainless steel for longer duration while aluminum was chosen for other parts for weight reduction.

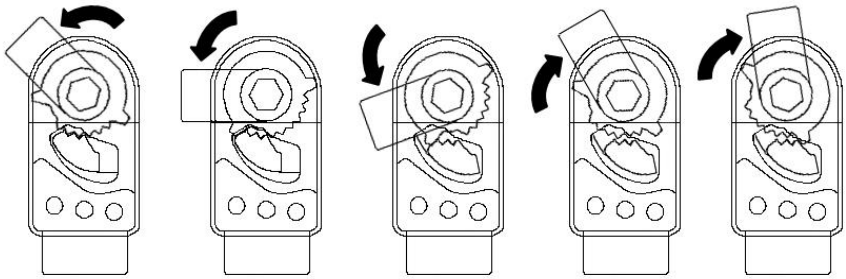

(a) (b)

(c) (d) (e)

Figure 4. Working principle of the progressive hinge lock

There were two attachment methods:

1) A non-invasive ring like structure was designed to attach the prosthesis to the stump of the metacarpal bone surrounding with muscles and soft tissue. The ring was made of sliver metal that allows easy and fine adjustment with manual strength. (Figure 5)
2) A silicon socket was designed for easy fitting for different patients. A serial of silicon sockets with different size was made. It is easy to mold to fit the patient's residue by heating. Moreover, it is much cheaper than sliver ring. (Figure 6)

A traditional silicon prosthesis can be used to cover the prosthesis to improve the appearance.

Figure 5. A non-invasive ring like structure for attachment

Figure 6. A set of silicon socket with different size

3.2. Clinical and biomechanical test

Efficacy of the finger prosthesis was evaluated by validated Jebsen hand function test. The patients conducted the Jebsen hand function test first without the prosthesis. Then, they conducted the test

again after prosthesis prescription.
Shorter time was recorded in each of the subtest with the use of prosthesis, except that in turning card. The percentage decrease ranged from 2% to 21% in the time required for performing the functional tasks. For turning card, the time usage was increased 28%. Most patients could not pick up large object (even for the light one) without the help of the prosthesis.

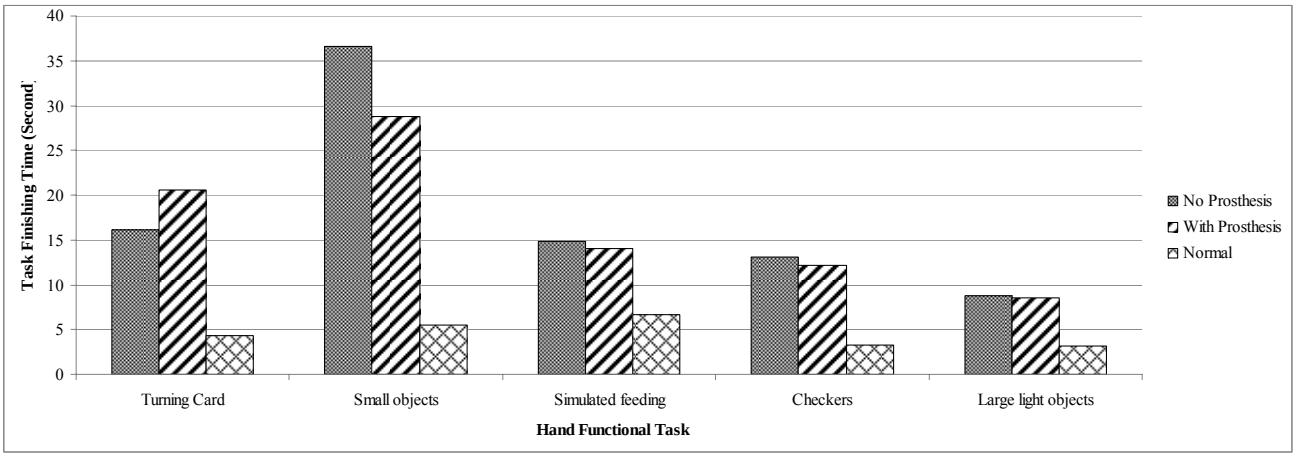

Figure 7. Time usage for performing different hand functional tasks

The pinch force was measured by a load cell (FUTEK, US). The maximum pinch force with and without prosthesis was 19.48N and 25.72N respectively. From the observation, it was difficult to apply pinch force to the load cell since the joint axis was not align with the apply force. This may be the reason that the prosthesis could not improve the maximum force exertion. We could not measure the gripping force since the value was below the measurement range of the pressure sensor. However, from the result of functional test, it was obvious that the prosthesis able to restore the gripping force since all patients able to pick up cylindrical mug with 0.5 kg.

Although the performance was not improved a lot, stable control and well adaptation to the prosthesis was observed. We believe that the performance can be further improved with longer training and adaptation time. The prosthesis can restore the opposition function of patient with multiple digit amputation. By applying enough prosthesis on the involved hand, it is possible for them to pick up large heavy object.

Figure 8. Pick up a heavy object with the help of prosthesis

4. PUBLICATION AND AWARDS

[1] D.T.P. Fong, Y.Y.W. Chan, Y.K. Fung, C.W.Y. Wong, L.K. Hung and W.H. Liao, "An inexpensive functional finger prosthesis," *In Proceedings of SMART - Sports Medicine And Rehabilitation Therapy 2010 Convention*, Hong Kong, China, pp. 10-11, Oct 9, 2010.
[2] P.S.H. Yung, Y.W. Chan, Y.K. Fung, M.M.L. Chung, D.T.P. Fong and K.M. Chan, "An inexpensive functional finger prosthesis with rebounded type progressive hinge lock," *In*

Proceedings of the 30th Annual Congress of The Hong Kong Orthopaedic Association, Hong Kong, China, pp. 95, Nov 27-28, 2010.
[3] D.T.P. Fong, Y.Y.W. Chan, M.M.L. Chung, W.H. Liao, A. Au-Yang, S.W. Sin, C.W.Y. Wong and L.K. Hung, "An Inexpensive Functional Finger Prosthesis with Rebounded Type Progressive Hinge Lock," *In Proceedings of the Symposium on Rehabilitation Technology - Interdisciplinary Approach from Theory to Practice (cum 7th Orthopaedic Rehabilitation Symposium, The Hong Kong College of Orthopaedic Surgeons)*, Hong Kong, China, pp. 32, Jan 15-16, 2011.
[4] M.M.L. Chung, D.T.P. Fong , A. Au-Yang, S.W. Sin, C.W.Y. Wong, P.S.H. Yung and K.M. Chan, "Clinical outcome after prescribing an inexpensive functional finger prosthesis for one month – a case study," *In Proceedings of the 31st Annual Congress of The Hong Kong Orthopaedic Association*, Hong Kong, China, pp. 100, Nov 19-20, 2011.

5. EXHIBITION

Date	**Event**	**Venue**
3rd -5th Nov 2010	The 2nd HKTDC Hong Kong International Medical Devices and Supplies Fair	Hong Kong Convention and Exhibition Centre
6th -14th Nov 2010	InnoCarnival	Hong Kong Science Park
16th -21st Nov 2010	China Hi-Tech Fair 2010	Shenzhen Convention and Exhibition Center
5th -13st Nov 2011	InnoCarnival 2011	Hong Kong Science Park
15th -21st Nov 2011	China Hi-Tech Fair 2011	Shenzhen Convention and Exhibition Center
13th Oct 2012	SMART Convention 2012	The Prince of Wales Hospital, Hong Kong

6. PATENT APPLICATION

US regular patent and PCT were applied in Jun 2012.

Diffusion Tensor MRI Predictors of Cognitive Impairment in Confluent White Matter Lesion

Principal Investigator: Prof. Xiaogang Wang [1]
Co-Investigator (if any): Prof. Vincent Mok [2], Prof. Winnie Chu [3], Prof. Jing Yuan [3]

Research Team Members: Chao Li, Research Assistant [1], Bo Xie, Research Assistant [1], Rui Zhao Research Assistant [1], Xingyu Zeng Research Assistant [1], Xiaotian He, Postgraduate Student [1]

[1] Dept. of Electronic Engineering, the Chinese University of Hong Kong
[2] Dept. of Medicine & Therapeutics, the Chinese University of Hong Kong
[3] Dept. of Imaging and Interventional Radiology, the Chinese University of Hong Kong

Project Start Date: 1st July 2010
Completion Date: 30th June 2012

ABSTRACT

Although age-related white matter lesion (WML) is an important substrate for cognitive impairment in the elderly, the mechanisms whereby WML induces cognitive impairment are uncertain. Recent findings based on small studies suggested that diffusion tensor imaging (DTI) measures might be the most sensitive imaging predictors in patients with WML. Understanding the imaging predictors for such disease will be useful in monitoring disease progression and in devising surrogate marker for treatment trials.

Our goal is to propose a set of new DTI measures, such as integrity, discontinuity and connectivity of white matter fiber bundles which correspond to anatomical structures, and to investigate their correlation with cognitive impairment. In order to obtain these measures from DTI properly, two technical challenges will be solved. First, model the pathways of white matter tracts by connecting local diffusion measurements into global fiber trajectories. Second, group fiber trajectories into anatomically meaningful bundles incorporating the prior knowledge input by neurologists. The proposed DTI measures reveal disruption of connections within anatomical structures of interest. They better indicate WML than the measures adopted in existing studies.

1. OBJECTIVES AND SIGNIFICANCE

- Investigate the proposed diffusion tensor MRI (DTI) measures as predictors of cognitive impairment in patients with white matter lesion (WML). The outcome of this project will help to understand the mechanisms whereby WML induces cognitive impairment. If DTI could be demonstrated as potent predictor for cognitive impairment, it can be used to monitor disease progression and in devising surrogate marker for treatment trials.
- Propose new algorithms which connect local diffusion measurements into global fiber trajectories and group fiber trajectories into anatomically meaningful bundles incorporating the prior knowledge from neurologists to guide grouping. It will make the obtained DTI measures more anatomically meaningful.
- Propose new DTI measures, such as integrity, discontinuity and connectivity of white matter fiber bundles, and they reveal disruption of connections within anatomical structures of interest.
- Study the correlation between the new DTI measurements and cognitive function scores. Compare the performance of the proposed DTI technologies with existing methodologies in terms of being used as potent predictor for cognitive impairment.

2. RESEARCH METHODOLOGY

- There are three Philips 3-tesla MRI scanners in the Department of Radiology & Organ Imaging of the Wales hospital available for this project. We plan to recruit 100 healthy subjects and 100 patients with small vessel diseases and collect their DTI data for experimental study.

- The research team of Prof. Vincent Mok will collect various cognitive function scores of these subjects for experimental study.
- Using tractography algorithms to generate fiber trajectories from the DTI data of a set of selected healthy subjects.
- In collaboration with neurologists, group the fibers of the selected subjects into anatomically meaningful bundles. It leads to the tractography atlas which will be used as a template later. We merge fiber tracts from multiple healthy subjects to construct our whole brain fiber model so that it is more representative than each individual model. In this merged fiber model, the common fiber structures have denser distributions of fiber points than those corresponding to individual differences and the local deformations are mainly determined by the common fiber structures.
- Register the DTI data of new healthy and patient subjects to the fixed tractography atlas obtained above. Both the fibers and the anatomical fiber bundles of the new subjects are automatically obtained after registration. We propose a free-form fibers model for fiber-to-DTI registration. It uses free-form-deformations (FFD) to globally but nonrigidly deform the fiber model to the input DTI. Instead of modeling the transformations of individual fiber points, FFD describes the deformation of the entire brain volume and thus serves as inter-fiber regularization and retains the relative positions of brain fibers. Besides, we also introduce the intra-fiber regularization to control the smoothness of individual fiber tracts.
- The proposed fiber-to-DTI registration scheme is applied to the clinical study of small vessel diseases (SVD). SVD subjects have WM lessons, which alter the micro-structures of axons and affect registration and tractography. We solve this challenge by proposing a two-round fiber-to-DTI registration with Robust Principal Component Analysis (PCA) and a contextual prior. Robust PCA is used to identify outlier fiber segments which are deformed into non-WM regions or WM lesion regions. Since WM lesions alter the micro-structures of axons, local affinity measures around these fiber segments are no longer reliable. Then a novel contextual descriptor, which characterizes non-local DTI features in larger regions, and its prior learned from healthy control subjects are introduced to guide the registration of these fiber segments.
- Compute structure-wise DIT measurements from the fibers and the anatomical fiber bundles. Study the correlations between the DIT measurements and the cognitive function scores.

3. RESULTS ACHIEVED

3.1. Obtaining the Tractography Atlas

Tractography atlas is a set of fiber bundle templates which correspond to the anatomical structures of the white matter in the brain. At the later stages, the DTI data of new subjects will be registered to the tractography atlas in order to compute structure-wise DIT measurements. The tractography atlas is computed from the DTI data of 10 selected healthy subjects recruited by the Prince of Whales Hospital. The fibers of each subject are generated by a tractography algorithm. We proposed and developed a novel nonparametric hierarchical Bayesian approach to cluster fibers into anatomical bundles. Compared with existing clustering methods, it has the following distinctive features.

- It can cluster fiber sets hundreds of times larger than existing methods. Thus, it is able to jointly cluster the fibers of ten subjects and achieves a more reliable tractography atlas.
- It can incorporate the prior knowledge provided by neurologists into the clustering process. Thus the produced fiber bundles better correlate with anatomical structures.
- It automatically learns the number of fiber clusters from data, while existing methods require manually inputting such information as *a priori*, which is hard to know in advance.

After the automatic clustering, further refinement is done by manually removing outlier fibers, splitting and merging improper clusters. The obtained final atlas is shown in Figure 1.

This part of work was published on *NeuroImage* [1], which has the highest impact factor (*Impact Factor = 5.739, 5-year Impact Factor = 7.168*) among all of the medical imaging journals.

Figure 1. Tractography atlas in different views. Colors indicate different anatomical structures.

3.2 Whole brain fiber-to-DTI registration

In order to generate the anatomically meaningful fiber bundles of new subjects, existing methods first generate fibers from DTI by tractography and then cluster fibers into bundles by tractography segmentation. However, tractography suffers from the problems of noise, partial volume effects, and early termination of fibers, especially when patients have white matter lesions. In tractography segmentation, it is difficult to obtain anatomically meaningful fiber bundles without human intervention.

To circumvent these challenges, we propose a novel whole brain fiber-to-DTI registration method. It deforms the manually annotated tractography atlas described in Section 3.1 to DTI of new subjects. Fiber trajectories and anatomically meaningful fiber bundles are automatically obtained by this registration. In our approach, the free-form deformations are used to regularize the transformations at the whole brain level and across fiber bundles. Fiber curvatures are penalized as the intra-fiber regularization to encourage the smoothness of transformed fibers.

Due to white matter lesions, existing registration methods perform poorly on patient subjects with small vessel diseases. To handle WM lesion, it is important to detect the fiber tract segments affected by WM lesion regions, where the local DTI measure is no longer reliable. Considering the influence of a WM lesion region, either the fiber tracts are inappropriately deformed to a non-WM region, or they measure the local DTI of the WM lesion region. In either case the resultant measure will be significantly different than that for other subjects. Taking healthy subjects into account, it is reasonable to assume that only a few subjects have WM lesions in the same region, meaning that measurements of the fiber segments affected by WM lesion are outliers among the subjects. Accordingly, we use robust PCA to detect these outliers and thus we will know which part of fibers will be unreliable under local DTI similarity measure. An example of the Robust PCA result is shown in Figure 2.

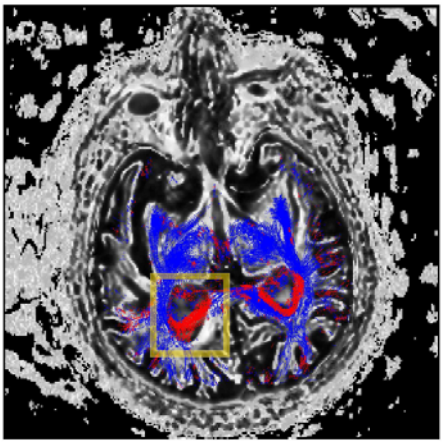

Figure 3. The Robust PCA result: The blue points plots the active fiber segments, while the red points plots the passive fiber segments, which are wrongly deformed to the lateral ventricle due to WM lesions. This figure should be viewed in color.

A Laplace along-fiber regional prior learned from healthy subjects is proposed to evaluate the match between fibers and tensors in patients. It effectively improves the registration performance in the presence of white matter lesions. The effectiveness of using the free-form deformations and regional prior is shown in Figure 3.

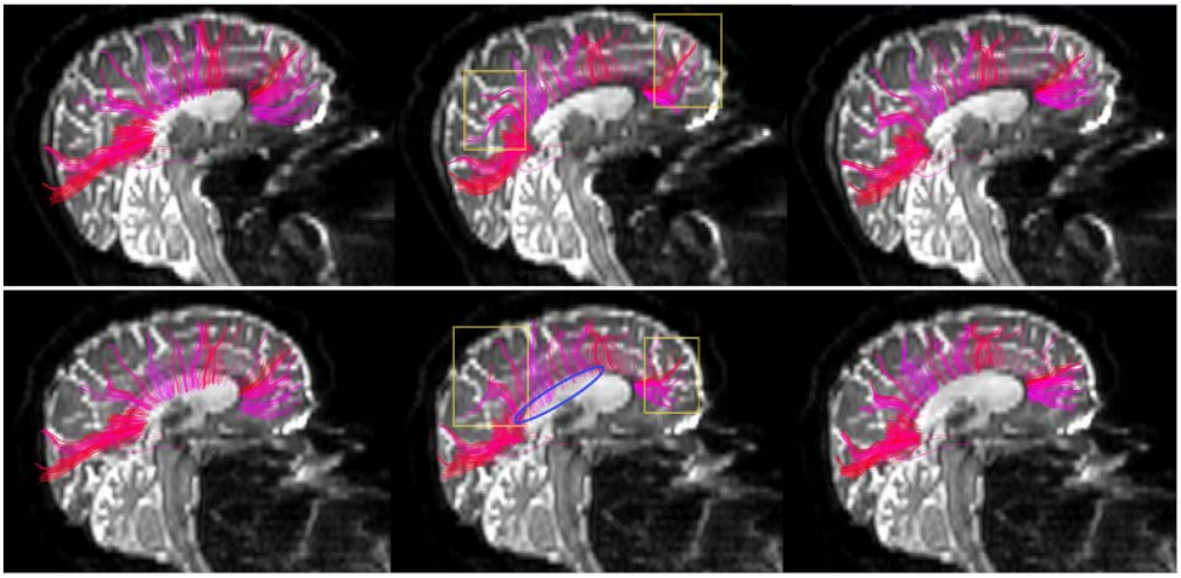

Figure 3. Comparison of the reconstructed corpus callosum fibers using different registration methods: affine alignment (left), fiber-tensor-fit under free-form deformations and fiber-tensor-fit with regional prior, for a healthy subject (top) and a patient subject (bottom). Affine alignment is widely used in existing registration methods. By using free-form deformations, our approach can improve the registration accuracy. However, its results on patient subjects are still not satisfactory. By using the regional prior learned from healthy subjects, the registration on patients with white matter lesions can be improved.

Fig. 4 compares the corpus callosum constructed by manually seeded tractography (middle) and by the proposed automatic fiber-to-DTI registration method. As shown, the shape of the deformed corpus callosum model well matches the fibers reconstructed by manually seeded tractography while the tractography result is incomplete, e.g., in the yellow rectangular region, due to early termination. Further, even with a carefully delineated seeding region, it is still difficult to avoid outlier fibers in tractography. A bundle of outlier fibers are highlighted in the red rectangle for example. Since outlier fibers in our fiber model have been removed by experts, the fibers reconstructed by our method is clean.

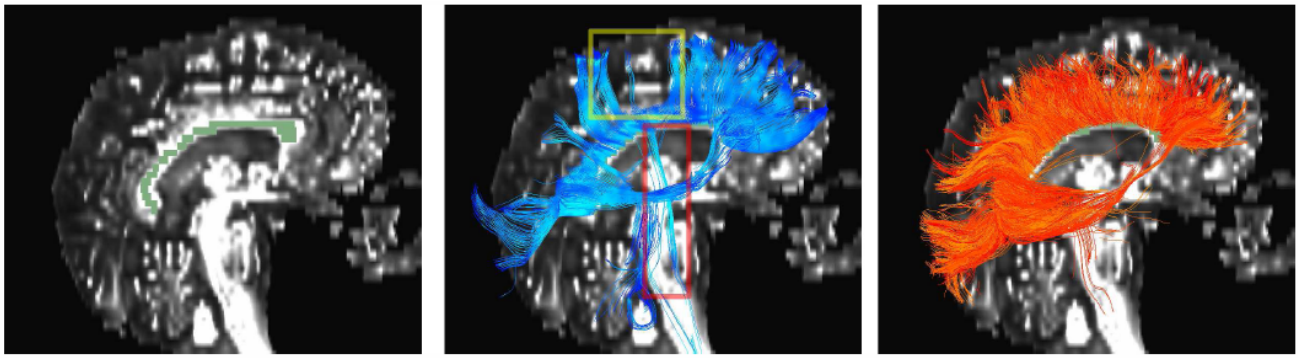

Figure 4. Comparison of corpus callosum bundles reconstructed by using manual seeding (middle) and our method (right). The left figure shows the label map for manual seeding.

To evaluate the consistency of this fiber-to-DTI registration among subjects, we warp backward the FA volume of each subject to the fiber model space and examine the averaged volume. Fig. 5 displays the averaged FA of all the subjects after back-warping. The averaged FA image appears rather blurry without using any registration due to the misalignment among subjects. The major skeleton of the WM becomes much clearer after affine registration which compensates variations of size, position, and orientation. As expected, the averaged images given by nonrigid fiber-to-DTI are the sharpest which demonstrated consistent alignment given by our fiber-to-DTI registration.

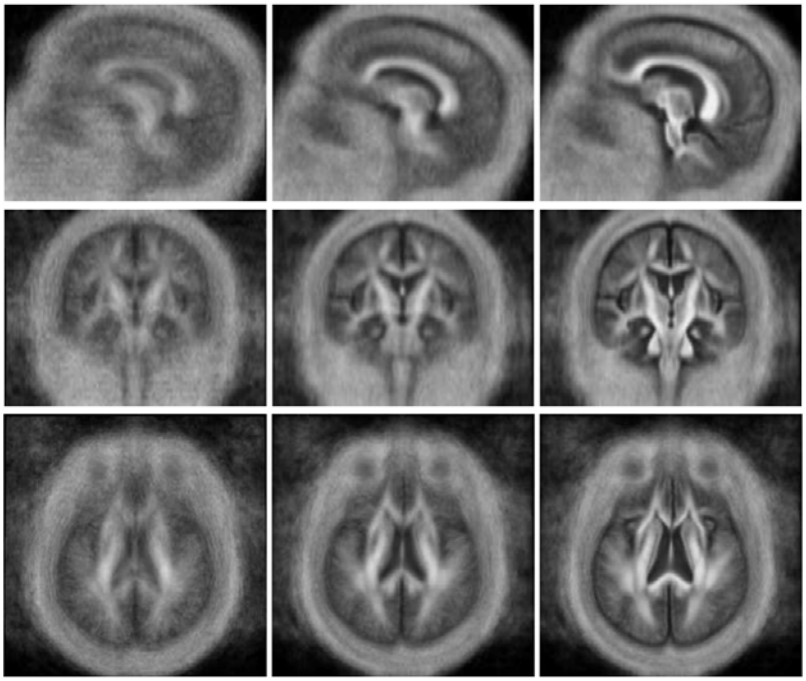

Figure 5. The average FA images after warping all the subject to the same domain. From left to right shows sagittal, coronal, and axial views. From top to bottom shows the results using no registration, affine registration andour non-rigid registration.

We also computed the pixel-wise standard deviations of back-warped FA volumes to quantitatively assess the group alignment. Fig. 6 shows the statistics of such pixel-wise standard deviations within the brain area. By using our nonrigid fiber-to-DTI registration, more points “move” to the left side 383 indicating the reduction of the standard deviations, i.e., the improvement of group alignments. The mean standard deviations are 0.25, 0.20, and 0.18 respectively for no registration, affine fiber-to-DTI registration and nonrigid fiber-to-DTI registration.

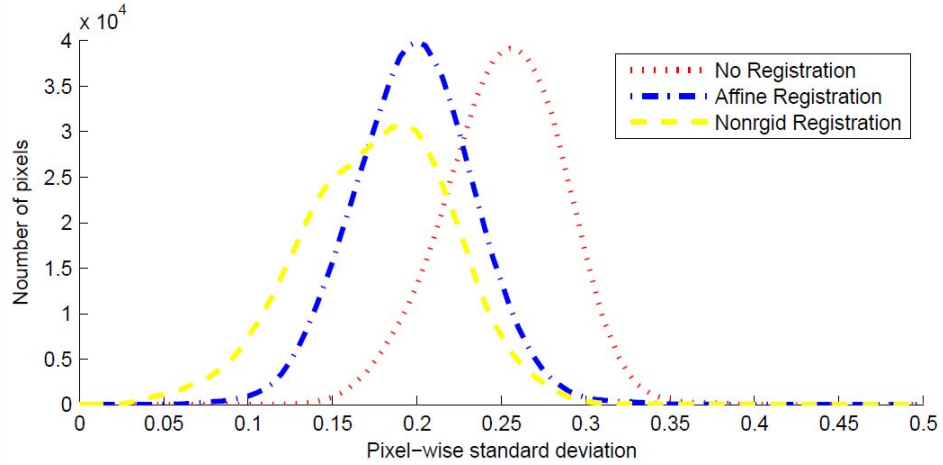

Figure 6. The histograms of pixel-wise FA standard deviations within the brain area after warping all the subjects to the brain fiber model domain.

This part of work has been accepted to *Workshop on Computational Diffusion MRI* [2]. The journal version of this work has been submitted to Medical Image Analysis and is under major revision.

3.3 Results of Clinical Study

48 elderly patients in various stages of Small Vessel Desease (SVD) are recruited for an experimental treatment. 52 healthy subjects are enrolled for reference. All subjects were recruited from the Whales hospital and underwent the same series of MRI scanning protocols. Based on the technologies developed in Section 3.1 and 3.2, we are able to compute DTI measurements from different anatomical bundles and study their correlations with various cognitive functions. Previous clinical studies [a] suggested that DTI measurements should have strong correlations with cognitive impairment than conventional MRI measurements. We therefore quantitatively validate our results by assessing the partial correlations (controlled for age, gender, and education) between the averaged FA and widely used cognitive scores: the Montreal Cognitive Assessment and the Mini-Mental State Examination. The correlation tests are performed among all the subjects with valid cognitive scores and there are about subjects for each cognitive score. Table 1 shows the correlation for the average FA along all the reigstered fibers, along four selected anatomical fiber bundles ("Corpus Callosum", "Occipito Frontal", "Brachia Conjunctiva" and "Inferior Cingulum"), among the whole brain volumes and the average skeletonised FA by TBSS (Smith et al., 2006). Strong correlation indicates that the DTI measurement has a good potential to be used as a predictor of cognitive impairment. With fiber-to-DTI registration, the cognitive scores have stronger correlation with the result of non-rigid registration than affine registration; the result after the second round non-rigid registration shows stronger correlation than after the first round non-rigid registration, since the second round registration well handles the WM lesion problem. Different anatomical fiber bundles correlate with cognitive scores in different ways. The fiber bundles of "Corpus Callosum" and "Occipito Frontal" have much higher correlation scores than those of "Brachia Conjunctiva" and "Inferior Cingulum". With our method, "Corpus Callosum" shows the strongest correlation with MMSE among all the anatomical structures and "Occipto Frontal" shows the strongest correlation with MoCA. This result confirms the conclusion drawn by some clinical study that MMSE is correlated with callosal lesion. MoCA is a cognitive test with stronger executive function components. Our resul hence explains the stronger association between MoCA and the frontal-occipital bundle, which is considered to subserve executive function. Compared with the skeletonished FA value of TBSS, our average FA along all fibers correlates better with the cognitive scores. It supasses TBSS by 8% on the correlation with MMSE. With our approach, the average FA on "Occipito Frontal" supasses TBSS by 5% on the correlation with MoCA. Besides, both our along fiber measure and TBSS skeletonised FA remarkably outperform the whole brain average. Figure 7 shows the scatter plots of our average FA values along all fibers versus cognitive scores on healthy controls and patients.

		MoCA	MMSE
Along All Fibers	Affine Reg.	0.392	0.383
	Non-rigid reg. (1st round)	0.587	0.616
	Non-rigid reg. (2nd round)	0.605	0.629
Corpus Callosum	Affine Reg.	0.368	0.407
	Non-rigid reg. (1st round)	0.535	0.579
	Non-rigid reg. (2nd round)	0.575	0.608
Occipito Frontal	Affine Reg.	0.323	0.157
	Non-rigid reg. (1st round)	0.605	0.545
	Non-rigid reg. (2nd round)	0.621	0.566
Brachia Conjunctiva	Affine Reg.	-0.229	-0.274
	Non-rigid reg. (1st round)	-0.145	-0.241
	Non-rigid reg. (2nd round)	-0.262	-0.363
Inferior Cingulum	Affine Reg.	-0.120	0.013
	Non-rigid reg. (1st round)	0.047	0.170
	Non-rigid reg. (2nd round)	0.223	0.322
Whole Brain Average of FA		0.456	0.396
Tract-Based Spatial Statistics (TBSS)		0.592	0.582

Table 1: Correlation between Neuro-assessment Scores and Specific FA Mea- surements. With our approach (i.e., the second round non-rigid registration), the p values of the t-test of our DTI measures for regions other than Brachia Conjunctiva (Superior Cerebellar Peduncle) and Inferior Cingulum are all below the 0.001 level.

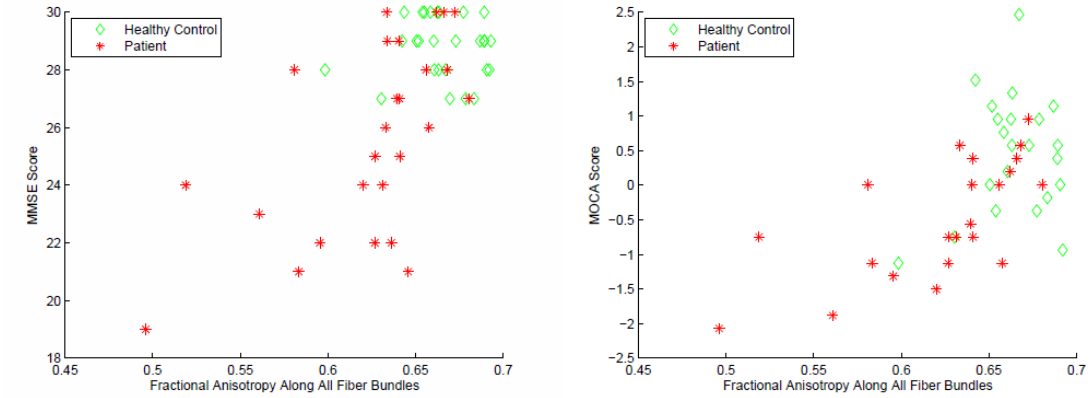

Figure 7: The scatter plots of our average FA values along all fibers versus cognitive scores on healthy controls and patients.

[a] Nitkunan et al. “Multimodal MRI in Cerebral Small Vessel Disease: Its Relationship with Cognition and Sensitivity to Change over Time,” Stroke, Vol. 39, pp. 1999-2005, 2008.

4. PUBLICATION AND AWARDS

[1] X. Wang, E. Grimson, and C. Westin, “Tractography Segmentation Using a Hierarchical Dirichlet Processes Mixture Model,” *NeuroImage*, pp. 290-302, Vol. 54, 2011.

[2] C. Li, X. He, V. Mok, W. Chu, J. Yuan, and X. Wang, “Free-Form Fibers: A Whole Brain Fiber-to-DTI Registration Method,” *Workshop on Computational Diffusion MRI*, 2011.

[3] C. Li, X. He, V. Mok, W. Chu, J. Yuan, and X. Wang, “Free Form Fibers: a Full-Brain Fiber-to-DTI Registration Method,” *Submitted to Medical Image Analysis* (under major revision).

LANTHANIDE-IMPREGNATED MOLECULARLY IMPRINTED POLYMER MICROSPHERES AS ANTIBODY MIMICS ON AN OPTOFLUIDIC PLATFORM FOR THE DETECTION OF DISEASE BIOMARKERS

Principal Investigator: YUNG Pun To [(1)]
Co-Investigator (if any): LEUNG Ka Nang [(1)], LEUNG Wing Nang [(2)]

Research Team Members: TAO Wenyan [(1)], Shun Hing Fellow; LI Lin Kai [(1)], research assistant; LIU Songlin [(1)], graduate student; YAO Na [(1)], research assistant, CHOY, Chi Tung, undergraduate research assistant [(1)]

[(1)] Dept. of Electronic Engineering, CUHK
[(2)] School of Chinese Medicine, CUHK

Reporting Period: 1 July 2010 – 31 June 2012

ABSTRACT

Antibodies bind with biomolecules and pathogenic bacteria with a very high specificity, which underlines their unparalleled importance in disease diagnosis and molecular biology research, as compared with other lengthy and laborious conventional methods. Antibodies, however, suffer from limitations such as difficulty in mass production, cost, instability, and limited shelf life. In this proposal, we use molecularly imprinted polymers (MIPs) to mimic artificial antibodies, which confer temperature stability, low production cost and convenience in handling. Molecular imprinting describes a process to fabricate a polymer matrix around a template (analyte or structural surrogate), which is subsequently removed to leave voids with high affinity for the target analyte. An all-in-one optofluidic platform will be developed utilizing lanthanide-impregnated MIP microspheres to extract, concentrate and detect biological markers from liquid samples. This sensitive, selective, and robust methodology potentially serves as a rapid point-of-care screening, diagnosis and therapeutic monitoring tool for many pathophysiological conditions. The dual-modality detection integrates molecular recognition and luminescence from lanthanide complex to serve as a universal sensing methodology at the interface of micro- and nano-scale to probe physiological phenomena at a cellular and molecular level.

1. OBJECTIVES AND SIGNIFICANCE

- To design a fabrication protocol for lanthanide-impregnated molecularly imprinted polymer microspheres
- To develop a universal optofluidic detection platform utilizing lanthanide-impregnated molecularly imprinted microspheres for detecting cells, proteins and other biomolecules of clinical and food hygiene significance
- To implement a preliminary commercial prototype for point-of-care microbial detection

Healthcare technology is essential in society nowadays because of aging population, pandemics and the quest for better quality of life. Conventional methods of identifying pathogenic bacteria and harmful biomolecules require lengthy cultivation and laborious chemical analysis, e.g., gas chromatography mass spectrometry, on the order of 2 - 7 days. Although the use of antibodies in detection has significantly cut down cost and time, there are still several limitations. For instance, antibodies are difficult to produce in large quantities, expensive, inherently unstable, and have a limited shelf life. This project uses molecularly imprinted polymers (MIPs) to mimic artificial antibodies, which confer temperature stability, low production cost and convenience in handling. MIPs can be stored in a dry state at ambient temperatures for several years without loss of recognition capabilities. In addition to this, here we will construct an all-in-one optofluidic platform utilizing lanthanide-impregnated MIP microspheres to extract, concentrate and detect biological markers from liquid samples. This sensitive, selective, and robust methodology serves as a rapid point-of-care screening, diagnosis and therapeutic monitoring tool for many pathophysiological conditions. The dual-modality detection integrates molecular recognition and luminescence from lanthanide complex to serve as a universal sensing methodology at the interface of micro- and nano-scale to probe physiological phenomena at a cellular and molecular level.

2. RESEARCH METHODOLOGY

Sol-gel synthesis of TiO_2 nanoparticle and TiO_2-MWCNT nanocomposite

Acetone concentration higher than 0.9 ppm in exhaled breath is a strong indication of ketoacidosis for diabetics. Titanium dioxide-multiwall carbon nanotubes (TiO_2-MWCNT) nanocomposite were prepared by sol-gel techniques to provide a sensing layer for the detection of acetone in air. Titanium tetraisopropoxide [$Ti(C_3H_6OH)_4$] was used as the precursors, anhydrous ethanol as the solvent, and acetic acid as the stabilizer. Firstly, specific amounts of $Ti(C_3H_6OH)_4$, ethanol and acetic acid (v/v=10:30:8) were mixed at room temperature, with vigorous stirring for 1 hour. Secondly, a mixture of 7.5 ml ethanol and 0.7 ml H_2O were added drop by drop to the above solution slowly to initiate the hydrolysis reaction. A sol-gel would be produced after 2 days. The preparation of TiO_2-MWCNT nanocomposite follows the aforementioned procedure except for the mixture of acetic acid and ethanol contained 0.05 g of carbon nanotubes, and dispersion of carbon nanotubes in the mixture by ultra-sonication for 1 hour, prior to the addition of the titanium precursor.

The non-metal coating surface of cantilevers was coated with as-prepared TiO_2 and TiO_2-MWCNT solution. Placing a drop of solution on a glass slide and sliding the cantilever into the solution until one side of the cantilever was completely wet. The cantilever was then pulled out and dried in desiccators for 2 days. The thickness was estimated by determining the change in resonance frequency of the coated cantilever. The vibration of microcantilever is subsequently controlled by the principle of electrostatic actuation at an ac voltage of 10 V.

Preparation and characterization of molecularly imprinted polymer

Molecular imprinting prepares tailor-made affinity adsorbents possessing specific binding sites within polymer matrices. We explored the utilization of MIPs as recognition unit for mononitrogen oxides (NO_x), biomarkers for inflammatory respiratory diseases. This molecular imprinting process involves three steps: (i) self-assembly of NO_x template and methacrylic acid as functional monomers, and dichloromethane and acetonitrile as porogenic solvents, (ii) polymerization of template-monomer complex with cross-linking monomers, and (iii) template removal to unveil binding cavities specific to mononitrogen oxides. Microspheres were prepared using precipitation polymerization. Molecular modeling was then used to analyze and discern the relative strength of molecular interaction between the template molecules and functional monomers. The surface morphology of MIP was characterized using scanning electron microscopy.

> Effectiveness of the MIPs is gauged by the binding constant between them and the respective analytes, measured by UV absorption spectroscopy. Uptake experiments are carried out in which aqueous solution of different analytes in methanol is added to the MIPs. Resultant suspension is shaken overnight. The polymer is then filtered and the remaining ligand concentration is determined by UV absorption spectroscopy. Further characterizations of MIPs include, gas chromatography–mass spectrometry, surface morphology electron microscopy, and binding assays. The surface morphology of MIPs was characterized using a JEOL JSM-5200 scanning electron microscope. The samples were gold sputtered under vacuum (with 10^3 Torr). The surface area and pore parameters of MIPs were measured using a N_2 Porosimeter Model JEOL JSM-6400 (Massachusetts, USA). A 100 mg quantity of dry MIP was used and degassed at 70°C under nitrogen flow for approximately 6 h prior to measurement. The MIP (10 mg) was weighed and placed in a 5-mL glass vial and 5 mL analyte in DCM solution of known concentration was added. The mixture was gently shaken on a horizontal shaker for 3 h and then filtered. The free PAHs in the filtrate were measured with a Varian 3800 gas chromatograph coupled to a Varian 4D MS ion trap detector. Other adsorbents—activated carbon and polystyrene-divinylbenzene (10 mesh)—were used to compare the PAHs extraction capacity with that of the MIP.

Fabrication of microcantilevers

Piezoelectric cantilevers were employed to translate the nanomechanical motion due to molecular recognition of disease analytes into a decrease in resonance frequency. The sensor consisted of a *p*-type silicon cantilever integrated with p-type silicon piezoresistors. The silicon wafer was firstly cleaned in hydrofluoric acid for 10 min to remove the native oxide layer, followed by cleaning in piranha solution to remove remaining organics. A layer of low-stress silicone dioxide layer was deposited by plasma-enhanced chemical vapor deposition, followed by a layer of low-stress silicon nitrogen layer as electrical isolation layer on front-side and also as backside masking layer during silicon etching. The silicon nitride/dioxide was then patterned by reactive ion etching. Titanium was sputtered on the patterned silicon nitride to serve as an adhesive layer. Platinum was then sputtered on top to form the lower electrodes, which were further patterned by a lift-off process. The

piezoelectric layer was deposited by RF sputtering of ZnO or sol-gel of PZT. The piezoelectric layer was patterned by reactive ion etching. A layer of platinum was deposited on top of the piezoelectric layer as the upper electrodes. The cantilever was finally realized by dry reactive ion etching to etch remaining silicon from the front side. MIPs in the form in micro-particles were spin-coated on the cantilever surface.

The sensing elements included an array of cantilever sensors enclosed in a cartridge. The use of a sensor cartridge enabled the sensor device to adapt to different applications according to the situation. In addition, it allowed a damaged cantilever to be replaced with ease. The cantilever signal was read out through piezoelectric methods. The bending of a cantilever was very sensitive to changes in the environment of the cantilever, which was used to detect changes upon structural modification in a pre-adsorbed layer. Under the frequency mode of operation, the mass of the cantilever sensor changed as a result of analyte binding to the polymer coating, leading to a change in resonant frequency. Analyte concentration could thus be determined from the change in resonant frequency.

High-throughput platform using arrays of cantilevers enables simultaneous and multivariate measurements. The array consisted of 7 cantilevers, including a number of beams with different MIPs specific to various individual or groups of disease analytes, one for sensing relative humidity, one for temperature and a few acting as the blank controls. The humidity sensor was a cantilever modified with a neutral polymer, e.g., polyacrylamide. Polyacrylamide is highly hydrophobic and attracts water molecules very well. The cantilevers could be used repeatedly and continuously with a purging process between sampling. A series of purge pulses would be applied *via* a zero filter to flush the cantilever with dry air and to remove any previously accumulated chemicals.

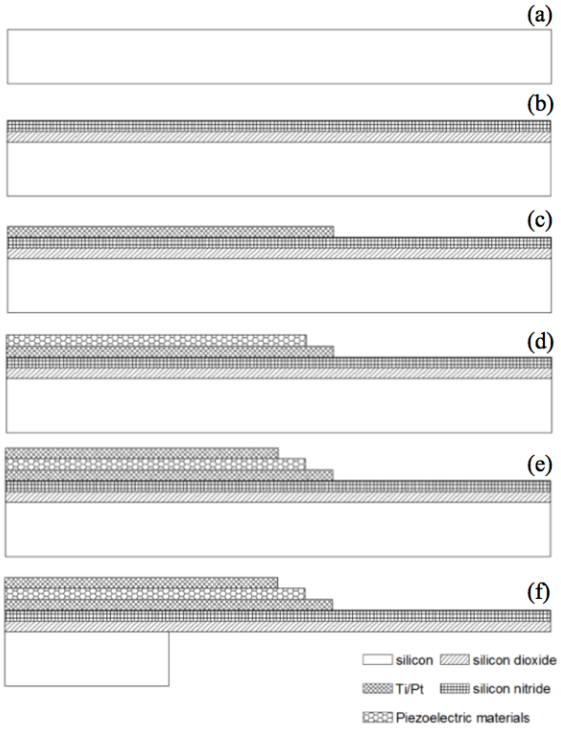

Fig. 1. Fabrication process flow of the piezoelectric microcantilever carried out at the CUHK cleanroom facilities. (a) Silicon wafer was rinsed by buffered HF and piranha solution to remove its native oxide layer and organic substances; (b) Silicon dioxide and silicon nitride were deposited on silicon wafer by PECVD. (c) Lower titanium/platinum electrode was sputtered on silicon nitride and patterned by lift off. (d) Piezoelectric material was deposited. (e) Upper titanium/platinum electrode was sputtered on silicon nitride and patterned by lift off. (f) Base silicon was further etched through by deep reactive ion etching and cantilever beams are released.

Detection mechanisms

Acetone molecules adsorbed on TiO_2-MWCNT nanocomposite dependent on the coordination environment around the surface titanium sites. This hydroxyl and carboxyl bonding manifests as a mechanical deflection when taking place on the surface of microcantilevers. This bending is statically measured using photodiodes with a high precision based on light beams reflecting off the cantilever surface. Further, to enhance the sensitivity, we will adopt the dynamic mode in which the adsorbed mass of acetone (Δm) will be obtained from the difference in vibration frequency of cantilever (Δf), as measured by an impedance analyzer.

3. RESULTS ACHIEVED

	2010		2011				2012	
	Q3	Q4	Q1	Q2	Q3	Q4	Q1	Q2
Milestone 1: Sol-gel preparation of sensing layer	Completed							
Milestone 2: Preparation and characterization of MIPs	Completed							
Milestone 3: Microcantilever design and fabrication	Completed							
Milestone 4: Validation and testing						Completed		

Characterization of TiO_2 and TiO_2- MWCNT nanocomposite and MIPs

Figure 2 shows SEM images of TiO_2 and TiO_2-MWCNT nanocomposite, respectively. Conducting paths formed by the carbon nanotubes determine the sensor's response to organic substances and gases. Swelling of the matrix caused by the adsorbed molecules increases the hopping resistance among carbon nanotubes. Not all nanoparticles were bonded to the carbon nanotubes and the carbon nanotubes were winding tightly. Further hydroxylation and carboxylation of the carbon nanotubes are needed to enhance the bonding efficiency and homogeneity of the nanocomposite. Figure 3 shows the electron micrographs of two types of MIPs prepared under different protocols.

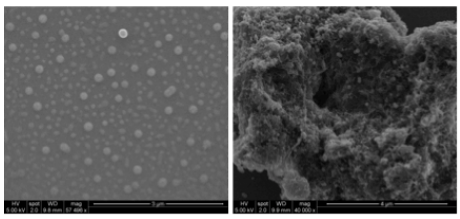

Figure 2 – The left figure shows TiO_2 nanoparticles (150 nm diameter) deposited on a silicon substrate after spin coating. The right figure shows carbon nanotubes with TiO_2 nanoparticles bonded on the surface.

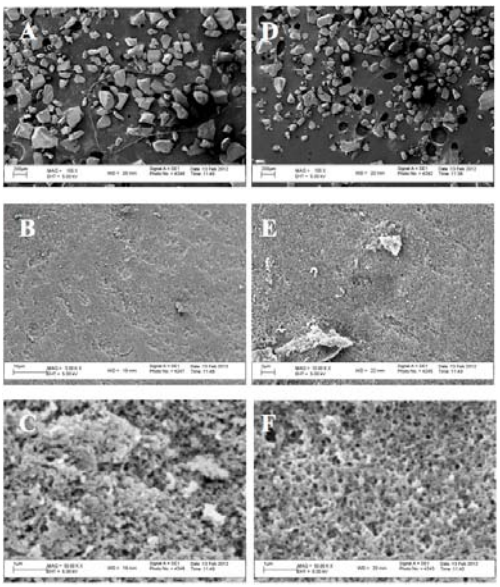

Figure 3 – Scanning electron microscope images of molecular imprinted polymers prepared using two different protocols showing the morphology of the synthesized polymers at (from left to right) 100×, 5000×, and 50,000×. The irregular and rough surfaces provide high adsorption capability. The images show obviously that the MIPs materials are homogeneous and densely packed. The 50,000× magnification also indicates that the porosity of the MIPs. Thus, the recognition sites on both the surface and inner part of the polymer can be used for affinity binding, providing higher extraction capability and capacity. Result shows that the MIPs could selectively extract acetone from array of volatile organic compounds commonly found in breath.

Fluorescence spectroscopy

Pyrene, a biomarker of carcinogenesis, was dissolved in different solvent, including DCM, acetone, ethanol, methane. The solutions were excited by UV and the emission spectrum was detected. Pyrene in different solvents such as heptane was further detected for fluorescent signal. 0.01 g/mL of pyrene was prepared in different solvents and transferred to quartz cuvettes. Fluorescence and phosphorescence scans were run using a Fluorolog-3 fluorometer (Fig. 4). Our MIPs can be produced in batch reproducibly. Batch-to-batch reproducibility was investigated by the MIPs prepared in 10 different batches, of which the relative standard deviation was determined to be 5.5%.

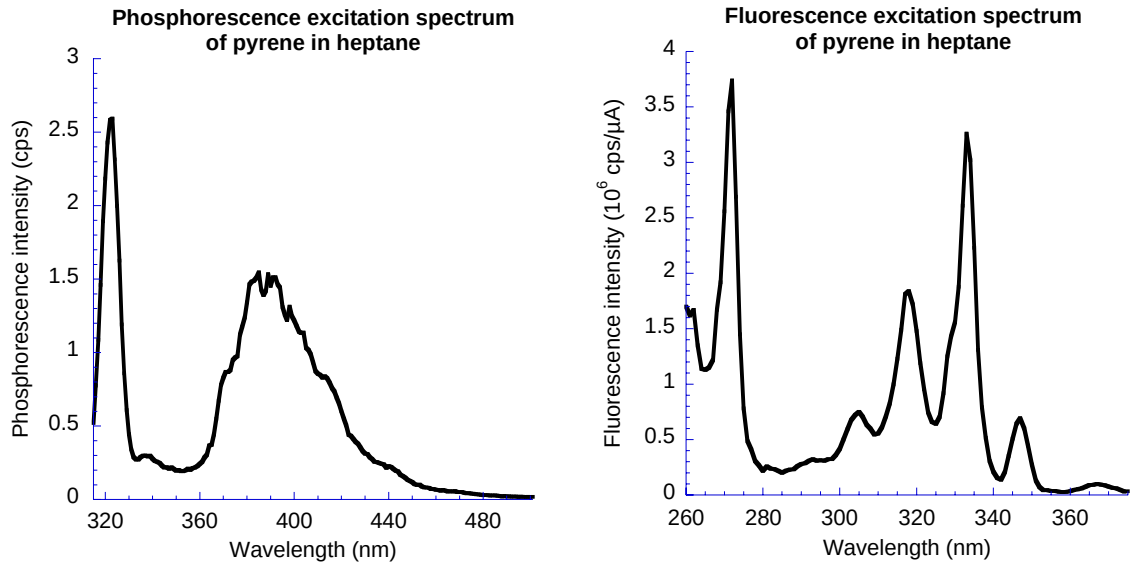

Figure 4 – Excitation spectra of pyrene (0.1 mg/L) in heptane take using (left) fluorescence spectroscopy and (right) phosphorescence spectroscopy. Distinct characteristic peaks in the fluorescence and phosphorescence plots indicated the presence of pyrene after a binding assay.

Fabrication of microcantilevers and prototyping

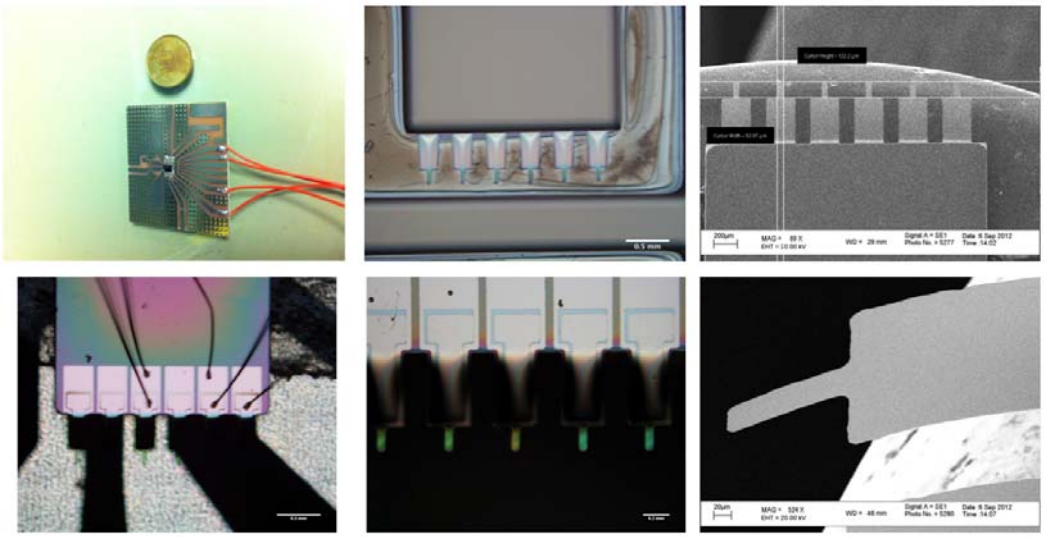

Fig. 5. (top left) One single cantilever mounted on a printed circuit board for testing. (top middle and right) The microcantilever is 200 μm long, 50 μm wide and 2 μm thick. Seven beams hang out over a silicon substrate etched by DRIE. The SEM image shows the completed microcantilever array. (bottom left) Wire bonding was shown. (bottom middle) Molecularly imprinted polymer has been coated and functionalized to the cantilevers by ink-jet spotting or spin coating. Ink-jet spotting is one of the reliable and rapid methods to functionalize cantilever array. It consists of three main parts, an *x*-*y*-*z* positioning system, piezo-driven ejection system and a ink-jet nozzle. It allows different coating for each cantilever. (bottom right) Bending of a cantilever observed under SEM.

Mechanical characterization

The natural frequency of the cantilever first mode of vibration can be derived as:

$$f = \frac{3.52}{2\pi}\sqrt{\frac{EI}{\rho A L^4}} = \frac{3.52}{4\pi}\frac{t}{L^2}\sqrt{\frac{E}{3\rho}}$$

Based on the physical dimension, the natural frequency can be calculated as around 68 kHz, and this value was consistent with our empirical values of 64.5 ± 3.5 kHz.

The equivalent mass of the cantilever beam is given by

$$M_{eff} = \frac{3}{8}\rho w t L = 21.5 \text{ ng}$$

Stiffness can therefore be calculated by

$$k_{eff} = \frac{3EI}{L^3} = 2.02 \text{ Nm}^{-1}$$

These values are all consistent with our experimental measurements performed using an atomic force microscope. Defection of the cantilever was also confirmed by an optical method utilizing a high-power laser diode, spatial filter and photodiode array.

Calibration curve

Fig. 6 shows measurements of different acetone concentrations ranging from 0 to 1410 ppmv. A linear response range from 7.05 ppmv to 705 ppmv was found. The regression equation is: Δf (Hz) = $3.49C_{acetone}$ (ppmv) + 5.29, with a correlation coefficient of 0.990. The slope of this linear zone is 3.49 Hz/ppmv, which could be viewed as the sensitivity of the sensor. The limit of detection is 5.0 ppmv. For diabetic patients under different conditions, mean acetone concentration is found from 2.05 to 5.58 ppmv. While in healthy individuals, the value is in the range of 0.48 to 0.51 ppmv. So in real situation, a 10-fold pre-concentration is needed. Meanwhile, the large response sensitivity is higher than previously reported values, such as 8.58×10^{-3} Hz/ppmv and 0.52 Hz/ppmv. Gas sensing experiments were performed inside a gas handling chamber.

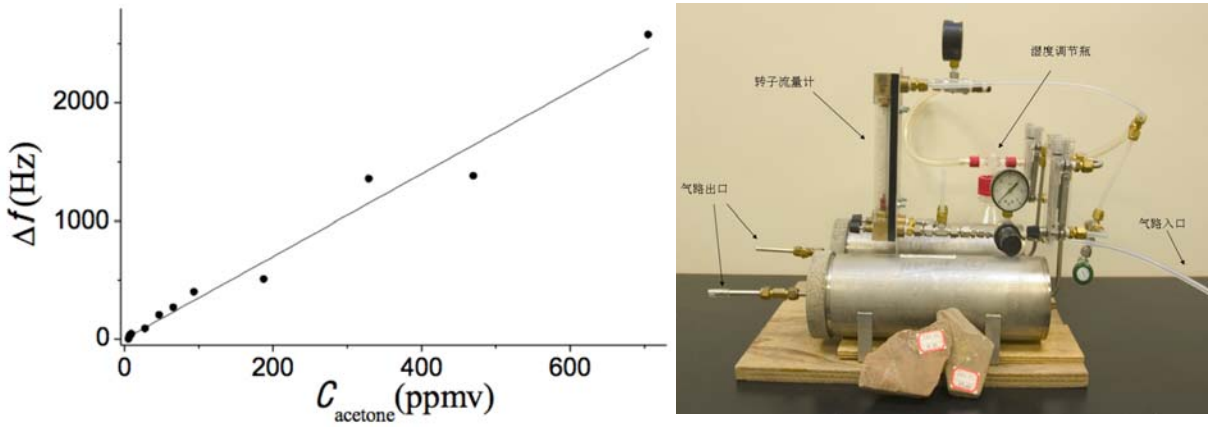

Fig. 6 (left) Calibration curve of acetone sensing using (right) a gas handling system.

4. PUBLICATION AND AWARDS

- W.Y. Tao, N. Yao, L.K. Li and P.T. Yung, "Development of room temperature ionic liquids coated quartz crystal microbalance for sensing acetone." *submitted to IEEE Sensors*.
- W.Y. Tao, N. Yao, L.K. Kai and P.T. Yung, "Detection of acetone and nitric oxide in human breath using a multichannel quartz crystal microbalance array". Proceeding of World Congress 2012 Medical Physics and Biomedical Engineering, Beijing, May 2012.
- N. Yao; L.K. Li; W.Y. Tao; C.T. Choy and P.T. Yung. "Synthesis of molecularly imprinted polymers for polycyclic aromatic hydrocarbon detection in air pollutants". Proceeding of World Congress 2012 Medical Physics and Biomedical Engineering, Beijing, May 2012.
- L.K. Li and P.T. Yung, "Automatic and continuous monitoring of polycyclic aromatic hydrocarbons in air using microcantilevers functionalized with molecularly imprinted polymers". *Patent application pending*.
- L.K. Li, W.Y. Tao, N. Yao and P.T. Yung, "Design, fabrication and characterization of piezoelectric microcantilevers integrated with capillary electrophoresis for rapid chemical separation and analysis". *Manuscript under preparation*.
- W.Y. Tao, L.K. Li, S. Liu and P.T. Yung, "Synthesis of molecularly imprinted polymer with lanthanide impregnation as point-of-care disease diagnostic tool." *Manuscript under preparation*.
- W.C. Chan, L.K. Li, W.Y. Tao, N. Yao and P.T. Yung, "Surface acoustic wave assisted piezoelectric microcantilevers". *Manuscript under preparation*.

SIGNAL PROCESSING STRATEGIES ON COCHLEAR IMPLANT DEVICES FOR EFFECTIVE SPEECH PERCEPTION OF TONAL LANGUAGES

Principal Investigator: Tan Lee [1]
Co-Investigators: Andrew. C. van Hasselt [2], Sigfrid Soli [3], Michael C.F. Tong [2]
Research Team Members: Meng Yuan [1][5], Wilson Yu [1], Ying-Yee Kong [4]

[1] Department of Electronic Engineering, CUHK
[2] Dept of Otorhinolaryngology, Head and Neck Surgery, CUHK
[3] House Ear Institute, USA
[4] Department of Speech-Language Pathology & Audiology, Northeastern University, USA
[5] Shanghai Acoustics Laboratory, Institute of Acoustics, Chinese Academy of Sciences, China

Project Start Date: 1st July 2009
Completion Date: 30th June 2012

ABSTRACT

This research aims at developing signal processing algorithms on cochlear implants (CI) for effective speech perception of Chinese languages, particularly Cantonese. Chinese dialects are tonal languages. A Chinese word carrying different tones may have totally different meanings. Existing CI devices are found to be inadequate in encoding and delivering tone-related information. Improved design of CI processing strategies is needed to provide maximum benefit to the huge population of Chinese-speaking CI recipients. Based on our previous psychophysical studies, new signal processing algorithms are designed to enhance the tone-related speech cues and the effectiveness of these algorithms is verified by acoustic simulation with normal-hearing listeners. Subsequently, tone-enhanced CI processing strategies are designed, implemented and evaluated with Cantonese-speaking CI users. The performance of these users in Cantonese tone recognition and word recognition with the tone-enhanced strategies are compared with those with the state-of-the-art strategies on commercial CI systems. This is an inter-disciplinary research that involves the participation of signal processing researchers, experienced medical doctors, audiologists, and hearing scientists.

1. OBJECTIVES AND SIGNIFICANCE

1) Design cochlear implant (CI) signal processing strategies for effective speech perception of tonal languages and verify their effectiveness by acoustic simulation with normal-hearing listeners
2) Implement the proposed strategies as signal processing algorithms for state-of-the-art CI products and test with CI patients who speak tone languages
3) Evaluate the performance of the new algorithms in realistic acoustic environments, with different noise conditions and reverberation
4) Compare the performance of the new algorithms with existing CI algorithms which were designed primarily for western languages

There have been many studies revealing that existing cochlear implant (CI) devices do not encode pitch and tone related information effectively and thus are not well suited for speech perception of tone languages. This research aims to develop tailor-made CI processing strategies for hearing-impaired tone-language speakers. The tone-enhanced processing strategies are implemented on state-of-the-art CI hardware and their effectiveness on improving speech recognition is evaluated with Cantonese-speaking CI users. In recent years, the population of CI recipients in China grows rapidly. This research will directly benefit these users and improve their

life quality. It is expected that the new processing strategies will also be useful in providing better music perception of CI users in general.

2. RESEARCH METHODOLOGY

2.1. Periodicity enhancement of speech signals

Periodicity is an important property of speech signals. It determines the pitch of speech, which is essential in speech communication, especially for tone languages. Restoring the periodicity of noise-corrupted speech is useful for improving the perceptibility of pitch. In a cochlear implant device, periodicity enhancement can be done at the acoustic frond-end or during the acoustic-electrical conversion process. Both approaches are investigated in this research.

For periodicity enhancement of noise-corrupted acoustic signals, we adopt a transform-domain approach, which is based on effective periodic-aperiodic decomposition of the linear prediction (LP) residual signal. By giving heavier weight to the periodic component, the signal periodicity is enhanced against noise, which is largely aperiodic.

To facilitate the identification and extraction of the periodic component from a noisy speech signal, prior knowledge about the signal's pitch trajectory must be available. We tackle the problem of robust pitch estimation by exploiting the temporal-spectral redundancy of speech signals. The problem is formulated as the reconstruction of a sparse combination of pitch peak spectrum templates.

2.2. Design of tone-enhanced CI processing strategies

The signal processing algorithm in the external sound processor is the "brain" of a CI. It determines the sound features that are used to stimulate the auditory nerves. In the latest commercial CI systems, the Continuous Interleaved Sampling (CIS) strategy and the Advanced Combination Encoder (ACE) strategy are most commonly used. These algorithms encode the temporal envelope and periodicity cues (TEPC) of speech signals in different frequency bands and use pulse train carriers to carry the envelope signals to the respective electrodes. We design tone-enhanced processing strategies on the basis of CIS and ACE so as to facilitate fair comparison among existing and new strategies. The temporal periodicity cues in the range of 20 – 500 Hz at all channels are simplified into a sinusoidal wave, and the temporal envelopes below 20 Hz are unmodified. The periodicity of the sinusoidal wave follows the pitch trajectory of the input signal, which is extracted using the robust algorithm as mentioned above.

2.3. Acoustic simulation with normal-hearing subjects

A multichannel noise-excited vocoder is used to simulate speech processing in cochlear implants. It is implemented by software. TEPCs below 500 Hz are extracted from four frequency bands: 60–500, 500–1000, 1000–2000, and 2000–4000 Hz. The test stimuli are obtained by combining TEPC-modulated noise signals from individual bands. For periodicity enhancement, temporal fluctuations in the range 20–500 Hz are replaced by a sinusoidal wave with frequency equal to the fundamental frequency of original speech. Word identification experiments with normal-hearing subjects are carried out. The test results are represented in terms of tone recognition accuracy and word recognition accuracy. The performances of the periodicity-enhanced vocoder are compared with those of the conventional vocoder under various noise conditions.

2.4. Tests on CI subjects

Patient tests are the most important part of this project. The proposed strategies of tone enhancement need to be transformed into CI processing algorithms that produce electrical stimuli. The study is carried out using the Nucleus Implant Communicator (NIC) system developed by Cochlear Ltd.,

which is a development and test platform that replicates the typical signals from CI speech processor. The NIC system is provided in the form of MATLAB toolbox, named NMT, which can run on desktop computers. The Laura 34 research processor, which is also provided by Cochlear Ltd., is used to transmit the generated stimuli to the implant.

The subjects must be patients who use the CI systems of Cochlear Ltd. They must have at least 6 months of experience with CI and with the CIS or ACE strategy. In addition, all subjects must use Cantonese as their first language. The selection and clinical screening of subjects are performed by experienced audiologists or ENT doctors at the Prince of Wales Hospital.

As in the acoustic simulation tests, both tone recognition and word recognition performances are assessed. The recognition performances attained with the proposed CI processing strategies are analyzed statistically and compared with the standard CIS and ACE.

3. RESULTS ACHIEVED

3.1. Periodicity enhancement of speech signals

We developed a novel approach to periodicity enhancement of speech signals based on transform-domain periodic-aperiodic decomposition. The method operates on the linear prediction error (residual) signal. The residual signal goes through a constant-pitch time warping process and two sequential lapped-frequency transforms, by which the periodic component is concentrated in the first modulation band. By emphasizing the respective transform coefficients, periodicity enhancement of noisy residual signals is achieved. The enhanced residual signal and estimated linear prediction filter parameters are used to re-synthesize the output speech.

We proposed to dynamically adjust the weights of the periodic component and the aperiodic component according to the signal characteristics. A Wiener filtering approach has been developed to restore the waveform periodicity and reduce noise. For the transform coefficients corresponding to the periodic component, the filter parameters are estimated using a template-based method. For the coefficients of the aperiodic component, the filter parameters are determined according to the local SNRs of the respective modulation bands. Experimental results show that the proposed methods perform significantly better than conventional methods in terms of both objective quality measures and subjective ratings.

This part of work was published in 3 conference papers (references [5],[7],[12]). A full paper is in preparation for submission to IEEE Transactions in Audio, Speech and Language Processing.

3.2. Robust pitch estimation from noisy speech

Reliable pitch estimation is a pre-requisite of periodicity enhancement. We have developed a highly robust pitch estimation algorithm that can perform well at very low SNRs, e.g., 0 dB or below. There are two novel elements that contribute to the robustness of the proposed method. First, a temporal-spectral representation of pitch is derived by accumulating spectral peaks over consecutive time frames. Since the harmonic structure of voiced speech changes much more slowly than noise spectrum in neighboring time frames, spectral peaks related to pitch harmonics would stand out over the noise through the temporal accumulation. Second, prior knowledge of speech and noise is incorporated with the use of sparse estimation techniques. Estimation algorithms for dealing with noise-corrupted peak spectra are developed based on sparse representation and reconstruction approaches. Unlike in conventional problem formulation where the noise is assumed to follow a zero-mean normal distribution, we use Gaussian mixture model (GMM) to approximate the probability distribution of noise spectrum peaks. With GMM, the objective function for sparse weight estimation becomes non-convex in general. By approximation and reformulation, we proposed two convex optimization approaches to estimate the sparse weights.

The proposed algorithm has been evaluated extensively with many different kinds of noise at SNRs from 15 dB to -15 dB. The results clearly showed the superior performance of our method. At the

SNR of -10 dB, for example, we could achieve an error rate of about 20% for non-stationary white noise, while the best performance of existing algorithms was around 40%.

In addition, we investigated the feasibility of using approximated pitch tracks in speech re-synthesis, in view of the fact that pitch detection errors are inevitable as the SNR decreases. It was found that linear approximation of Cantonese pitch contours would not cause noticeable perceptual difference from the original contours.

This part of work on pitch estimation and pitch contour approximation was published in 5 conference papers and 1 journal paper (references [2],[4],[6],[9],[10],[11])

3.3. Subjective listening tests

3.3.1 With normal-hearing subjects

Five male and five female normal-hearing subjects participated in the tests. The accuracy of both tone identification and word identification were found to be consistently better with temporal cues from the high-frequency band than with those from the low-frequency band. When the SNR of input speech was decreased, the speech recognition performance degraded significantly when the standard processing strategy was used. The use of tone-enhanced processing strategy led to substantial performance improvement in noise, especially for female voice.

3.3.2 With CI subjects

A research license agreement was established in July 2009 with Cochlear Ltd., which allows our project team to use the L34 research processor, the NIC library and the NMT toolbox for the study. The subjective listening tests with CI patients were carried out in two different modes of stimuli generation and presentation as described below.

Mode I: Commercial processor in sound field

In this mode, the subject uses his/her own CI system to listen to acoustical signals played from a loudspeaker. The acoustical signals are picked up by the external microphone and the electrical stimuli are generated by the commercial speech processor in the subject's CI system.

Mode II: Direct stimulation using a research processor

In this mode, the electrical stimuli are generated by a computer using software-implemented signal processing algorithms and presented via the Laura 34 research processor to the subject's internal implant. The software being used includes the Nucleus MATLAB Toolbox (NMT) and Nucleus Implant Communicator (NIC).

We have successfully completed listening tests with four male and three female subjects, aged 43 to 60. All of them were post-lingually deafened adults and native speakers of Cantonese with 6 months experience in listening with a CI. All subjects use the ACE strategy in their daily communication. Each subject was required to complete five test sessions on different days. A validation experiment was carried out in the first two sessions to compare the word and tone recognition performance in quiet with the subject's own CI processor (Session 1) and with the experimental platform. In the remaining three sessions, electrical stimuli were generated from noisy speech materials and delivered by direct stimulation via the Laura 34 experimental platform.

The average percent correct scores on word and tone identification in quiet attained by direct stimulation (Test Session 2) were compared with that by sound-field listening (Test Session 1). For all of the seven subjects, the word identification scores from listening with the Laura 34 research processor were very close to those of listening with their own CI systems. This confirmed that the experimental platform was functioning properly and the subjects adapted very well to the electrical stimuli generated by the MATLAB-implemented ACE strategy.

With the presence of noise, the speech recognition performance of CI subjects declined considerably. The average accuracy of tone identification dropped from 85% to 76%. The degradation of

performance with noise was greater for the female voice than for the male voice. With the tone-enhanced processing strategy, the accuracy of tone identification in noise was improved significantly from 76% to 82% and more improvement was observed for female voice than for male voice. The improvement was also found for all of the six tones of Cantonese.

This part of research was presented as an invited paper in the annual meeting of the Acoustical Society of America and a research abstract has been published in the Journal of the Acoustical Society of America (reference [3]). Recently, a journal paper that contains full details of this study has been prepared and submitted to Ear and Hearing for peer review (reference [1]).

4. PUBLICATION AND AWARDS

[1] Tan Lee, Wilson Yu, Meng Yuan and Ying-Yee Kong, "The effect of enhancing temporal periodicity cues on Cantonese tone recognition by cochlear implantees," submitted to *Ear and Hearing*.

[2] Tan Lee and Feng Huang, "Pitch estimation in noisy speech using accumulated peak spectrum and sparse estimation technique," accepted for publication in IEEE Transactions on Audio, Speech and Language Processing.

[3] Ying-Yee Kong, Tan Lee, Meng Yuan and Wilson Yu, "Relative contributions of temporal and spectral cues for Mandarin and Cantonese tone recognition," invited presentation at *the 163rd meeting of Acoustical Society of America*, April 2012.

[4] Feng Huang and Tan Lee, "Robust pitch estimation using l1-regularized maximum likelihood estimation," *Proceedings of Interspeech 2012*, Oregon, USA, September 2012.

[5] Feng Huang, Tan Lee, and W. Bastiaan Kleijn, "Transform-domain wiener filter for speech periodicity enhancement," *Proceedings of IEEE International Conference on Acoustic Speech and Signal Processing*, Kyoto, Japan, pp. 4577-4580, March 2012.

[6] Feng Huang and Tan Lee, "Sparsity-based confidence measure for pitch estimation in noisy speech," *Proceedings of IEEE International Conference on Acoustic Speech and Signal Processing*, Kyoto, Japan, pp. 4601-4604, March 2012.

[7] Feng Huang, Tan Lee, and W. B. Kleijn, "Transform-domain speech periodicity enhancement with adaptive coefficient weighting," *Proceedings of IEEE International Symposium on Intelligent Signal Processing and Communication Systems*, Thailand, December 2011.

[8] Tan Lee and P. C. Ching, "Dealing with imperfections in human speech communication with advanced speech processing techniques," (invited paper in) *Proceedings of International Symposium on Signals, Circuits and Systems 2011,* Iasi, Romania, June 2011.

[9] Yujia LI and Tan Lee, "Perception and analysis of linearly approximated F0 contours in Cantonese speech", *Proc. International Symposium on Chinese Spoken Language Processing (ISCSLP) 2010*, pp. 435-439, Tainan & Sun Moon Lack, Taiwan, Nov. 2010.

[10] Feng Huang, Tan Lee, "Pitch estimation in noisy speech based on temporal accumulation of spectrum peaks", *Proceedings of Interspeech 2010*, pp. 641-644, Chiba, Japan, Sep. 2010.

[11] Yujia Li and Tan Lee, "Perception-based automatic approximation of F0 contours in Cantonese speech", *Proceedings of Interspeech 2010*, pp. 1425-1428, Chiba, Japan, Sep. 2010.

[12] Feng Huang, Tan Lee, W. Bastiaan Kleijn, "A method of speech periodicity enhancement based on transform-domain signal decomposition," *Proc. EUSIPCO*, Aalborg, Denmark, pp. 984-988, August 2010.

TERAHERTZ PROBE FOR IN VIVO IMAGING

Principal Investigator: Thierry Blu[1]
Co-Investigator: E MacPherson[1], A T Ahuja[2] and W H Cheung[3]

Research Team Members:
Mr SY My[1]
MS YW Sun[1]
Ms W C Kan[1]
Dr Edward Parrott[1]
Dr Yang Chen[1]
Dr Shengyang Huang[1]
Dr Y X Wang[3]
Dr K.W. Yeung[3]
Ms W S LEE[4]
Mr Paddy O'Kelly (Collaborator)[5]

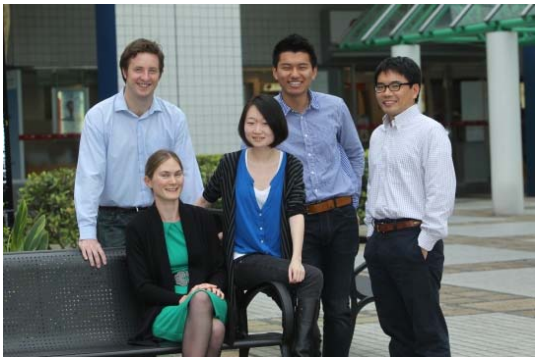

(1) Dept. of Electronic Engineering, Chinese University of Hong Kong
(2) Dept. of Diagnostic Radiology and Organ Imaging, Prince of Wales Hospital, Chinese University of Hong Kong
(3) Dept. of Orthopaedics and Traumatology, Chinese University of Hong Kong
(4) TeraView Ltd, Cambridge, UK

Reporting Period: 1st October 2009 – 30th Sept 2012

ABSTRACT

Terahertz frequency radiation lies between the millimetre and infrared regions of the electromagnetic spectrum (THz = 10^{12} Hz, 1 THz corresponds to 4.14 meV). In addition to terahertz radiation being non-ionising, its reflection geometry imaging modality means that data can also be taken non-invasively. Due to its sensitivity to hydrogen bonds and therefore water, terahertz radiation has been able to reveal contrast in terahertz images of skin cancer as tumour has a higher water content than healthy tissue. It is not just variations in water content that terahertz radiation is able to detect as contrast has also been see in terahertz images of dehydrated and wax embedded samples. This implies that the discriminatory aspects relate to the change in vascularity and matrix organization of the pathological tissue.

Therefore, if terahertz imaging could be used in vivo then it has the potential to be a valuable clinical tool for instance to determine tumour excision margins or to monitor changes in matrix organization as for example in scar maturation. We therefore plan to collaborate with TeraView Ltd to investigate how the terahertz probe can be improved so that it can be more suitable for clinical use in vivo.

1. OBJECTIVES AND SIGNIFICANCE

- Design and develop a new terahertz probe with improved image registration and signal to noise that can be used in vivo
- Improve the analysis of the data by using novel signal processing techniques
- Demonstrate its success by characterizing inhomogeneous biological samples
- Investigate potential medical applications that have been hitherto difficult due to poor image registration of the present terahertz probe

2. RESEARCH METHODOLOGY

Our research is divided into two main areas namely probe design and data processing.

2.1 Probe design

We collaborated with Teraview Ltd, Cambridge to draw up designs and select components for the improved probe. We have recruited (Dr) Edward Parrott from Cambridge University to work on this aspect of the project and he started 1st June 2010. During his post, Dr Parrott has built a fiber based transmission spectroscopy module for the terahertz system.

2.2 Data processing

Previously we have been using deconvolution with a simple double Gaussian filter (DGIF) to process our data, however recently we have applied a new approach, Frequency-wavelet domain deconvolution (FWDD) to our data and achieved significant improvements (see section 3).

We also investigated other processing methods that do not involve direct deconvolution, but instead use recently developed sparse restoration techniques (aka, compressed sensing) which typically amount to regularize the deconvolution problem with a non-Euclidean norm. The rationale for using this approach is that the THz measurements essentially result from reflections caused by strong refractive index changes. The preliminary results on simulations (using real THz impulse responses) are very promising: they indicate that, without baseline extracton, it is is possible to retrieve very accurately (within one sample at PSNR = 25 dB) the location of the sudden refractive index changes, even in the presence of substantial noise. This is exemplified in the plots below

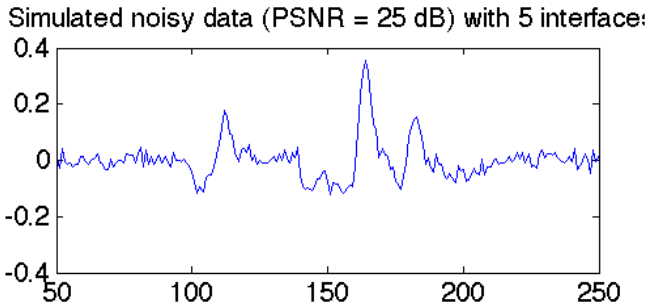

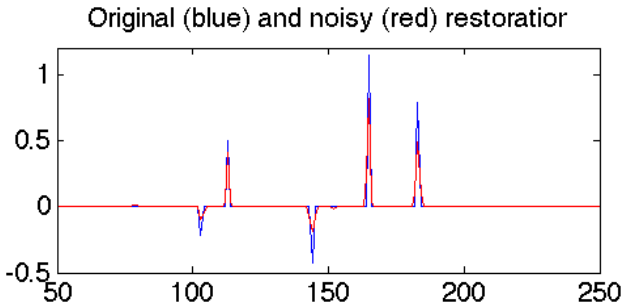

An even higher accuracy may be achievable by carefully modelizing the THz impulse response and using another approach to sparse restoration: the "Finite Rate of Innovation" setting (see Blu *et al.*,"Sparse Sampling of Signal Innovations", IEEE Signal Processing Magazine, Vol. 25 (2), pp. 31-40, March 2008).

3. RESULTS ACHIEVED SO FAR

3.1 Data processing

In Figure 1 (taken form our published journal article [1]) the improved resolution achievable using FWDD (Fig. 1d) rather than DGIF (Fig 1b) is clear – no matter how much the filter parameters are tweaked (illustrated in Fig 1c) the two reflections cannot be clearly resolved using this approach. However using the FWDD method, the reflections can be seen clearly.

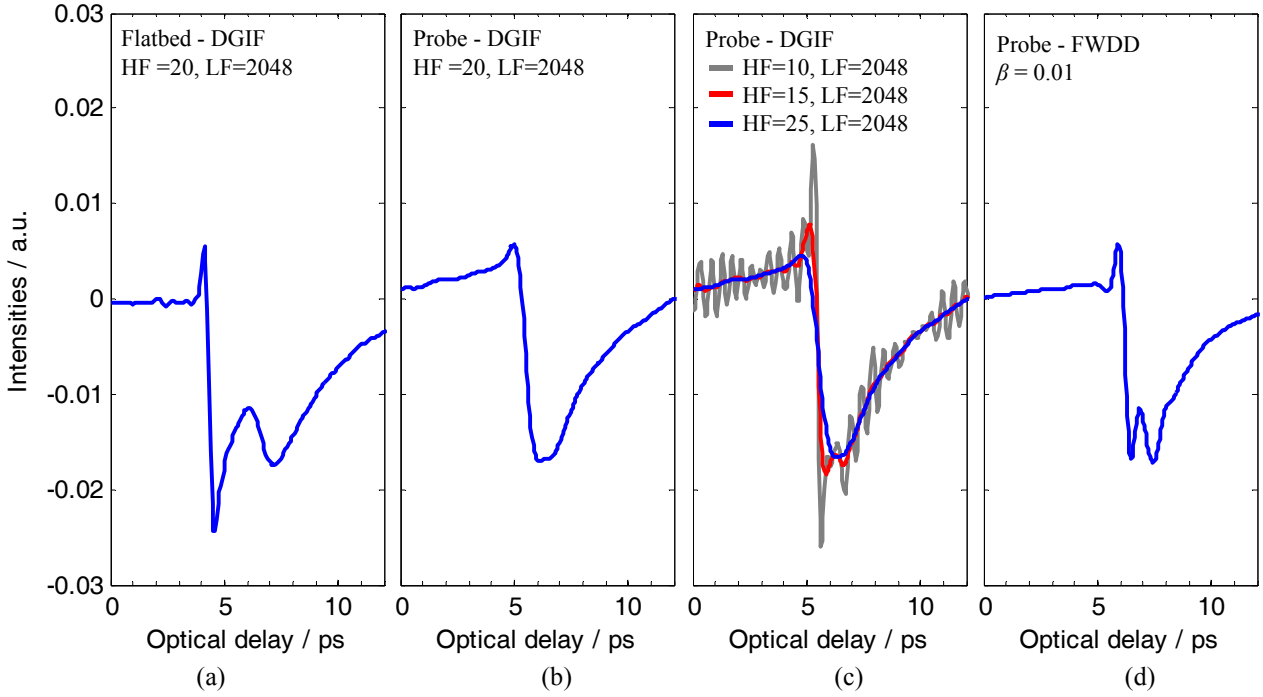

Figure 1. The resulting response functions calculated using palm data from a) the flat-bed imaging system, processed using a double Gaussian filter; b) the probe, processed using the same double Gaussian as in (a); c) the probe, processed with various double Gaussian filters; and d) the probe, processed using the new (FWDD) approach.

Figure 2 is taken from our publication on terahertz processing techniques [3.]. We used sparse deconvolution to better determine the thickness of a thin sample.

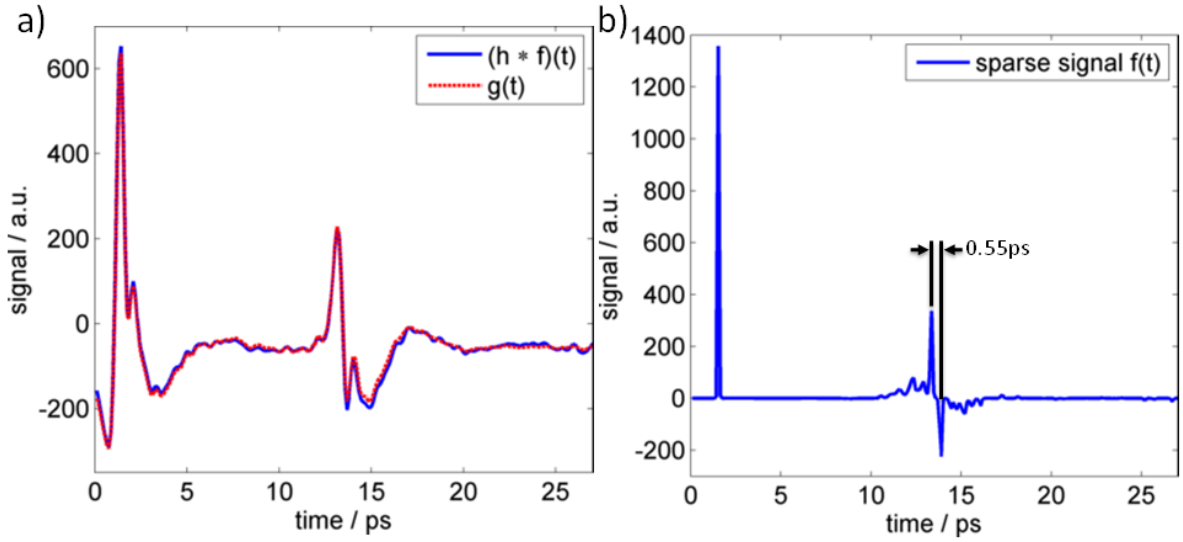

Figure 2: (a) The measured terahertz signal [g(t)] (red dotted line) and the reconstructed terahertz signal (blue solid line) obtained by convolving the sparse deconvolution result f(t) with an estimate of the system impulse response h(t) (not shown here). (b) The sparse deconvolution result f(t).

3.2 New transmission module

The THz signal from the new fiber based transmission spectroscopy module has a higher signal to noise ratio than the previous probe and is pictured in Figure 3.

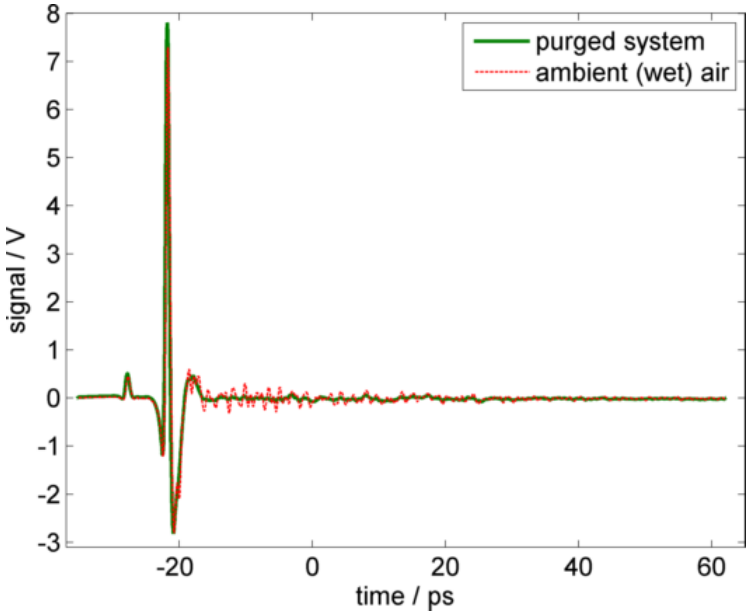

Figure 3. Sample time domain taken in transmission mode. Green solid line is the system signal when purged with dry air, and the red dashed line is the ambient atmosphere signal, clearly showing the water vapour absorption features.

3.3 Sample characterization

One of the findings we have shown in this project is that structural changes occurring in tissues contribute significantly to the terahertz image contrast – more so than initially thought. In our study of liver cirrhosis we showed that structural changes contributed upto 66% of the change in absorption coefficient, meaning that this contrast was greater than that due to changes in water content alone [9.]. This paper was well received and had two news articles reporting on its findings namely in SPIE Newsroom http://spie.org/x44146.xml?ArticleID=x44146 and in BioPhotonics http://www.photonics.com/Article.aspx?AID=46015 Figure 4 illustrates the key result.

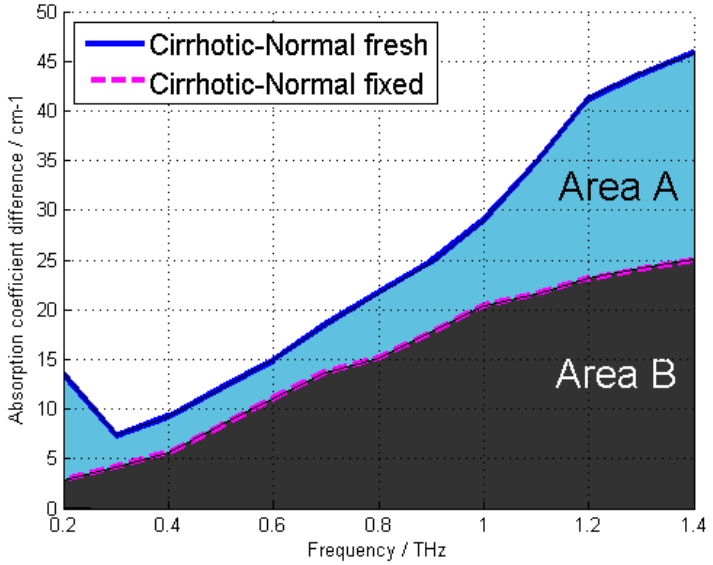

Figure 4: The blue line indicates the absorption coefficient of freshly excised cirrhotic rat tissue, minus that of the fresh healthy tissue. The pink line represents the same calculation for samples that were later fixed in formalin. Thus, the area labeled "A" predominantly represents the difference in absorption due to water, whereas area "B" represents the difference due to structural changes, such as nodules and fibrosis.

Another high impact publication was in the BioPhysical journal (impact factor 4.4) showing how terahertz spectroscopy could be used to distinguish between antibodies with different labels [7.], this result is given in Figure 5.

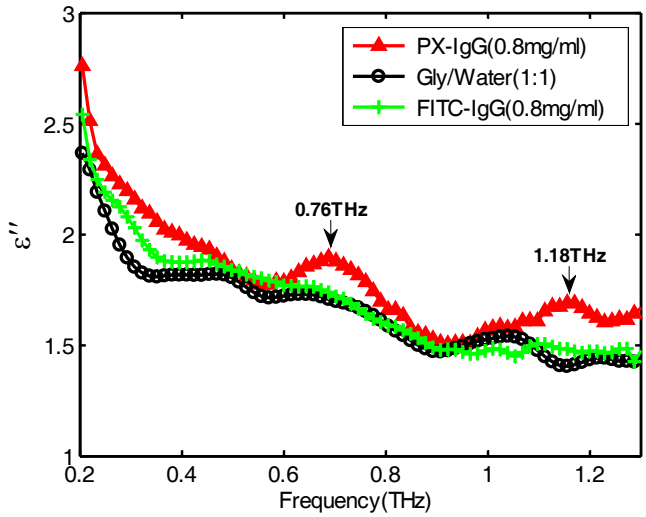

Figure 5: ε" is the imaginary part of the permittivity, which is related to the dissipation (or loss) of energy within the medium. The peroxidase (PX) labeled antibody has features at 0.76 THz and 1.18 THz which are not present in the fluorescein (FITC) labeled antibody nor the glucose solution in which the samples were dissolved.

As well as characterizing biological samples we have also characterized liquid crystals as we are developing a liquid crystal based terahertz device (a spatial light modulator) to improve the image acquisition speed and image registration issues. Our characterization and analysis of liquid crystals for terahertz devices has also resulted in a high impact journal publication [1.] and several international invited talks.

4. PUBLICATION AND AWARDS

Journal Papers :

1. Hongkyu Park, Edward P. J. Parrott, Fan Fan, Meehyun Lim, Haewook Han, Vladimir G. Chigrinov, and Emma Pickwell-MacPherson, Evaluating liquid crystal properties for use in terahertz devices. Optics Express Vol. 20, Issue 11, pp. 11899-11905 (2012)

2. Calvin Yu, Shuting Fan, Yiwen Sun, Emma Pickwell-MacPherson, "The potential of terahertz imaging for cancer diagnosis: A review of investigations to date". Quant Imaging Med Surg, Vol 2, p33-45, 2012.

3. Edward Parrott, M. Y. Sy, V. P. Wallace, T. Blu, Emma Pickwell-MacPherson, "Terahertz pulsed imaging in vivo: measurements and processing methods", J. Biomed. Opt. 16, 106010 (2011).

4. Edward Parrott, Yiwen Sun, Emma Pickwell-MacPherson, "Terahertz spectroscopy: its future role in medical diagnoses", Journal of Molecular Structure, Volume 1006, Issue 1, p. 66-76 (2011).

5. Yiwen Sun, Ming Yiu Sy, Yi-Xiang J Wang, Anil T Ahuja, Yuan-Ting Zhang and Emma Pickwell-MacPherson, "A promising diagnostic method: Terahertz pulsed imaging and spectroscopy". World J Radiol 3(3):55-65, 2011.

6. Yang Chen, Yiwen Sun, Emma Pickwell-MacPherson, "Total Variation Deconvolution for Terahertz Pulsed Imaging", Inverse Problems in Science & Engineering. Vol 19, Issue 2, 2011, 223- 232

7. Yiwen Sun, Yuanting Zhang and Emma Pickwell-MacPherson, "Investigating antibody interactions with polar liquids using terahertz pulsed spectroscopy". Biophysical Journal, Volume 100, Issue 1, 5 January 2011, Pages 225-231.

8. E Pickwell-MacPherson, "Practical considerations for *in vivo* THz imaging", invited paper for J. Terahertz Science and Technology, Vol 3, No. 4, Dec 2010.

9. Stanley Sy, Shengyang Huang, Yi-Xiang J Wang, Jun Yu, Anil T Ahuja, Yuan-ting Zhang and Emma Pickwell-MacPherson "Terahertz spectroscopy of liver cirrhosis: investigating the origin of contrast", Physics and Medicine in Biology, Phys. Med. Biol. 55 (2010) 7587-7596.

10. W. C. Kan, W S Lee, W. H. Cheung and E Pickwell-MacPherson, "Terahertz Pulsed Imaging of knee cartilage", Biomedical Optics Express Vol. 1, Iss. 3, pp. 967–974 , 2010.

11. Yang Chen, Emma Pickwell-MacPherson, "Improving extraction of impulse response functions using stationary wavelet shrinkage in terahertz reflection imaging." Fluctuation and Noise Letters, Vol. 9, No. 4 (2010) 1–8.

Conference papers:

1. **THz-IRMMW, Keynote invited talk,** Hongkyu Park; Zhe Huang; Edward Parrott; Hau Ping Chan and Emma Pickwell-MacPherson "Novel wire grid polarizer for accurate antenna characterization", Sept 2012

2. **THz-IRMMW:** Edward P. J. Parrott, Hongkyu Park and Emma Pickwell-MacPherson, "Compensating for fibre-coupled power drift in THz-TDS systems", Sept 2012.

3. **THz-IRMMW:** Shuting Fan, Edward P. J. Parrott, and Emma Pickwell-MacPherson, "Removing the 'double-pulse' problem in polarization maintaining fiber delivery of femtosecond laser in terahertz systems", Sept 2012

4. **SPIE International Symposium on Optics and Photonics**, Invited talk: E. Pickwell-MacPherson, E. P. J. Parrott, H. Park, F. Fan, V. G. Chigrinov, "Tailoring liquid crystals to become fast and efficient terahertz devices", San Diego, August 2012

5. **SPIE International Symposium on Optics and Photonics**, Invited talk: **E. Pickwell-MacPherson,** E PJ Parrott, Y Sun, "Probing biological systems with terahertz spectroscopy", San Diego, August 2012

6. **IEEE Radio Frequency Integrated Circuit Symposium** Workshop on THz imaging for biomedical applications at, Invited talk: **E. Pickwell-MacPherson,** "Biomedical THz studies: from in vivo skin imaging to molecular spectroscopy", Montreal, Canada June 2012.

7. **THz-Bio Workshop Invited Talk: E. Pickwell-MacPherson,** "Bio-chemical sensing with THz spectroscopy", Seoul National University, Korea, Feb 2012

8. **SPIE Photonics West BiOS invited talk, E. Pickwell-MacPherson,** AJ Fitzgerald and VP Wallace "Breast cancer tissue diagnosis at terahertz frequencies", San Francisco, Jan 2012.

9. **Shenzhen International Conference on Advanced Science and Technology, Invited Plenary talk**, "Biomedical terahertz imaging and spectroscopy", **E. Pickwell-MacPherson** and V. P Wallace, Shenzhen, China, Nov 2011

10. **THz-IRMMW, Invited keynote talk:** Hongkyu Park; Fan Fan; Meehyun Lim; Haewook Han; Vladimir Chigrinov; **E Pickwell-MacPherson "**Terahertz properties of liquid crystals", Houston, USA, Oct. 2011.

11. **SPIE Photonics West BiOS invited talk, E. Pickwell-MacPherson,** "Terahertz pulsed imaging in vivo", San Francisco, Jan 2011.

12. **Liquid Crystals for Photonics invited talk: E. Pickwell-MacPherson**, E. P. J. Parrott, H. Park, V. G. Chigrinov, "Liquid Crystal Quest for Terahertz Imaging", Hong Kong, Dec 2010

13. **THz-IRMMW:** M.Y. SY, S.Y. Huang, Y.X. Wang, J Yuc, A.T. Ahuja, Y.T. Zhang, V.P. Wallace, and **E. Pickwell-MacPherson**, "Investigating the Role of Water Content on the Terahertz Properties of Rat Liver Cirrhosis", THz-IRMMW, Rome 2010.

14. **THz-IRMMW:** Yiwen Sun, Y.T.Zhang, **E. Pickwell-MacPherson**, “Probing Dielectric Relaxation Models of Polar Liquids using Terahertz Time-domain Pulsed Spectroscopy”, THz-IRMMW, Rome 2010.

15. **THz-IRMMW:** M.Y. SY, Y.T. Zhang, and **E. Pickwell-MacPherson**, “A Study of TPI of Human Skin under Different Temperature and Humidity”, THz-IRMMW, Rome 2010.

Awards:
Mr Stanly Sy won the Engineering Faculty best MPhil Thesis Prize 2011.

[1] Yang Chen, Shengyang Huang, and Emma Pickwell-MacPherson, "Frequency-wavelet domain deconvolution for terahertz reflection imaging and spectroscopy," Opt. Express 18, 1177-1190, 2010, Jan 2010. 5 year IF 4.6.

[2] YW Sun, B M Fischer, E Pickwell-MacPherson, “The Effects of Formalin Fixing on Terahertz Image Contrast”, J. Biomedical Optics, vol. 14, issue 6, p. 064017, Dec 2009. IF 3.9

[3] MY. SY, YT. Zhang , E. Pickwell-MacPherson, “A Study of Terahertz Pulsed Imaging of Human Skin”, IEEE EMBS International symposium on Medical Devices and Biosensors and Biomedical Health Engineering (MDBS-BHE), Shenzhen, China, Dec 2009.

[4] Y Chen, E. Pickwell-MacPherson, “Stationary-Wavelet Regularized Inverse Filtering for Terahertz Reflection Spectroscopy of Liquid Samples”, MDBS-BHE, Shenzhen, China, Dec 2009.

[5] Shengyang Huang, Y.T.Zhang, E. Pickwell-MacPherson, “Quantitative Estimation of Calculation Accuracy from Dynamic Range in Terahertz Pulsed Imaging”, MDBS-BHE, Shenzhen, China, Dec 2009.

[6] Yiwen Sun, Y.T.Zhang, E. Pickwell-MacPherson, “Terahertz Dielectric Properties of Monoclonal Antibodies to Influenza”, MDBS-BHE, Shenzhen, China, Dec 2009.

DEVELOPMENT OF A ROBOTIC ENDOSCOPE HOLDER FOR NASAL SURGERY

Principal Investigator: Professor Yunhui Liu [1]

Co-Investigator (if any): Professor Michael C. H. Tong [2]
Dr. Siu Kwan Ng [2,3]
Dr. Vlantis, Alexander Chris [2]
Dr. Hing Sang Chan [2,3]

Research Team Members: Mr. D. Navarro-Alarcon [1] , Dr. Peng Li [1] , and Miss. H. M . Yip [1]

[1] Department of Mechanical and Automation Engineering, The Chinese University of Hong Kong
[2] Department of Department of Otorhinolaryngology, The Chinese University of Hong Kong
[3] Department of Head and Neck Surgery, Prince of Wales Hospital.

Project Start Date: 1st July 2009
Completion Date: 30th November, 2011

ABSTRACT

To carry out surgical operations in the nasal cavity, a surgeon needs to use one hand to hold and control an endoscope that views the nasal cavity and the other hand to manipulate surgical tools. In this project, we propose to develop a robot manipulator to hold and control the endoscope so that the surgeon can use both his/her hands to perform the operational procedure, which is highly preferable. The robot manipulator consists of a positioning device, which is to be manually set up before the operation, and a compact dexterous endoscope holder with fine motion and force control, which is to be controlled by the surgeon. The dexterous endoscope holder will have five degrees of freedom that are specially designed so as to realize fine motion of the endoscope inside the narrow nasal cavity. The operational safety of the proposed robotic system is guaranteed by a passive safety mechanism and an active force controller. The hand-busy surgeon controls motion of the endoscope by a friendly force-reflecting foot-controlled or voice-controlled interface, which enables the surgeon to feel or understand the interaction forces of the endoscope with the nasal cavity. To guarantee stability of the system, we will develop a sensor-based motion planner that maps the surgeon's motion commands to the motion of the endoscope based on the compliance of tissues in the nasal cavity, which is estimated on-line using the force and position measurements. The performance of the robotic endoscope holder will be verified by experiments. The results will advance research of robotics technology for nasal surgery and have direct applications for medical services in Hong Kong.

1. OBJECTIVES AND SIGNIFICANCE

In nasal surgery, surgeon needs to simultaneously manipulate the surgical tools and an endoscope that captures images of the nasal cavity (Fig. 1). To improve the efficiency and quality of the surgical operation, it is highly demanded to release the hand-busy surgeon from controlling the endoscope so that his/her both hands can be focused on manipulation of surgical tools. As an innovative solution, we propose to develop a compact and dexterous robot manipulator for controlling fine motion of the endoscope and the interaction force of its tip with nasal cavity. There are several challenges in developing the robotic endoscope holder. First, nasal surgery has a small workspace where the robot and the surgeon must work together, so how to guarantee safety of both the surgeon and patient is one of the major concerns. Second, the endoscope tip needs to conduct fine motion of position and orientation in the small nasal cavity, so special efforts must be made to the mechanism design and the motion controller. Furthermore, a friendly and effective interface must be developed to facilitate collaboration of the hand-busy surgeon with the robot. Existing surgical robots are too big to be used

in nasal surgery. Moreover, most of existing surgical robots are controlled by a hand-controlled interface. This hand-control method is not suitable for nasal surgery because the surgeon wants to focus his/her both hands on the surgical procedure and to control the endoscope directly by himself/herself instead of an assistant. Therefore, it is highly demanded to develop a new robot manipulator with a surgeon-friendly interface that enables the surgeon to control the endoscope without using hands. In this project, we addressed mechanism design, safety, motion and force control, and human-robot interactions of such a robotic endoscope holder. An innovative technology for nasal surgery has been developed.

The project objectives are as follows:

- Design of a compact, dexterous and surgeon-friendly robotic arm with the capability of realizing fine and dexterous motion of the endoscope in the narrow nasal cavity;
- Development of a new mechanism for guaranteeing operation safety;
- Development of a friendly surgeon-robot interface to facilitate interactions between the robot and the hand-busy surgeon by voice or foot.; and
- Experimental validation of the developed system in a simulated environment.

2. RESEARCH METHODOLOGY

2.1. System Requirements

The robot is to release the hand manipulating the endoscope so that both hands of the surgeon can be focused on the procedures. Based on interviews with the surgeons at the Prince of Wales Hospital and the medical experts in our team, and ex-vivo measurements of 6 human cadaver heads, we identified the following functional requirements and technical specifications of the robot:

(1) The robot must be able to conduct the endoscope manipulation task while satisfying the specific dimensional requirements of nasal surgery, i.e. it must be able to work in the narrow workspace without obstructing the surgeon;
(2) The robot must be able to reorient the yaw and pitch angles in a range of about ±60° , and to insert the constrained endoscope about 10 cm inside the nasal cavity.
(3) The robot must satisfy strict safety requirements. It must not, under any circumstances. threaten the safety of the patient or surgeon. The robot must not generate large interaction forces at the entry point or inside the nasal cavity during the procedure.
(4) The robot should have a surgeon-friendly interface that enables surgeon to control the robot easily.

2.2. Outline of the Robotic System

To meet the functional and technical requirements, we iteratively optimized the configuration, the mechanism and kinematic parameters of the robotic endoscope holder, and finally developed a prototype (Fig. 2). The developed robotic system has the following features:

(1) It is composed of a 3 degrees of freedom (DOF) positioning platform and a 4 DOF dexterous orientation arm (Fig. 2). The decoupled design allows surgeon to independently control the orientation-insertion task and the contact point positioning task of the endoscope.
(2) The orientation arm can accomplish a decoupled control of the pitch and yaw angles of the endoscope. The arm uses a *double parallelogram* mechanism to control the picth angle and an *arc-guide* mechanism to change the yaw angle so as to realize a remote center motion.
(3) To control the endoscope insertion and roll along the *z* axis, we investigated two designs: a *Double Screw Drive Mechanism* that uses two actuators to change the roll angle and the insertion depth in a decoupled manner, and a mechanism that uses two motors to control the two DOF independently.
(4) The positioning platform, which serves as a mobile base for the orientation arm, is a 3 DOF robot with the so called Cartesian configuration to independently control the *x, y, z* position of the RCM.

(5) The yaw and pitch actuators of the orientation arm are placed at the mobile platform base to reduce the size and weight. The power is transmitted to the joints through tendons.
(6) Specially designed passive mechanisms are used to protect safety of the patient, the surgeon as well as the robot itself.

Fig. 1 The nasal surgery.

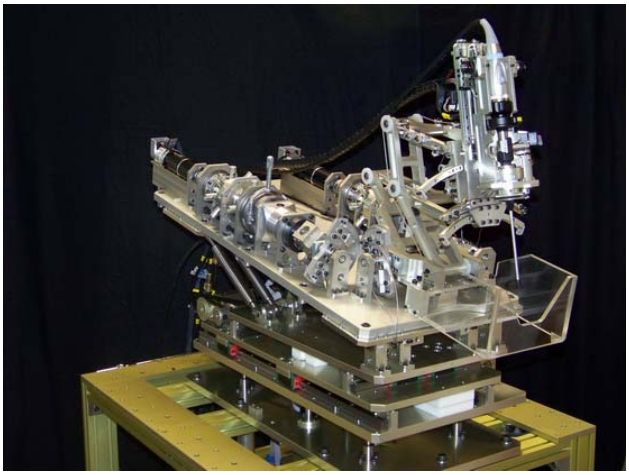

Fig. 2 The developed robotic endoscope holder.

2.3. Safety Protection Mechanism

Since the medical robot will inevitably have direct contact with the patient and the surgeon during the surgical procedures, it is important to design safety mechanisms to prevent the patient and surgeon from injuries. The safety of our system is protected in two levels. In the first level, the safety is protected passively by the mechanisms themselves. We have newly developed a passive safety protection unit, which is installed at the robot joints (Fig. 3). No matter whether the controllers and sensors work well, the mechanism will guarantee the interaction forces below thresholds when the robot is interacting or colliding with people. In the second level, the safety of the system is guaranteed by active force control. An on-line monitoring system is developed for monitoring the interaction forces between the endoscope and the surgeon. When the forces are greater than thresholds, the power supply will be cut off automatically.

2.4. Surgeon-Robot Interface

To enable the surgeon to focus his/her both hands on the surgical procedures, a hand-free control interface has been developed for this robotic system. The interface includes a foot-controlled interface and a speech-controlled interface. The developed speech-controlled interface enables the surgeon to control the robot using voice commands. It can be used independently or together with the foot-controlled interface. Voice commands have been carefully designed to improve the robustness of the speech-recognition. When used together with the foot-controlled interface, the speech-controlled interface requests the user to use three voice commands such as “moving pan”, “moving tilt”, or “moving zoom” to select the motion axis. Once the axis has been selected, the surgeon inputs the desired motion using the control pedal. As shown in Fig. 4, the foot-controlled interface is composed of 2 pedals, one for selecting the moving axis of the robot and one for commanding the moving speed and moving directions. The pedal for the selection of moving axis is simply a foot switch. The two directional swinging pedal is for controlling the direction and speed of the motion.

Fig. 3 The passive safety protection mechanism installed at the joints.

Fig. 4 The foot-controlled interface.

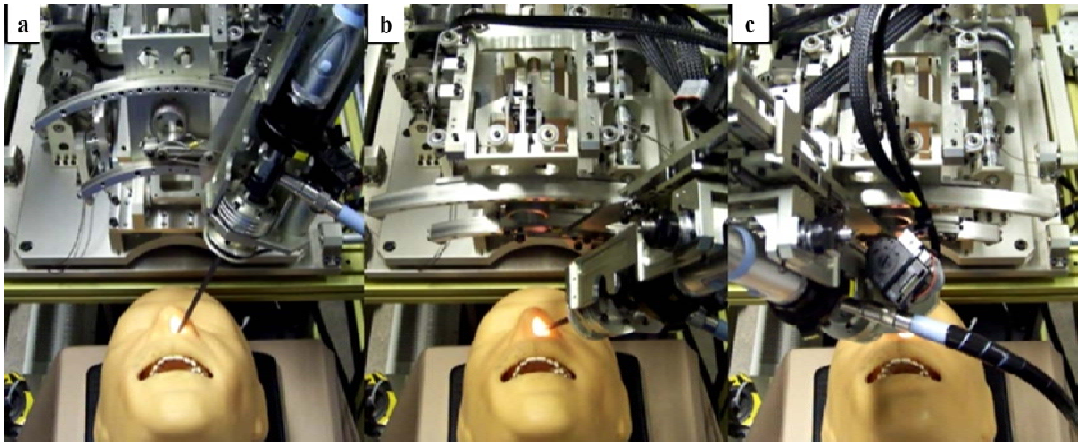

Fig. 5 The experiment using a manikin head.

2.5. Experimental Verification

To validate the developed robotic system, we have used the prototype to conduct experiments on a manikin, a pig head and cadaver head with help from the surgical experts of the Prince of Wales Hospital. Dr. Iris Leung and Dr. Samuel Chow conducted the experiments on the cadaver head. Fig. 5 shows the robot manipulating an endoscope in the nasal cavity of a manikin head. Fig. 6 presents the experiment using a pig head. Fig. 7 shows the experimental setup and the doctors using the robotic system to conduct the surgical procedures when a cadaver head was used.

It was found in the experiments that the developed robot could successfully control the orientation and insertion depth of an endoscope in the narrow nasal cavity. The robot did not obstruct hands of the surgeons. The forces measured by a force sensor during the procedures were about 3-5 N, which certainly meets the safety requirement. It was also found that the foot-controlled interface can provide satisfactory performance. The feedback from the surgeons who performed the experiments and the other surgeons who tried in other occasion are very positive.

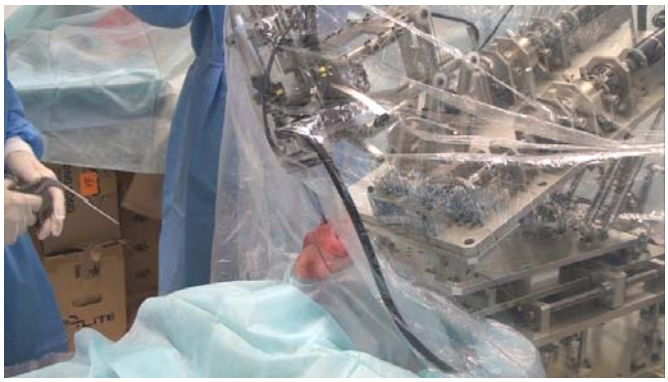

Fig. 5 The experiment using a pig head.

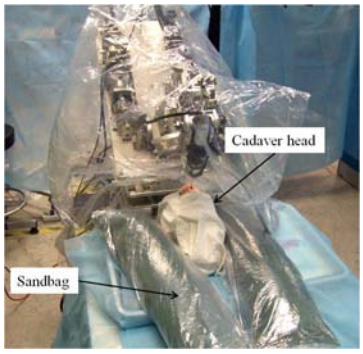

(a) The setup using a cadaver head.

(b) Dr. Leung in the experiment.

(c) Dr. Chow in the experiment.

(d) Nasal surgery using two hands.

Fig. 6 The experiment using a cadaver head.

3. RESULTS ACHIEVED

In this project, we have developed a robotic system for holding and manipulating the endoscope for a surgeon carrying out surgical procedures in a nasal cavity. The major results achieved are as follows:

(1) A robotic system has been designed and prototyped for manipulating the endoscope for a surgeon during nasal surgical procedures. The robotic system consists of a 4 DOF orientation arm and a 3 DOF positioning platform.

(2) A safety protection system has been develop to protect the safety of the surgeons, the patient and the system itself by combining specially designed passive safety mechanisms with an active force control method.

(3) A hand-free interface has been designed and prototyped for the surgeon to control the robot assistant for manipulating the endoscope using foot or voice.

(4) The performance of the system has been verified with help from surgeons of the Prince of Wales Hospital by experiments using a manikin head, a pig head and a cadaver head. The surgeon was satisfied with the performance of the system.

(5) We have published or submitted 5 papers. A patent is being applied.

(6) An ITF project “Development of a Robotic System for Nasal Surgery (ITS/475/09)”and a RGC project “Passivity-based Force Control of Medical Robots Interacting with Soft Tissues” were awarded from the research of this project.

4. PUBLICATION AND AWARDS

This research led to awards of two projects from external sources:

(1) ITF Project: Development of a Robotic System for Nasal Surgery (ITS/475/09), PI: Yunhui Liu, HK$998,021, November 1st, 2010,-April 30, 2012.
(2) RGC GRF Project: Passivity-based force control of medical robots interacting with soft tissues (415011),PI: Yunhui Liu, HK$681,195, Dec. 1st, 2011-Nov. 31st, 2014.

This research also led to the following publications:

(1) D. Navarro-Alarcon, Y.H. Liu, P. Li; , "Stable force/position control of a robotic endoscope holder for constrained tasks in nasal surgery," Proceedings of World Congress on Intelligent Control and Automation, pp. 1195-1120, 2011.
(2) D. Navarro-Alarcon, P. Li, H. M. Yip, "Energy shaping control for robot manipulators in explicit force regulation tasks with elastic environments," Proceedings of IEEE Int. Conference on Intelligent Robots and Systems, pp. 4222-4228, 2011.
(3) D. Navarro-Alarcon, Y. H. Liu and J. G. Romero, "Visually servoed deformation control by robot manipulators," Submitted to 2013 IEEE Int. Conf. on Robotics and Automation, 2012.
(4) D. Navarro-Alarcon, Y. H. Liu and J. G. Romero, and P. Li, "Exploiting force feedback within robust energy sharping control," Submitted to Automatica (under review), 2011.
(5) P. Li, Y. H. Liu, D. Navarro-Alarcon and H. M. Yip, "A novel robotic system for manipulating endoscope in nasal cavity: design and experimentation", in preparation, to be submitted to IEEE/ASME Trans. on Mechatronics, 2012.

In addition, we exhibited the robotic system in 2011 International ICT Expo, the Faculty 20th Anniversary Innovation and Technology Fair, 2011 China High-Tech Fair Shenzhen, and the InnoCarnival 2011. The robotic system was widely reported by local newspapers and newspapers in the Mainland. Those publicity activities greatly helped promotion of the university.

Development of high sensitive and throughput surface enhanced Raman scattering (SERS) substrates for molecular diagnosis

Principal Investigator: Jianbin Xu[1)]
Co-Investigator (if any): H.C. Ong[2)], Mary Waye[3)], and Aaron H.P. Ho[1)]

Research Team Members: C.Y. Chan[1)], K.C. Hui[1)], J. Li[1)] and Chuanlai Shen[1)]

[1)] Dept. of Electronic Engineering, [2)] Dept. of Physics, and [3)] Dept. of Biochemistry, The Chinese University of Hong Kong

Project Start Date: 1st July 2008
Completion Date: 30th June 2010

ABSTRACT

This project aims at developing production scalable surface enhanced Raman scattering (SERS) substrates that have ultra-high sensitivity. In fact, we have developed a bottom-up approach that allows one to systematically optimize the SERS effect while at the same time maintaining good reproducibility in sample fabrication. One- and two-dimensional periodic metallic arrays have been fabricated by using interference lithography and their band structures have been determined both experimentally and theoretically. By varying the size and shape of arrays in a step-by-step manner, we have obtained arrays that produce desirable local field. In addition, strong correlation between band structures and SERS mappings of arrays has been found, which unambiguously identifies the electromagnetic origin of SERS effects. These studies lay out general guidelines on how to optimize the field strength by tailoring the geometry of arrays. As a proof of concept, we have demonstrated strong SERS signal from one single organic molecular layer attached on 2-D Ag hole arrays. In addition, the detection of 68 ng/ml ARL-1 proteins by our arrays presents a feasible method that goes beyond the regular detection limit given by Enzyme-linked immunosorbent assay (ELISA). More importantly, our arrays in fact outperform the commercially available Klarite SERS substrates, pointing to a new direction of creating a potential market in developing more powerful SERS substrates for trace level detection with the same level of stability and reproducibility but at lower cost and higher throughput.

1. OBJECTIVES AND SIGNIFICANCE

The objectives of this project include implementation of periodic metallic arrays as SERS substrates that have single molecular sensitivity, good reproducibility, and high throughput, and development of an approach to identify the optimal condition for producing SERS effects.

The identification of molecular species at low concentration is of great importance in chip scale molecular diagnosis. Among different developing techniques, surface-enhanced Raman scattering (SERS) provides an optical means for the identification of molecules by detecting their distinct signature of vibrational modes and therefore is suitable for label-free detection. However, SERS has long been known to be quite elusive and stable Raman signal cannot be obtained consistently even under the same condition. This drawback hinders the fabrication of cost-effective SERS substrates at production level. Therefore, how to fabricate good SERS substrates that on one hand produce intense Raman signal while on the other hand are highly reproducible has become an important issue in this area. We propose to use interference lithography, which is a production scaleable method, to fabricate periodic metallic arrays for SERS. By combining theory and experiment, we have developed a bottom-up approach that allows us to systematically obtain arrays with Raman sensitivity down to single molecule. At the end of this project, we foresee a general recipe in making high sensitivity SERS substrates will be demonstrated.

2. RESEARCH METHODOLOGY

This methodology is divided into three parts: sample preparation, band structure determination, and SERS related studies. 1-D and 2-D metallic arrays are fabricated by using interference lithography and thin film deposition. By changing the processing conditions, which include incident angle, exposure time, etc, arrays with different sizes and shapes can be produced. Once the samples are ready, they are transferred to a home-built computer controlled goniometer for different optical measurements including SPR spectroscopy, reflection and transmission, fluorescence spectroscopy, Raman scattering spectroscopy, etc. In particular, by measuring the angle-dependent reflectivity (or transmission), the band structures of samples can be mapped out accordingly. From band structures, all surface plasmon resonance modes as well as other resonances can be identified unambiguously. In parallel with experiment, we use electrodynamics modeling to further understand the underlying physics of our experiments. Rigorous coupled wave analysis (RCWA) and finite-difference-time-domain (FDTD) are used to calculate the band structures, field patterns, etc. Finally, the connection between array geometry and plasmonic field profile can be identified and this provides a general guideline for maximizing field strength.

Once all factors have been optimized, molecular species that exhibits distinct Raman spectrum will be attached on arrays for SERS characterizations. Commercially available Raman microscope will be used to test out the suitability and scalability of arrays. In particular, we eventually expect the substrates can achieve almost single molecular level.

3. RESULTS ACHIEVED

We list out our achievements as follows:

1. We have developed interference lithography (IL) as a simple and cost-effective tool for fabricating two-dimensional periodic metallic arrays, as shown in Fig. 1. IL allows us to fabricate large area (> 3 cm^2) and uniform periodic arrays with great precision and good reproducibility (Fig. 2), thus offering the scalability to production level. In particular, by using IL, array geometries including hole size, shape, periodicity, etc, can be varied from >2 microns to 10 nm and from circular to elliptical by changing the processing parameters. A few examples are given in Fig. 2.

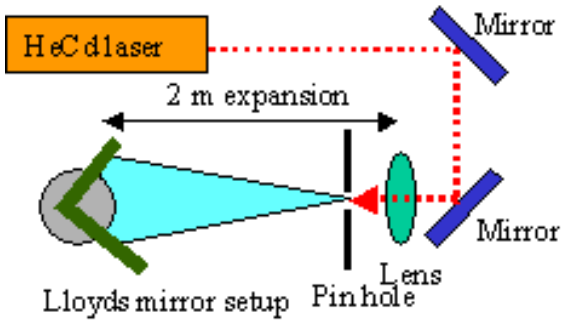

Fig. 1. Schematic setup for Lloyds interference lithography.

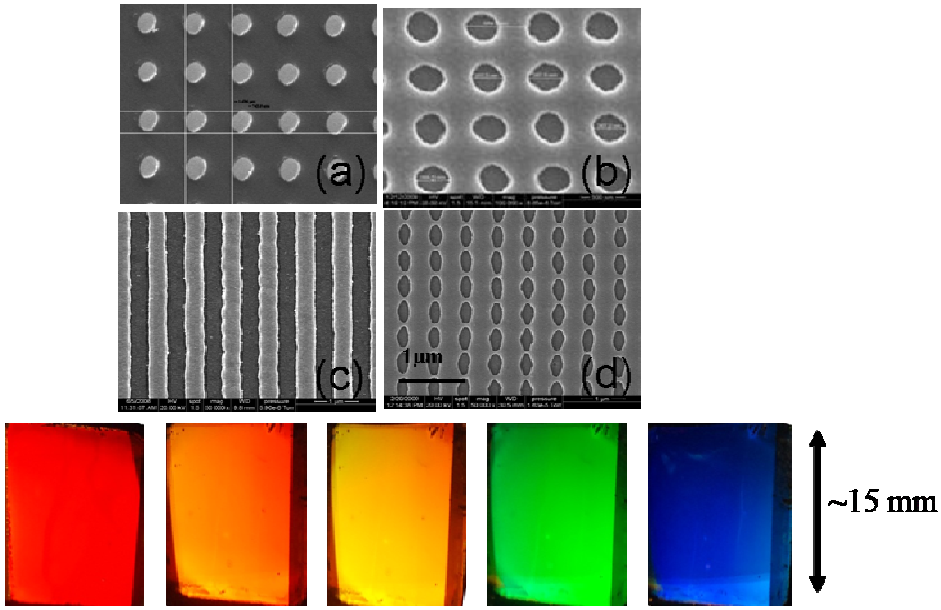

Fig. 2. The scanning electron microscopy (SEM) images of different periodic arrays fabricated by interference lithography (top). A typical sample is viewed at different angles and monochromatic colors are displayed at each viewing angle indicating the sample is uniform (bottom).

2. We have set up angle-dependent reflectivity system for measuring the dispersion relations of the arrays. Dispersion relations are important tool for understanding the basic optical properties of the arrays as they indicate the spectral position, decay lifetime, coupling efficiency, etc, of various electromagnetic resonances. The p- and s-polarized dispersion relations of typical two-dimensional circular Ag hole arrays with different hole diameters are given in Fig. 3. The corresponding SEM images are shown in the insets. The dark reflectivity regions represent the excitations of SPPs and other resonance modes. The red solid lines are deduced from theoretical simulations indicating (1,0), (-2,0), and $(-1,\pm1)_s$ SPPs are excited under p-polarization while $(0,\pm1)_a$ and $(-1,\pm1)_a$ SPPs are excited under s-polarization. The decay lifetime and coupling efficiency can be obtained by fitting the reflectivity spectra by using analytical Fano line shape function. As will be discussed later, lifetime and coupling efficiency are two important parameters for determining the resulting SERS responses.

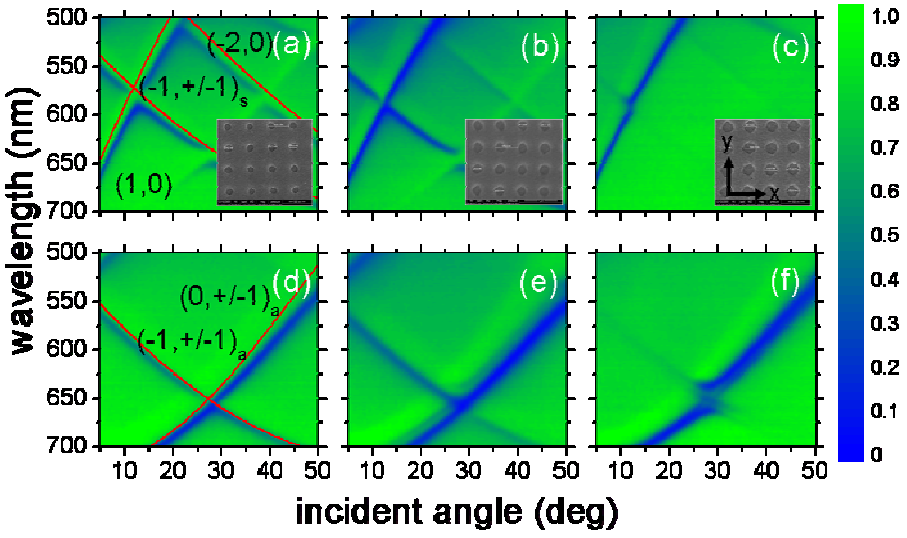

Fig. 3. The a) - c) p-p and d) – f) s-s reflectivity mappings of 2D Ag circular hole arrays with hole diameter = 204, 280, and 360 nm (from left to right) and depth = 100 nm. The dash lines are deduced from theoretical simulations indicating (1,0), (-2,0), and $(-1,\pm1)_s$ SPPs are excited under p-polarization

while $(0,\pm1)_a$ and $(-1,\pm1)_a$ SPPs are excited under s-polarization. The corresponding SEM images are shown in the insets with period = 670 nm.

3. As the properties of metallic arrays are highly geometry dependent, simulations based on Rigorous Coupled Wave Analysis (RCWA) and Finite-Difference Time-Domain (FDTD) have been developed for optimizing the geometry of arrays. An example is given in Fig. 4, the band structure of 1D metallic grating is calculated by RCWA and it is compared with the experimental result. Good agreement between theory and experiment is seen, indicating the presence of dispersive SPP modes and non-dispersive localized mode. In addition, complete field patterns arising from the arrays can be computed by simulations.

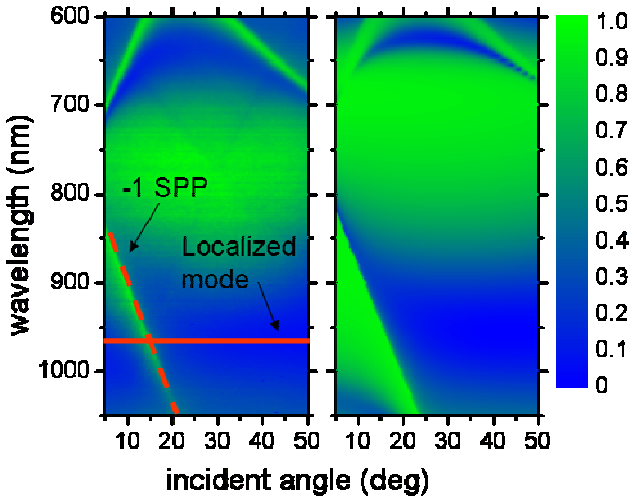

Fig. 4. (a) The experimental p-polarized dispersion relation (reflectivity) of Fig 2(c) Au grating. (b) The dispersion relation of the corresponding grating simulated by RCWA. The theory is found to agree well with the experiment, indicating the presence of SPP and localized mode.

4. Since SERS from periodic arrays is strongly angle-dependent, we have developed angle-resolved Raman spectroscopy for detailed understanding of the underlying physics of SERS. For example, p-polarized dispersion relation of a 2D hole array and its corresponding p-polarized angle-dependent Raman mapping excited by 514 nm laser are given in Fig. 5. The array, given in the inset of Fig. 5(a), is capped with a self-assembled monolayer (SAM), 6-mercaptopurine, to serve as Raman probe. In fact, the bright lines at 538, 542, 550, 560 nm, etc, in Fig. 5(b) are the peaks that are attributable to the Stoke Raman signatures of 6-mercaptopurine. A clear one-to-one correspondence is seen between the dispersion relation and the Raman mapping, indicating SERS is of SPP electromagnetic origin in this case. More importantly, while the dispersion relation provides the information of all individual electromagnetic modes including SPPs and other localized modes, the corresponding Raman mapping reveals the contributions of each mode to the resulting SERS. As a result, the combination of dispersion relation and angle-dependent Raman mapping offers us a valuable tool in studying the underlying of SERS, possibly leading us to rationally design effective SERS substrates.

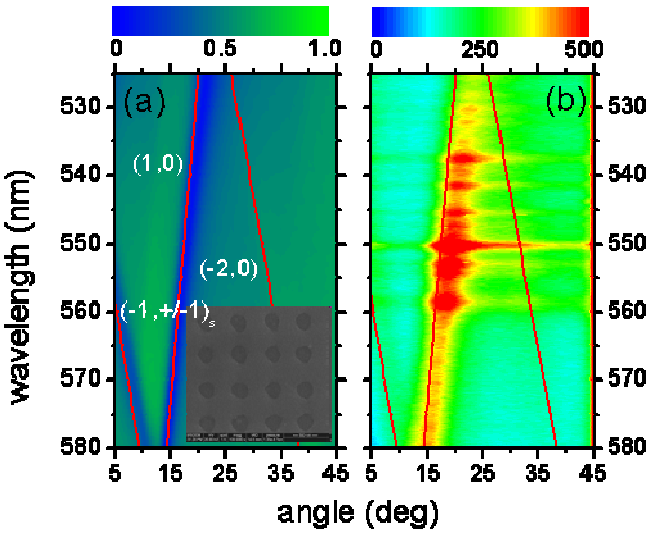

Fig. 5. The p-polarized (a) dispersion relation and (b) angle-dependent Raman mapping of 2D Ag hole array covered with 6-mercaptopurine to serve as Raman probe. The inset shows the array has period = 670 nm, hole depth and radius = 120 and 150 nm, respectively. A one-to-one-correspondence is clearly seen by comparing the dispersion relation with the Raman mapping, indicating strong Raman emission arises from the (1,0) SPP mode. As a result, the combination of dispersion relation and angle-dependent Raman mapping offers a good tool in understanding the underlying physics of SERS.

5. It is found that the SERS response is strongly geometry-dependent and is associated with the decay lifetime and coupling efficiency of the electromagnetic modes. We have fabricated 2D hole arrays with period = 670 nm, hole depth = 120 nm and radius varying from 85 to 200 nm. Fig. 6(a)-(c) show the p-polarized dispersion relations of 2D hole arrays covered with 6-mercaptopurine taken at radius = 85, 118 and 200 nm. One can see the SPP modes (dark bands) change as a function of hole radius. In particular, the (1,0) dark SPP band becomes darker when the hole radius increases, signifying stronger (1,0) SPPs are being excited. On the other hand, from Fig. 6(d)-(f), it is found that the corresponding Raman mappings correlate well with the dispersion relations, with the Raman emissions arising from (1,0) SPPs also increase consistently with increasing hole radius. The Raman spectra taken at angle = 20^{o} for all arrays are plotted in Fig. 7(a), showing the Raman peaks become more and more pronounced when radius increases. The spectrum taken from Ag film is also shown for reference. Therefore, our results strongly suggest it is possible to obtain strong SERS by tailoring the geometry of the arrays once the dependence of the behaviors of SPPs on geometry is fully understood.

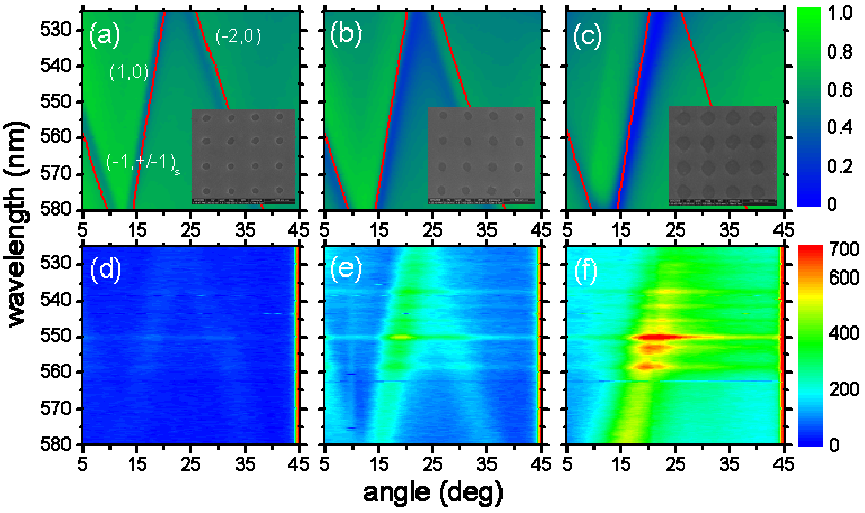

Fig. 6. The p-polarized (a)-(c) dispersion relations and (d)-(f) angle-dependent Raman mappings of 2D Ag hole arrays with period = 670 nm, hole depth = 120 nm, and hole radius = 85, 118, and 200 nm (insets). It seems from the figures that increasing the excitation of (1,0) SPP modes would increase the SERS intensity.

We also have attempted to correlate the decay lifetime and coupling efficiency of (1,0) SPPs with the resulting Raman enhancement factor. We have determined the SERS enhancement factor by comparing with the SERS obtained from bulk solution and plot the enhancement factor as a function of hole radius in Fig. 7(b). A typical of 10^6 in enhancement has been reached. More importantly, it is found that the enhancement factor is governed by (1,0) SPP decay lifetime as well as coupling efficiency. Shorter lifetime and higher efficiency, implying the presence of strong radiative SPPs, lead to larger Raman enhancement factor. As a result, it is possible to control the Raman enhancement once the underlying physics of SPPs is understood.

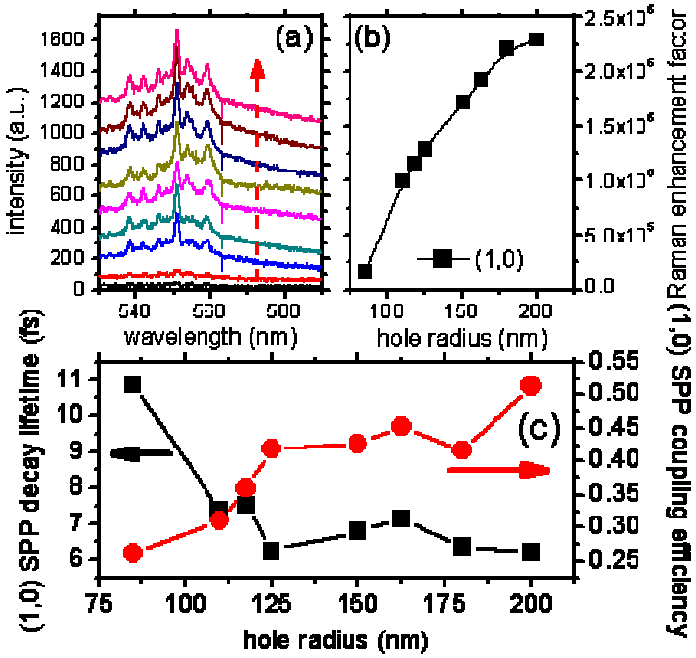

Fig. 7. (a) The (1,0) Raman spectra of the arrays taken from hole diameters of 85, 110, 118, 125, 150, 163, 180 and 200 nm. The solid arrow span from small to large hole size. The spectra are vertical shifted for visualization. The Raman spectrum taken from Ag film is also shown at the bottom for

reference. (b) The plot of SERS enhancement factor against hole radius for (1,0) SPP mode. (c) The plots of (1,0) SPP decay lifetime and coupling efficiency against hole radius.

6. To the best of our knowledge, we are a few to build a library of SERS mapping at different periods, hole depths and radii so that the dependence of SERS on geometry can be completely understood. In fact, very strong Raman enhancement is observed in thick arrays when localized mode is involved and interacts with SPPs. When the hole depth increases, localized mode begins to evolve. Fig. 8 shows the dispersion relation of 2D Ag hole array taken at period = 670 nm, hole depth and radius = 280 and 190 nm, respectively. Clearly, at the central low reflectivity region where the localized mode interact with (1,0) SPP, circled by the dash ellipse, the corresponding Raman mapping shown in Fig. 8(b) shows very strong Raman enhancement. In contrast to the shallow hole arrays where only SPPs prevail, thick hole arrays in general exhibit stronger Raman enhancement. More importantly, the SERS enhancement factor estimated from our thick arrays is ~ 10^{8-9} and they are able to detect Rhodamine 6G at concentration as low as 8 pM with high consistence and reproducibility.

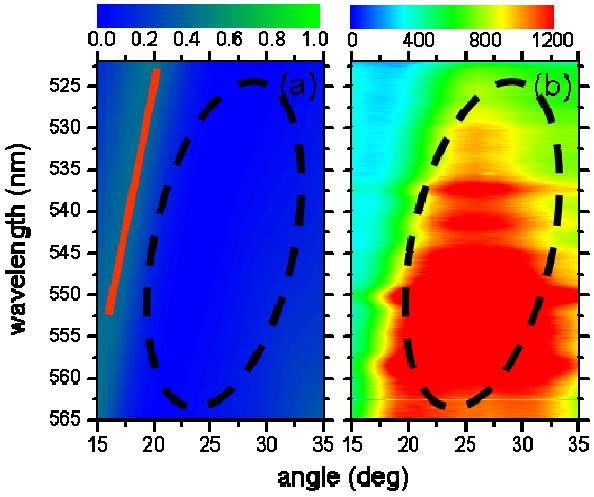

Fig. 8. The p-polarized (a) dispersion relation and (b) angle-dependent Raman mapping of thick 2D Ag hole array covered with 6-mercaptopurine. The dash circle in (a) defines the excitation of localized resonance mode, which gives rise to very low reflectivity. On the other hand, the localized mode produces very strong SERS emission in (b). The solid line indicates (1,0) SPP mode.

7. We have developed general guideline in designing the geometry of arrays to suit for any specific target analytes. By knowing the optical absorption spectrum of the analytes and matching the absorption peak with the localized resonance mode, it is possible to maximize the excitation as well as Raman emission enhancements, thus producing the strongest possible SERS.

8. Our "not-yet-optimized" SERS substrate already outperforms the commercial Klarite™ SERS substrate purchased from Renishaw Diagnostics (http://www.renishawdiagnostics.com/en/Renishaw-diagnostics--9944). Fig. 9 shows the Raman spectra of (a) 6-mercaptopurine and (b) aldose reductase like protein-1 (ARL-1) protein (68ng/ml) functionalized with 4, 4'-Bipyridine taken from Klarite™ and our 2D Ag arrays (period = 670 nm, hole depth and radius = 380 and 150 nm) by using 633 nm micro-Raman spectrometer (collaborated with Dr. Shen Chuanlai from Department of Microbiology and Immunology, School of Medicine, Southeast University, Nanjing). Apparently, the overall intensities of two target analytes obtained from our substrate are higher than that from Klarite™, indicating superior performance. More importantly, the detection of 68 ng/ml ARL-1 proteins by our arrays presents a feasible method that goes beyond the regular detection limit given by Enzyme-linked immunosorbent assay (ELISA).

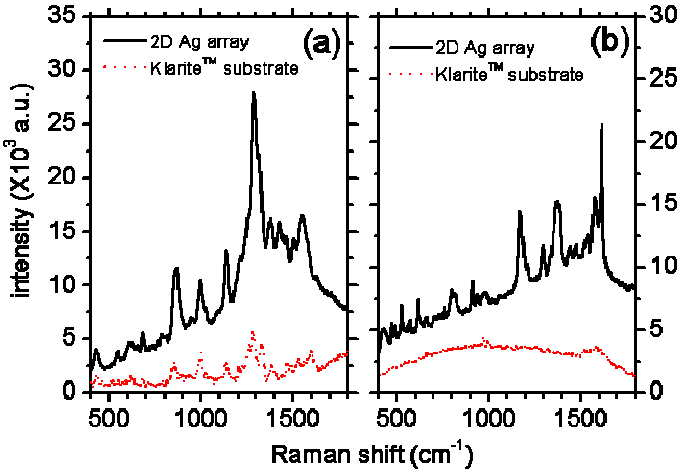

Fig. 9. The Raman spectra of (a) 6-mercaptopurine and (b) ARL-1 protein functionalized with 4, 4'-Bipyridine taken from Klarite™ (dash lines) and our 2D Ag arrays (solid lines) by using a 633 nm micro-Raman spectrometer. Apparently, our arrays show much stronger SERS intensities.

4. PUBLICATION AND AWARDS

Please list out and number all the publications produced under the funded project. All these publications must be directly acknowledged the SHIAE funding support and stated the affiliation with the Institute. The list can be numbered in alphabetic order. When referring to them for the submission in CD, name the file with corresponding reference number in square brackets as "81150xx-Pub[1].pdf".

1. J. Li, H. Iu, J.T.K. Wan, H.C. Ong, The plasmonic properties of elliptical metallic hole arrays, Applied Physics Letters, American Institute of Physics, 94, 03101 (2009).

2. J. Li, H. Iu, D.Y. Lei, J.T.K. Wan, J.B. Xu, H.P. Ho, M.Y. Waye and H.C. Ong, Dependence of surface plasmon lifetimes on the hole size in two-dimensional metallic arrays, Applied Physics Letters, American Institute of Physics, 94, 183112 (2009).

3. C.Y. Chan, J. Li, J.B. Xu, and H.C. Ong, The dependence of surface enhanced Raman scattering on the groove size of one-dimensional metallic gratings, Materials Research Society Spring Meeting, San Francisco, April (2009).

4. K.C. Hui, J.T.K. Wan, J.B. Xu and H.C. Ong, Dependence of anisotropic surface plasmon lifetimes of two-dimensional hole arrays on hole geometry, Appl. Phys. Lett. 95, 063110 (2009).

5. J. Li, J.B. Xu, and H.C. Ong, Hole size dependence of forward emission from organic dyes coated with two-dimensional metallic arrays, Appl. Phys. Lett. 94, 241114 (2009).

6. D.Y. Lei, J. Li, A.I. Fernandez-Dominguez, H.C. Ong, and S.A. Maier, Geometry dependence of surface plasmon polariton lifetimes in nanohole arrays, ACS Nano 4, 432 (2010).

7. C.Y. Chan, J.B. Xu, M.Y. Waye and H.C. Ong, Dependence of surface enhanced Raman scattering (SERS) from two-dimensional metallic arrays on hole size, Appl. Phys. Lett. 96, 033014 (2010).

8. C.Y. Chan, H.C. Ong, J.B. Xu, and M.Y. Waye, Angle-resolved surface enhanced Raman scattering" Springer (in press).

RESEARCH ON LANGUAGE AND BRAIN WAVES

Principal Investigator: Prof. William S-Y. WANG [1]
Co-Investigator (if any): N/A

Research Team Members: James W. Minett, Dr. [1], Gang Peng, Dr. [1], Lan Shuai, Dr. [1], Hong-Ying Zheng, Dr. [1] Ying Wai Wong, Mr. [2]
[1] Department of Electronic Engineering
[2] Centre for East Asian Studies

Project Start Date: 1st July 2008
Completion Date: 31th July 2010

ABSTRACT

Language is a fundamental aspect of everyday life without which exchange of information between people and accumulation of knowledge across generations would not be possible. Yet, we know very little about how language is implemented in the brain. The central goal of this project is to understand the biological bases of language via observations of brain activities using electroencephalography (EEG), i.e., brain waves, and behavioral experiments, with particular focus on the brain mechanisms of two distinctive features of Chinese language: lexical tones and Chinese characters.

1. OBJECTIVES AND SIGNIFICANCE

We design our EEG experiments with the following objectives:

- To investigate the neuropsychological bases of language processing
- To study the influence of language on the brain
- To examine the influence of language experience on auditory (lexical tones) and visual (Chinese characters) perception
- To harness brain activities to assist communication

We anticipate that this project will shed light on the neuroscience of human language, particularly of Chinese, as current studies being done in most other laboratories are based, in general, on European languages [references a-f]. Toward this goal, we will focus on the distinctive features of Chinese, including Mandarin and Cantonese, such as its use of a morphosyllabic writing system (Chinese characters), and the use of voice pitch to distinguish lexical meanings (lexical tones) [references g-j].

2. RESEARCH METHODOLOGY

We used both behavioral and electro-physiological approaches to investigate our target problems. One of our main research tools was a 128-channel EEG System (GES 250) manufactured by Electrical Geodesics, Inc. In the later stages of the project period, we switched to using an ActiveTwo EEG system manufactured by Biosemi B.V., which comprises a set of 32 active electrodes for signal acquisition.

Figure 1. Our EEG system recording the brain waves of a participant.

Participants of our experiments were given simple linguistic tasks, such as reading characters or sentences and identification of auditorily presented lexical tones. During the electrophysiological experiments, an array of electrodes was placed on the participant's head to measure changes in

electrical potential at various locations on the scalp (see **Error! Reference source not found.**). The measured EEG signal is believed to reflect, in part, the summed activities of pyramidal neurons in different layers of the cortex that are active during the performance of particular cognitive tasks [reference e].

The brain waves that are elicited by these tasks also contain noise of different kinds, such as spontaneous, task-irrelevant brain activities, changes in electrical potential due to muscle movements, and interference from the external environment. To enhance the signal-to-noise ratio, event-related brain potentials (ERPs, from which the dependent variables of a study are obtained) are derived by time-locking EEG segments to the onset of events that trigger certain cognitive processes, after which averaging can be done across experimental trials as well as across subjects.

3. RESULTS ACHIEVED

During the project period, six papers were submitted to leading international journals in the area of language and cognition [1-6], of which five have been accepted or published [1-4]. A further four papers are currently being written up for submission [7-10]. Moreover, two books on language and the brain edited by the P.I. and team members were published [11, 12]. SHIAE is duly acknowledged in all these publications. In addition to the above publications, our research has been publicized in public lectures by the P.I. [15-18], as well as by team members at various conferences [13, 14].

These papers can be summarized into three aspects: cross-linguistic studies of language processing, hemispheric lateralization patterns of language processing, and brain-computer interfaces.

3.1 Cross-linguistic Studies of Language Processing

Cross-linguistic studies have shown that long-term language experience affects how humans perceive and interpret the world [reference h, j-n]. Hong Kong Cantonese (HKC) and Putonghua (PTH) are two dialects of Chinese whose speakers have distinct sociolinguistic backgrounds as summarized in Table 1 (replicated from [2]). In this research, we investigated how these sociolinguistic differences affect the production and perception of speech sounds, as well as the perception of written words.

Table 1
Sociolinguistic differences between native Putonghua and Hong Kong Cantonese speakers.

	Mother tongue	Character set	Phonemic coding system	Primary school medium of instruction		Secondary school medium of instruction	
				Spoken	Written	Spoken	Written
PTH speakers	Putonghua	Simplified	*Pinyin*	Putonghua	Chinese	Putonghua	Chinese
HKC speakers	Cantonese	Traditional	None[a]	Cantonese	Chinese	Cantonese; some English	Chinese; some English

[a] Note that a phonemic coding system – *The Linguistic Society of Hong Kong Romanization Scheme*, more commonly known as *Jyutping* – for Hong Kong Cantonese does exist, but it is not in widespread use (Lun, S. C. (2008). The road of Jyutping (Cantonese Romanization) in Hong Kong and its social implications and applications. *Sociolinguistics Symposium: Micro and Macro Connections*, Amsterdam, The Netherlands, 3–5 April, 2008).

An earlier work done by our team members reported that HKC and PTH have different distributions of tonal space [reference o], with HKC having more tones (six tones, without consideration of speech duration) than PTH (four tones, without consideration of the neutral tone). Therefore, even though the tonal contours of a syllable can physically vary continuously, native speakers of PTH and HKC perceive the continuum as different series of discrete categories. These discrete categories induce *categorical perception* along the continuum [reference p]. Categorical perception refers to the phenomenon that when a speaker is asked to discriminate pairs of stimuli, his performance for pairs that cross a category boundary is much better than for within-category pairs. In both the behavioral [3] and electrophysiological [4] experiments conducted in the project, our results suggest that differences in tonal inventory affect the categorical perception of the same tones (level and rising) by native speakers of each language. Paper [3] investigates the factor of tonal inventories

(HKC vs. PTH), as well as the factor of tone language vs. non-tone language (German vs. Chinese), on categorical perception of different pitch contours. We confirm that nontone-language-speaking subjects exhibit only psychophysical boundaries, whereas tone-language-speaking subjects exhibit linguistic boundaries [reference g]. Moreover, we find these linguistic boundaries are further shaped by different tone inventories. Paper [4] is a follow-up study to paper [3] that investigates the factor of tonal inventories and the factor of speech and nonspeech on perception of pitch contours. By using both behavioral and EEG experiments, we report how the experience of different tonal inventories affects the perception of lexical tones and nonspeech pitches at both the behavioral and brain mechanism level.

While Papers [3] and [4] both target the tonal inventory of HKC and PTH, Papers [5] and [7] examine other aspects of speech processing. The acoustic properties of vowels were examined in Paper [5] to investigate the distribution of vowel spaces in these two dialects. Paper [7] investigates the relationship between syllabic rates and intelligibility of Chinese speech as compared to English which was reported earlier [reference q].

Spoken language is encoded in written language using graphemes. Two character sets are commonly used in written Chinese: Traditional characters, which are now used in Hong Kong, Macau, Taiwan, and some other Chinese-speaking communities around the world, and Simplified characters, which are now used in Mainland China, Singapore and Malaysia. The Simplified characters were designed with fewer strokes than their Traditional counterparts with the aim of making the task of learning the written language easier. The two character sets nevertheless share a subset of characters that have identical forms in each set, and which are therefore familiar to all literate Chinese individuals. Paper [2] investigates the brain's response to this subset of Chinese characters as well as to non-characters (the latter formed by adding or removing strokes from real characters). We find a systematic difference in the brain waves of native speakers of PTH and native speakers of HKC, suggesting that cultural difference, particularly differences in language experience, can bring about differences in cognition.

3.2 Hemispheric Lateralization of Language Processing

In the social sciences, there is a famous hypothesis—the Sapir–Whorf Hypothesis. The Whorf hypothesis states that the way people think is strongly affected by their native languages [reference r]. Moreover, the nature of neural organization predicts that if language affects perception, it will do so more in left hemisphere of the brain than in the right hemisphere [reference s]. Paper [1] investigates the brain mechanisms related to the lateralization of color perception using functional magnetic resonance imaging (fMRI). Compared with colors from the same lexical category, discrimination of colors from different linguistic categories provokes stronger and faster responses in the left hemisphere language regions. Collaboration among researchers at CUHK, HKU, and Berkeley was enhanced when H-Y. Zheng, a member of our team, spent the Summer of 2008 at Berkeley under the tutelage of Paul Kay, a member of the U.S. National Academy of Sciences. In contrast with Paper [4], which deals with color perception, Papers [8], [9], and [13] investigate hemispheric lateralization of specific language features from different aspects. Paper [8] focuses on the visual domain, and investigates the influence of linguistic experience and word compositionality on hemispheric lateralization during word reading. Papers [9] and [13] focus on the auditory domain, and investigate the influence of pitch features, as well as speech versus non-speech mode, on the hemispheric lateralization of tone perception by measuring brain waves. These studies all shed light on the brain mechanisms that underlie the influence of language on hemispheric lateralization in visual and auditory perception.

3.3 Brain–Computer Interfaces

A brain–computer interface, or BCI for short, is a system that provides a direct channel for communication between the brain and an external device, usually a computer. Typically, BCIs are used to restore functionality that has been lost by some form of disability. In this project, our focus has been on restoring the ability to communicate to individuals who are severely paralyzed. In particular, we have used scalp-recorded EEG signals to as a means to write Chinese characters on a computer, allowing users to communicate with others without speaking, writing, or signing. This system will benefit those patients who have experienced nervous system damage, for example motor

neuron disease or brain-stem stroke, which limits their ability to control voluntary muscle movement, thus preventing them from communicating by conventional means. Papers [10] and [14] describe and provide a performance analysis of a prototype BCI system for encoding and typing Chinese characters on a computer. Paper [6] provides a review of the present status and future directions of research into P300-based BCIs, which currently offer the best performance among assistive communication BCIs.

3.4 Other achievements

The P.I. was awarded two honors during the project period for contributions to the research of language [19, 20]. Moreover, two applications for project funding on relevant research areas stimulated by this project were awarded [21, 22]. Two further research grant applications on relevant research areas were submitted directly after the project period [23, 24].

4. PUBLICATION AND AWARDS

4.1 Peer Reviewed Journal Papers

[1]. W-T. Siok, P. Kay, W.S-Y. Wang, A.H.-D. Chan, L. Chen, K-K. Luk, and L-H. Tan, "Language regions of brain are operative in color perception," *Proceedings of National Academy of Sciences of the United States of America, 106*(20), 8140-8145, 2009.

[2]. G. Peng, J.W. Minett, and W.S-Y. Wang, "Cultural background influences the liminal perception of Chinese characters: An ERP study," *Journal of Neurolinguistics, 23*(4), 416-426. 2010.

[3]. G. Peng, H-Y. Zheng, T. Gong, R-X.Yang, J-P. Kong, and W.S-Y. Wang, "The influence of language experience on categorical perception of pitch contours," *Journal of Phonetics*, doi:10.1016/j.wocn.2010.09.003, in press.

[4]. H-Y. Zheng, J.W. Minett, G. Peng, and W.S-Y. Wang, "The impact of tone systems on the categorical perception of lexical tones: An event-related potentials study," *Language and Cognitive Processes*. doi: 10.1080/01690965.2010.520493 , in press.

[5]. G. Peng, Y.-W. Wong, and W. S-Y. Wang, Comparative formant analysis of the vowels in Cantonese and Mandarin continuous speech. *Journal of the Acoustical Society of America*, under review.

[6]. J.N. Mak, Y. Arbel, J.W. Minett, L.M. McCane, B. Yuksel, D. Ryan, D.Thompson, L. Bianchi, and D. Erdogmus, "Optimizing the P300-based BCI: current status, limitations and future directions," *Journal of Neural Engineering*, under review.

[7]. G. Peng, G-T. Mai, and W.S-Y. Wang, "The intelligibility of speech is modulated by syllabic rates: Evidence from time-compressed speech with periodic insertions of silence," to be submitted to *Phonetica*, under preparation.

[8]. G. Peng and W.S-Y. Wang, "Hemisphere lateralization is influenced by bilingual status and fractionation of word," to be submitted to *Proceedings of the National Academy of Sciences*, under preparation.

[9]. L. Shuai, J. Ho, and W.S-Y. Wang, "Hemispheric lateralization is modulated by tone features: An ERP study on Cantonese tones," to be submitted to *Laterality*, under preparation.

[10]. J.W. Minett, H-Y. Zheng, M. Fong, L. Zhou, G. Peng, and W.S-Y. Wang, "A Chinese Text Input Brain–Computer Interface Based on the P300 Speller," to be submitted to *IEEE Transactions on Neural Systems and Rehabilitation Engineering*, under preparation.

4.2 Books

[11]. W.S-Y. Wang, *Yuyan Yongxian:* Fazhan *yu Yanhua (語言湧現：發展與演化)*, Academia Sinica, 2008.

[12]. J.W. Minett and W.S-Y. Wang (Eds.), *Language, Evolution, and the Brain.* City University of Hong Kong Press, 2009.

4.3 Conference Papers

[13]. L. Shuai, "Tone lateralization is affected by both linguistic roles and physical properties," Paper presented at *The 8th Göttingen Meeting of the German Neuroscience Society*, 2009.

[14]. J.W. Minett, G. Peng, L. Zhou, H-Y. Zheng, and W.S-Y. Wang, "An assistive communication

brain–computer interface for Chinese Text Input," *Proceedings of the Fourth International Conference on Bioinformatics and Biomedical Engineering (iCBBE 2010), June* 2010, Paper 41183, 4 pages.

4.4 Keynote Speeches

[15]. Wang, W.S-Y., Explorations on tones (聲調探索), *International Symposium of Dialects of South-East China (歷時演變與語言接觸：中國東南方言國際研討會)*, Hong Kong CUHK, December 15, 2009.

[16]. Wang, W.S-Y., Information processing by human and by computer: the case of language, *International Conference on Computer Processing of Oriental Languages*, Hong Kong PolyU, March 26, 2009.

[17]. Wang, W.S-Y., Evolution of tones (聲調的演化), *Conference in Evolutionary Linguistics (演化音法學討論會)*, Guangzhou, March 30, 2009.

[18]. Wang, W.S-Y., Recent developments on language learning and the brain, *International Conference on Applied Linguistics and Language Teaching*, Taipei, April 16, 2009.

4.5 Honors

[19]. William Shi-Yuan Wang was awarded an Honorary Professorship by Peking University, China, 2010.

[20]. William Shi-Yuan Wang was awarded the Golden Language Award by Taiwan University of Science & Technology, Taiwan, 2010.

4.6 Funding

[21]. W. S-Y. Wang (PI), "An Assistive Communication Brain–Computer Interface for Traditional Chinese Character Input: the P300 Chinese Speller", *Application for the Innovation and Technology Fund Innovation and Technology Support Programme tier 3.* Awarded September 1, 2009 – February 28, 2011. Grant No.: ITS/068/09.

[22]. G. Peng (PI), "Sensorimotor Adaptation in Speech Production: The Case of Tones", *Application for General Program, National Natural Science Foundation of China*, Awarded January 2011 - December 2013. Grant No.: 11074267.

[23]. W. S-Y. Wang (PI), "Language-dependent and Independent Indices of Dyslexia: Linking EEG and Behavior", *Application has been submitted to the National Institute of Health*, *USA* on October 2010.

[24]. W. S-Y. Wang (PI), "Linguistic Pitch Perception and the Acoustic Density Hypothesis", *Application has been submitted to the General Research Fund (Research Grants Council)* on October 2010.

5. REFERENCES

[a]. Hagoort, P., Hald, L., Bastiaansen, M., and Petersson, K. M. (2004). *Integration of word meaning and world knowledge in language comprehension*. Science, 304(5669):438-441.

[b]. Friederici, A. D. (2002). Towards a neural basis of auditory sentence processing. *Trends in Cognitive Sciences,* 6(2):78-84.

[c]. Kutas, M., and Federmeier, K. D. (2000). Electrophysiology reveals semantic memory use in language comprehension. *Trends in Cognitive Sciences,* 4(12):463-470.

[d]. Penolazzi, B., Hauk, O., and Pulvermüller, F. (2007). Early semantic context integration and lexical access as revealed by event-related brain potentials. *Biological Psychology,* 74(3):374-388.

[e]. Pizzagalli, D. A. (2007). Electroencephalography and high-density electrophysiological source localization. In J. T. Cacioppo, L. G. Tassinary and G. G. Berntson (Eds.), *Handbook of phychophysiology* (3rd ed.). New York: Cambridge University Press.

[f]. Kutas, M., and Hillyard, S. A. (1980). Reading senseless sentences - brain potentials reflect semantic incongruity. *Science,* 207(4427):203-205.

[g]. Wang, W. S.-Y. (1991) Explorations *in Language*. Taipei: Pyramid Press.

[h]. Wang, W. S.-Y. (1976) Language change. *Annals of the New York Academy of Science*, 280:61-72.

[i]. Luo, H., Ni, J.-T., Li, Z.-H., Li, X.-O., Zhang, D.-R., Zeng, F.-G., and Chen, L. (2006). Opposite patterns of hemisphere dominance for early auditory processing of lexical tones and consonants. *Proceedings of the National Academy of Sciences of the United States of America,* 103(51):19558-19563.

[j]. Tan, L.-H., Spinks, J. A., Eden, G. F., Perfetti, C. A., and Siok, W. T. (2005). Reading depends on writing, in Chinese. *Proceedings of the National Academy of Sciences of the United States of America,* 102(24):8781-8785.

[k]. Hot, P., Saito, Y., Mandai, O., Kobayashi, T., & Sequeira, H. (2006). An ERP investigation of emotional processing in European and Japanese individuals. *Brain Research*, 1122(1):171-178.

[l]. Gandour, J. T., Dzemidzic, M., Wong, D., Lowe, M., Tong, Y., Hsieh, L., et al. (2003). Temporal integration of speech prosody is shaped by language experience: An fMRI study. *Brain and Language,* 84(3):318-336.

[m]. Majid, A., Boster, J. S., & Bowerman, M. (2008). The cross-linguistic categorization of everyday events: A study of cutting and breaking. *Cognition,* 109(2):235-250.

[n]. Boroditsky, L., Fuhrman, O., & McCormick, K. (2010). Do English and Mandarin speakers think about time differently? *Cognition, In Press, Corrected Proof*.

[o]. Peng, G. (2006). Temporal and tonal aspects of Chinese syllables: A corpus-based comparative study of Mandarin and Cantonese. *Journal of Chinese Linguistics,* 34(1):134-154.

[p]. Liberman, A. M., Harris, K. S., Hoffman, H. S., & Griffith, B. C. (1957). The discrimination of speech sounds within and across phoneme boundaries. *Journal of Experimental Psychology*, 54(5):358-368.

[q]. Ghitza, O.; Greenberg, S. (2009) On the possible role of brain rhythms in speech perception: intelligibility of time-compressed speech with periodic and aperiodic insertions of silence. *Phonetica*, 66:113–126.

[r]. Kay P, Kempton W (1984) What is the Sapir-Whorf hypothesis? *American Anthropologist* 86:65–79.

[s]. Gilbert, A. L., Regier, T., Kay, P., & Ivry, R. B. (2006). Whorf hypothesis is supported in the right visual field but not the left. *Proceedings of the National Academy of Sciences of the United States of America*, 103(2):489-494.

HYBRID ASSISTIVE KNEE BRACES WITH SMART ACTUATORS

Principal Investigator:
Professor Wei-Hsin Liao [(1)]

Co-Investigators:
Professor Yunhui Liu [(1)]
Professor Ling Qin [(2)]
Professor Kai-Ming Chan [(2)]

Research Team Members:
Mr. Chi Chong Chan, Carl, MPhil student [(1)]
Dr. Jinzhou Chen, Research Associate [(1)]
Mr. Hongtao Guo, PhD student [(1)]
Dr. Lu Liu, Postdoctoral Fellow [(1)]
Dr. Daihua Wang, Postdoctoral Fellow [(1)]
Dr. Zhehua Wu, Research Associate [(1,2)]

[(1)] Dept. of Mechanical and Automation Engineering, CUHK
[(2)] Dept. of Orthopaedics and Traumatology, CUHK

Project Start Date: 1st June 2007
Completion Date: 31th May 2010

ABSTRACT

Exoskeleton systems that can assist disabled people have been investigated in recent years. However, most exoskeletons use DC motors as actuators and batteries as power sources. While a DC motor consumes a lot of power and limits the working time of the exoskeleton, it produces large impedance that would cause discomfort and danger to people. Magnetorheological (MR) fluid is a smart fluid that can change its rheological behavior under applied magnetic field. Rotary devices using MR fluids have the benefits of high torque, good controllability, low power requirement, and safety. In this research, we developed a new MR actuator for an assistive knee brace to provide assistance to the elderly or disabled. The MR actuator consists of a DC motor and an MR brake/clutch. When active torque is desired, the DC motor works and the MR actuator functions as a clutch to transfer the torque generated by the motor to the leg; when passive torque is desired, the DC motor is turned off and the MR actuator functions as a brake to provide controllable passive torque. The prototype of this MR actuator was fabricated and experiments were carried out to investigate the characteristics of the MR actuator. The results showed that the MR actuator is able to provide sufficient torque needed for normal human activities. Adaptive control was proposed for controlling the MR actuator. Experiments of the MR actuator under control were performed to study the torque tracking ability of the system. A testing structure was developed for testing the knee brace with motor/MR actuator. In addition, a new MR fluid based multifunctional actuator was designed, analyzed, fabricated, and tested. It is the first in the world for a single device to have three functions (motor, clutch, and brake).

1. OBJECTIVES AND SIGNIFICANCE

In this project, a new hybrid assistive knee brace will be developed. The idea is to use the MR actuator to provide controllable assistive torque to the knee joint and thus make the knee brace adaptable to the person while interacting with environment. The MR device can function as a clutch or a brake while the motor will be turned on when needed. Comparing with previous leg exoskeletons, the new hybrid assistive knee brace with MR actuator will have the following benefits:

1) Better safety: While functioning as clutch, the MR device transfers the torque generated by the motor to the human body. Using MR device as clutch, the inertia of output shaft can be made very small and low impedance can be achieved, thus the system is much safer than the existing exoskeleton, which assistive torque is directly provided by the motor.
2) Longer working life: While functioning as brake, the MR device can produce large torque while consuming little power. A prosthetic leg using an MR damper powered by a small Li-ion battery can work about 2 days between two charges. For comparison, the RoboKnee can only work 30-60 minutes even the battery used is much larger. MR devices can be much more energy efficient.

The new hybrid assistive knee brace with MR actuator been developed have the following advantages: compact in size, low power consumption, safe, and adaptive. It provides the disabled people with user-adaptive knee braces compared to passive knee braces.

2. RESEARCH METHODOLOGY

The configuration of an assistive knee brace is shown in Fig. 1, where the MR actuator provides assistive torque to help people for their mobility. The main parts of the system include: braces, MR actuator, sensors. The braces include upper brace and lower brace. The upper brace is bound to the upper leg and the lower brace is bound to the lower leg. The lower brace is connected to the foot, and the upper brace is connected to the waist. The braces transfer the assistive torque generated by the actuator to the lower limb. The sensors are used to detect the user's walking condition and estimate the needed assistive torque. Two force sensors are mounted on the front and rear sole of the foot to measure the reaction force from the floor. Two strain gages are mounted on the aft and fore of the lower brace to measure the force acting on the actuator. The torque produced by the actuator can be measured using these strain gages. An angular sensor is to measure the knee joint angle. The knee angular velocity can be derived by differentiation of the angle signal.

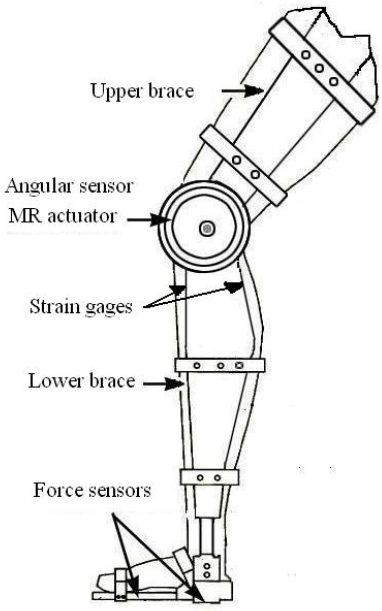

Fig. 1 Configuration of knee brace with MR actuator

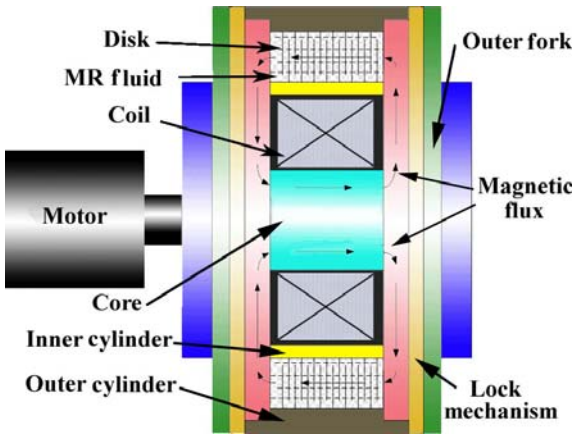

Fig. 2 Schematic diagram of MR actuator

There are three working conditions:

1) The shaft is locked to the lower brace and the magnetic field is on. The MR device acts as a brake, which can provide controllable passive torque.
2) The magnetic field is off. The MR device doesn't work and the knee joint can rotate freely.

3) The shaft is unlocked to the lower brace and the magnetic field is on, while the motor is working. As the shaft is unlocked to the lower brace, the shaft can rotate relatively to the lower leg, thus the MR device acts as a clutch to transfer the torque from the motor to the upper leg.

3. RESULTS ACHIEVED

3.1. Design and analysis of MR actuator

To produce large torque and keep the MR actuator compact in size, the MR actuator utilizes a plurality of interspersed and alternating rotors and stators. The principle of the MR actuator is shown in Fig. 2. It consists of a DC motor, which provides active torque when needed, an outer cylinder, which is connected to the upper leg, MR fluids that are used in shear mode to produce or transfer torque, and an inner cylinder, which is connected to the lower leg. The outer disks (stators) are engaged in outer cylinder; the inner disks (rotors) are engaged in inner cylinder. MR fluids are filled between the outer and inner disks. The shaft is connected to the motor, and the motor is mounted on the lower brace. The shaft can be locked to the inner cylinder, which is connected to lower brace. For the MR actuator, the magnetic field applied to MR fluids determines the on-state torque. Therefore it is important to design an appropriate magnetic circuit. The finite element method (FEM) was used to analyze the magnetic circuit. The magnetic flux density in the MR fluid is between 0.268 T and 0.402 T. Let N = 20, the calculated torque generated by the MR actuator is about 19 Nm.

3.2. Fabrication of MR actuator

A prototype was fabricated. A pair of one-way bearings are used to shift the MR fluids to function between brake and clutch. The lower brace is mechanically communicating with the shaft core through the one-way bearings. At the same time, the lower brace is communicating with the upper brace by normal ball bearings. If no magnetic field is applied to MR fluids, the lower brace can freely rotate respect to the upper brace. If magnetic field is applied to the MR fluids and the knee joint is extending, the one-way bearings are unlocked and torque generated by the motor (which is mounted on the lower brace) can be passed to the upper brace through one-way bearings and MR fluids. If magnetic field is applied to MR fluids and the knee is bending, the one-way bearings are locked so that the MR device functions as brake to provide passive torque.

3.3. Testing of MR actuator

Experiments were carried out in order to investigate the characteristics of the developed MR actuator. Fig. 3 shows the photo of experimental setup. The shaft core of the MR actuator is rotated at a certain speed in one direction by an AC motor through a 10:1 gearbox. Here the MR actuator functions as a clutch. The torque is transmitted from the shaft core to the outer cylinder by applying the current to the coil. In order to measure the output torque of the MR actuator, a load cell (Model 28c02 from PCB Inc.) is mounted on the outer cylinder of the MR actuator, which is fixed on a vibration free table. The MR actuator rotates at a constant speed of 1.4 rad/sec, the output torque is measured by the load cell under a step input coil current of 0.5, 1.0, 1.5, 1.8 A, respectively.

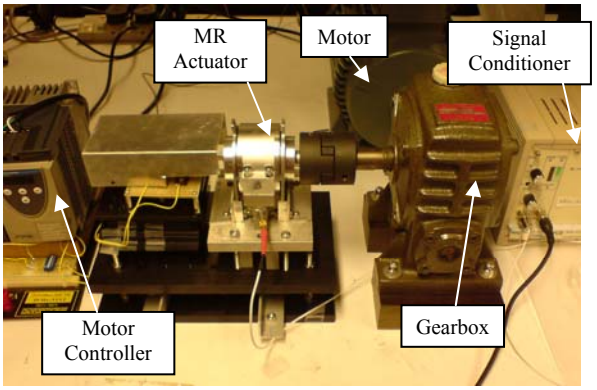

Fig. 3 Photo of the experimental setup

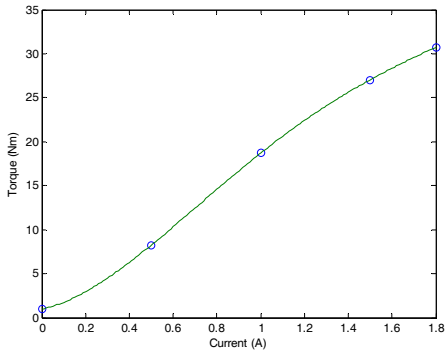

Fig. 4 Output torque versus applied current

Fig. 4 shows the relationship between average torque and applied coil current. We can see that the torque increases as the coil current increases, and when I = 1.8 A, the torque reaches a value of larger than 30 Nm. When the coil current is 1 A, the torque is about 18 Nm, which is close to the calculated torque 19 Nm. The estimated torque of the knee joint during normal walking and standing up is smaller than 20 Nm. Therefore, the torque generated by the developed MR actuator is sufficient for normal activities of knee joint.

3.4. Control of MR actuator

As the MR actuator exhibits nonlinear behaviors and system parameters may vary with time and environment, adaptive control is used to control MR actuator here. Fig. 5 shows the experimental results. It shows that the system has good torque tracking ability under the adaptive control.

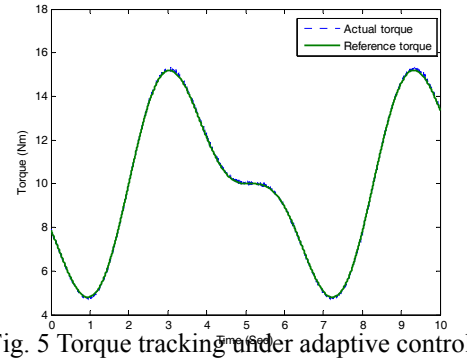

Fig. 5 Torque tracking under adaptive control

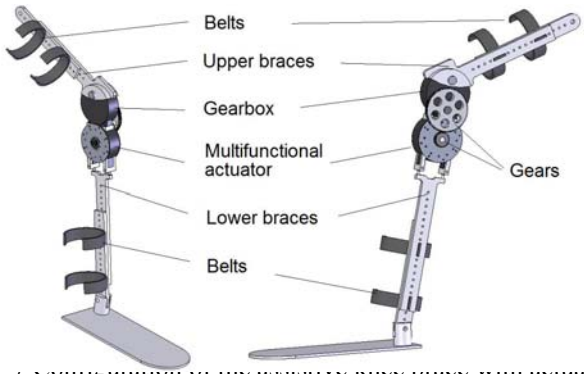

Fig. 7 Configuration of the assistive knee brace with actuator

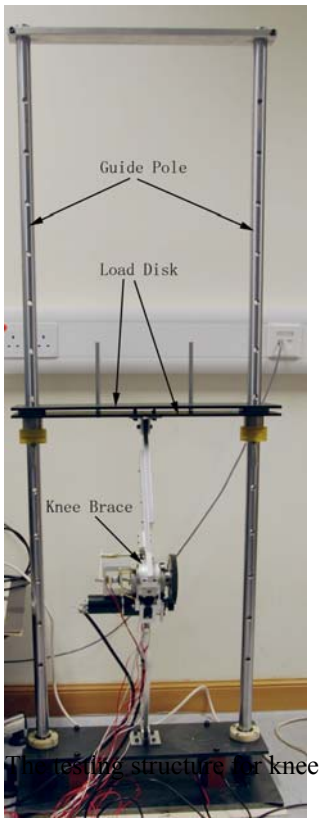

Fig. 6 The testing structure for knee brace

3.5. Testing of knee brace with motor/MR actuator

We developed an assistive knee brace that utilizing this MR actuator together with a DC motor. When active torque is desired, the DC motor works and the MR actuator functions as a clutch to transfer the torque generated by the motor to the leg; when passive torque is desired, the DC motor is turned off and the MR actuator functions as a brake to provide controllable passive torque. Potentiometer and strain gauges were used to detect the position and force information of the knee brace. The knee brace can provide active or passive assistive torque based on the working condition of the knee brace. A testing structure was developed for testing the knee brace (see Figs. 6 & 7). The motion of the knee brace in the testing structure was analysed. Preliminary experiments were carried out and the results showed that this knee brace can provide proper assisting torque as expected. The knee brace with MR actuator was evaluated as compared to that without MR actuator in three aspects: power consumption, performance, and safety.

3.6. Development of multifunctional actuator

The above developed MR actuator with separate DC motor seemed a bit bulky to be used on human body. A more compact, multifunctional actuator is desired for assistive knee braces. Therefore, a new MR fluid based multifunctional actuator used in assistive knee braces was designed and analyzed using finite element method. The influence of permanent magnets on MR fluids was discussed. Modeling of the actuator in different functions was developed. The prototype of the actuator was fabricated and tested. Torques of the motor part and inner clutch/brake part were measured. Braking torque control of the actuator was investigated. Although the measured torque is not high, by adding transmission mechanisms like gearbox or harmonic drive, the torque will be increased while the speed is reduced. With appropriate gear ratio (e.g., 100:1), the actuator would fulfill the requirement of normal walking (about 20 Nm torque). Therefore, the new multifunctional actuator is promising for assistive knee braces.

4. PUBLICATIONS AND AWARDS

[1] J.Z. Chen and W.H. Liao, “Design and Control of a Magnetorheological Actuator for Leg Exoskeleton,” *Proceedings of 2007 IEEE International Conference on Robotics and Biomimetics*, pp. 1388-1393, 15 - 18 December 2007.

[2] J.Z. Chen and W.H. Liao, “Development and Testing of a Magnetorheological Actuator for an Assistive Knee Brace,” *Proceedings of SPIE Conference on Smart Structures and Materials*, SPIE Vol. 6928, 69281G1-12, doi: 10.1117/12.776194, 9-13 March 2008.

[3] J.Z. Chen and W.H. Liao, “Design and Testing of Assistive Knee Brace with Magnetorheological Actuator,” *Proceedings of 2008 IEEE International Conference on Robotics and Biomimetics*, pp. 512-517, 21 - 26 February 2009.

[4] H.T. Guo and W.H. Liao, “Integrated Design and Analysis of Smart Actuators for Assistive Knee Braces,” *Proceedings of SPIE Conference on Smart Structures and Materials: Active and Passive Smart Structures and Integrated Systems 2009*, SPIE Vol. 7288, 72881U1-11, doi: 10.1117/12.815964, 9-12 March 2009.

[5] H.T. Guo and W.H. Liao, “Magnetorheological Fluids Based Multifunctional Actuator for Assistive Knee Braces,” *Proceedings of 2009 IEEE International Conference on Robotics and Biomimetics*, pp. 1883-1888, 19 - 23 December 2009.

[6] H.T. Guo and W.H. Liao, “Design and Control of Multifunctional Magnetorheological Actuators for Assistive Knee Braces,” *Proceedings of SPIE Conference on Smart Structures and Materials: Active and Passive Smart Structures and Integrated Systems 2010*, SPIE Vol. 7643, 764310 (11 pages); doi:10.1117/12.847530, 7-11 March 2010.

[7] J.Z. Chen and W.H. Liao, "Design, Testing, and Control of a Magnetorheological Actuator for Assistive Knee Braces," *Smart Materials and Structures*, Vol. 19, 035029, 2010, doi:10.1088/0964-1726/19/3/035029.

[8] J.Z. Chen and W.H. Liao, "Development and Experimental Evaluation of an Assistive Knee Brace with Magnetorheological Actuator," *Journal of Intelligent Material Systems and Structures*, submitted (under review), 2010.

[9] H.T. Guo and W.H. Liao, "Design and Analysis of a Multifunctional Actuator with Magnetorheological Fluids," *Smart Materials and Structures*, to be submitted.

[10] H.T. Guo and W.H. Liao, "Design and Control of Magnetorheological Actuators for Assistive Knee Braces," *Advancement in Biologically Inspired Robotics*, Invited Book Chapter, to be submitted.

[11] *Magnetorheological Actuator with Multiple Functions*, CUHK Technology Disclosure 09/ENG/318, U. S. Provisional Patent Application, No. 61/202,539, March 11, 2009; *U. S. Patent Application*, No. 12/722,146, March 11, 2010.

[12] J. Z. Chen, *A Magneto-rheological Actuator for Assistive Knee Braces*, Ph.D. Thesis, The Chinese University of Hong Kong, July 2009.

[13] H. T. Guo, *Design and Analysis of Multifunctional Actuators for Assistive Knee Braces*, Ph.D. Thesis, The Chinese University of Hong Kong, August 2010.

[14] C.C. Chan, *Gait Experiments and Analysis for Assistive Knee Braces*, Final Year Project Report, The Chinese University of Hong Kong, May 2009.

[15] H.T. Guo, 2nd Prize of Paper Presentation in the 228th Tsinghua Forum for Doctoral Candidates, November 2009.

[16] *Press Release*, The Chinese University of Hong Kong, 5 January 2010

[17] Newspaper Reports: *Hybrid Assistive Knee Braces with Smart Actuators*, Ming Pao, Singtao Daily, Hong Kong Economic Times, Apple Daily, Oriental Daily, Wen Wei Po, Ta Kung Pao, South China Morning Post, AM 730, Metro, Headline Daily, Sing Pao, Hong Kong Commercial Newspapers, Hong Kong Daily News, 6 January 2010

[18] Interviewed TV Program: *Hybrid Assistive Knee Braces with Smart Actuators*, by RTHK, Shown on TVB-Jade, 12 November 2008

5. REMARKS

Under the support of SHIAE, significant results have been obtained for this project. Besides several conference/journal papers and book chapter that have been published [1-7] and/or under review/in preparation [8-10], one technology disclosure (CUHK 09/ERG/318) was submitted to Technology Licensing Office, CUHK. A US provisional patent application (entitled 'Magnetorheological Actuator with Multiple Functions') has also been filed in March 2009, and the corresponding regular US patent application was filed in March 2010 [11]. A PhD thesis was completed [12] and the other one was submitted in July 2010 [13]. A final year student (currently MPhil student) did excellent work (see report [14]) while participating in this project. A PhD student presented some of the work done for this project and received the 2nd Prize of Paper Presentation in the 228th Tsinghua Forum for Doctoral Candidates [15].

A 'Press Conference' was arranged on 5 January 2010 by Miss Onki Yeung of CINTEC and the Communications and Public Relations Office [16], The Chinese University of Hong Kong. This project was reported in the TV news (TVB-Jade, TVB-Pearl, ATV, and HKBN) on 5 January 2010,

and reported by 14 local newspapers the next day (6 January 2010). The news clippings are provided [17]. Moreover, additional HK$994,554 from Hong Kong Innovation and Technology Commission has just been secured to support the further development on 'Smart Assistive Knee Braces Utilizing MR Fluids' (ITS/308/09, Tier 3). Human trials with more testing and refinement will be carried out in the one and half years to come (1 March 2010 – 31 August 2011).

STUDY ON RF RADIATION EFFECT AND SIGNAL EFFICIENCY OF WIRELESS MEDICAL DEVICES

Principal Investigator:
Prof. Max Q-H Meng [(1)]

Co-Investigator (if any):
Prof. Yuan-Ting Zhang [(1)];
Prof. Ke-Li Wu [(1)] and Justin Wu [(2)]

Research Team Members:
Dr. Lisheng Xu, Postdoctoral Fellow [(1)];
Dr. Xiaona Wang, Research Assistant [(1)];
Dr. Rong Liu, Research Assistant [(1)];
Mr. Hongliang Ren, Ph.D student [(1)]

[(1)] Dept of Electronic Engineering
[(2)] Dept of Medicine and Therapeutics

Project Start Date: 1st May 2006
Completion Date: 31st May 2008

ABSTRACT

In this project, we have systematically studied the radiation effects and communication link performance of Ingested Wireless Devices (IWD) through numerical and experimental techniques. Having analyzed the radiation characteristics of implantable and ingestible exposure sources in 5-year old children, 10-year old children and adults via numerical simulations, we recommend that different transmission power levels should be used for children and adults, respectively. We also studied the variation of radiation efficiency in the bi-directional communication of IWD in relation to the distance between an antenna and a homogenous human trunk. The distance had little influence on communication performance, although the Specific Absorption Rate (SAR) values and port impedances varied significantly in relation to the distance. We also found that the influence of human legs and head on the maximum SARs was negligible and we proposed a human body trunk model for testing the compliance with safety levels. Our simulation studies on the radiation characteristics of IWD showed that the radiation intensity outside the body decreased with frequency. Furthermore, the orientation and position of the IWD, which gave maximum radiation efficiency, was frequency dependent. In addition, we found that the operation frequencies increased from 1.42, 1.0, and 2.2 *GHz* to 1.62, 1.15, and 2.85 *GHz* after the pig's euthanasia within one hour through animal experiments. Our measurement tests further validated the decrease of the dielectric properties of the animal tissues after death. These differences need to be taken into account before the design of ingested antennas. Lots of our further simulation studies demonstrate that variation of radiation intensity near the surface of abdomen are around 1, 1.6 and 2.5 *dB* within 20% variation of dielectric values corresponding to the frequency of 430, 800 and 1200 *MHz*, respectively. An increment up to 20% in dielectric properties always cause a SAR variation less than 7%, 10% and 20% at the frequency of 430, 800 and 1200 *MHz*, respectively.

1. OBJECTIVES AND SIGNIFICANCE

The demand to utilize Radio Frequency (RF) antenna inside a human body has risen for biomedical application. However, the radiation characteristics of implantable and ingestible wireless devices are scarcely studied until recently. Our research in this project provides a better guideline for compliance checking and design of various wireless medical devices, in addition to our work on the optimization

of communication link performance in relation to antenna and medical sensory devices. Furthermore, this project proposed and used a conservative homogeneous body trunk model for efficient estimation of the radiation effects and link performance so that more accurate compliance tests and design on the body-worn and ingestible wireless devices can be achieved. Nor does it stop there; the tests of radiation characteristics of capsule antenna via animal were performed for further validation.

2. RESEARCH METHODOLOGY AND RESULTS ACHIEVED

2.1. Effect of trunk size on electromagnetic radiation from a source inside human body

There have been many investigations on biologic effects in the heads of children and adults. However, investigations on the human body trunk are rarely reported. For assessment of compliance with the safety guidelines, the radiation effects and efficiency of IWDs inside human body trunk models of five-year-old children, ten-year-old children and adult were studied by using developed homogenous models at the frequency of 2.4 *GHz*. The simulation results indicated that the radiation efficiency ranged from –53.39 *dB* to –116.4 *dB* and almost all the radiation power was dissipated in the tissues of the body trunk models. In order to reduce the radiation harm of wireless device while keep the link performance, we recommend using different power levels for children and adults.

2.2. Variation of radiation effects with distance between RF source and trunk model

We analyzed the variation of biological effects and signal efficiency with distance between electromagnetic source and human body model. The SAR distributions and electric fields for various vertical and horizontal slices of the human trunk were calculated, showing that distance had little influence on signal efficiency within the range of $\lambda/2\pi$. Considering the radiation efficiency of wireless devices and safety guidelines for radiation exposure, we recommend that body-worn antenna should be kept at a suitable distance (i.e., 12 *mm*) from human body.

2.3. Electromagnetic radiation characteristics from ingested sources inside the human intestine

The widespread use of IWD during the past few years has attracted a great deal of social and scientific concerns about RF exposure. As IWD could travel and rotate at any direction in GI tract, we only selected seven positions in small intestine as illustrated in Fig. 1. Figs. 1 (a)-(b) illustrate one sagittal slice and one transverse slice of the body model. The human body model was constructed from visible human body data and the electric characteristic data of human biological tissues were referred to international published results.

Figs. 2(a)-(d) demonstrate the near-field intensities of a XY planar slice both inside and outside the human body model when the IWD is positioned at C with X orientation at frequencies of 430 *MHz*, 800 *MHz*, 1.2 *GHz*, and 2.4 *GHz*, respectively. The near field outside the human body is symmetric along X-axis at the frequency of 430 *MHz*. However, the pattern becomes irregular when frequency increases. The electric fields in anterior part of the human body are higher than those in the posterior. The far electric fields decrease greatly with frequency, while the number of side lobes of the far field increase with frequency.

(a) (b)

Fig. 1. Simulation configuration. (a) Sagittal slice of human model; (b) Transverse slice of human model. C, F, B, T, M, L and R are the center, anterior, posterior, superior, inferior, left lateral and right lateral position of the abdomen area, respectively.

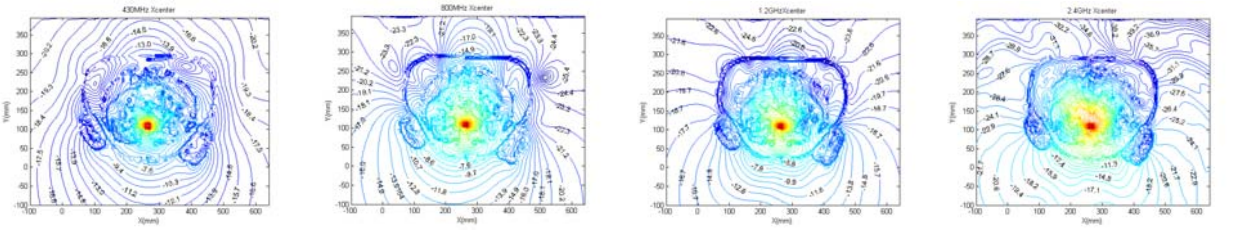

(a) (b) (c)

(d)

Fig. 2. Near fields of XY planar slice (where Z=1000 *mm*) in decibels for ingested wireless source at position of C with X orientation. (a) 430 *MHz*; (b) 800 *MHz*; (c) 1.2 *GHz*; (d) 2.4 *GHz*.

2.4. Influence of head and legs on the realistic human body model simulation

In this project, we studied the influence of head and legs on the signal efficiency and found that both head and legs could influence the distributions of electric fields and SAR, but rather insignificantly. The electric fields distribution along the human body horizontal slices nearly superposes with that along the human body without legs and head. The influence on the electric filed in human body is less than the external electric field. The simplified human body model without head and legs can be used as a reference for testing the safety compliance of body-worn, implantable, and ingestible medical devices.

2.5. Suitability of using homogeneous phantom for compliance testing

The suitability of homogeneous trunk phantoms for RF compliance testing of wireless medical devices was studied at the 900 *MHz* frequency band using simplified homogeneous phantom and anatomical human body models. The simulation results demonstrated that a homogenous representation of human body was suited for assessing the averaged SARs in human body and confirmed that the local energy absorption details still need to be analyzed by using anatomical models or by combining with the worst-case consideration.

2.6. Influence of Anesthetic and Dead Pig Body on Ingested Wireless Device

For the *in situ* measurement of the radiation characteristics of IWD in animal, three designed capsule antennas were surgically embedded in small intestine of an adult female pig. We selected two positions (the superior and inferior positions) in the intestine of the pig for analyzing the influence of the position on the radiation characteristics of the ingested capsule antenna, illustrating in Fig. 3. The middle-line incision was cut paralleling to the cranial-caudal line. These two positions located at two sections of small intestine parallel to the cranical-caudal line, 8 *cm* below the surface of the pig's skin. Three capsules with printed monopole antennas were placed by an experienced surgeon from the incision into the two positions of the intestine, respectively. The orientations in this experiment were parallel to X-axis in order to keep the constant position for different measurements when the pig was anesthetic and after euthanasia within one hour. The accuracy of the position for the different capsules can be controlled within 5 percent. We found that the frequencies increased greatly from 1.42, 1.0 and 2.2 *GHz* to 1.62, 1.15 and 2.85 *GHz* after the pig's euthanasia within one hour when the antennas were put in the superior position of the intestine. The frequencies increased from 1.5, 1.03 and 2.3 *GHz* to 1.67, 1.13 and 2.8 *GHz* when the antennas were put in the inferior position after its euthanasia within one hour. Our measurement results further validated the decrease of the dielectric properties of the animal tissues after death. These differences need to be taken into account in electromagnetic modeling.

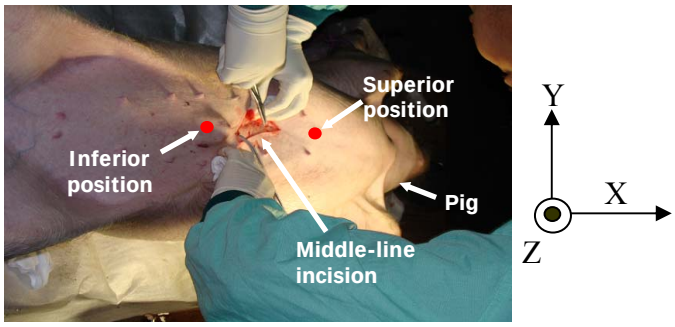

Fig. 3. Configuration of animal experiment.

2.7. Effects of dielectric parameters of human body on SAR for ingestible wireless device at operating frequencies 430, 800 and 1200 MHz

We analyzed the influence of dielectric properties of human body tissues on radiation characteristics of IWD placed in small intestine at the operation frequencies of 430, 800 and 1200 *MHz* with X, Y and Z orientations. As demonstrated in Table I, the input impedance increases as the conductivity increases. The image part of the input impedance increases with relative permittivity, while the real part of input impedance decreases with the increment of relative permittivity. Both the female and male body models confirm these findings.

Fig. 4 demonstrates the calculated SAR values as bar graphs in percentage, each corresponding to a scenario of increased dielectric parameters. The variations of maximum of un-averaged and averaged SARs are less than 7%, 10% and 20% when the conductivities and permittivities of human body tissues increase up to 20% at the frequency of 430, 800 and 1200 *MHz*, respectively. When the conductivities increase, the maximum of averaged and un-averaged SAR values will increase. When the relative permittivity increases, the maximum of SAR usually decreases. In the near-field radiation of IWD, the peak-to-average value of SAR is typically larger than the ratio in the radiation from cell phone. Therefore, the high-local RF energy deposition in human body needs to be considered carefully even though the input power of IWD is low. The intensity of electric field has 1, 1.5 and 2.5 *dB* variations when dielectric parameters increased within 20% at the frequency of 430, 800 and 1200 *MHz*, respectively. This study also shows that the same increment in dielectric values in female and male body models resulted in mostly same variations of SAR and electric field even though their SARs and electric field distributions were different at same dielectric values. These results suggest that some estimation on the dependence of the calculated radiation characteristics of IWD and the SARs in human body on the variability in dielectric values of surrounding human body tissues should be determined.

TABLE I. SAR_{peak}, maximums of SAR_{1g} and SAR_{10g} in the female and male body models, and the impedances of the IWD which was placed in center position at X orientation with the delivered power of 25 *mW* at the frequency of 800 *MHz*.

Model	Dielectric Parameter	Maximum of SAR [W/kg]			Impedance [Ohms]
		Un-averaged	1-g	10-g	
800 MHz Female Body X Orientation Center	Original	43.31	3.90	0.76	44.2+j15.3
	+5%σ	43.76	3.94	0.77	45.9+j15.9
	+10%σ	44.19	3.97	0.77	47.6+j16.5
	+20%σ	44.46	3.99	0.75	51.4+j17.4
	+5%ε	43.34	3.87	0.75	42.4+j22.0
	+10%ε	43.35	3.85	0.75	40.6+j28.4
	+20%ε	42.67	3.74	0.72	38.0+j39.2
	+5%σ&+5%ε	42.77	3.75	0.73	39.8+j39.2
	+10%σ&+10%ε	43.63	3.87	0.75	44.2+j28.7
	+20%σ&+20%ε	44.68	3.91	0.75	43.4+j41.1
	Original	18.94	2.24	0.64	30.1-j23.1

800 MHz Male Body X Orientation Center	+5%σ	19.13	2.28	0.65	31.1-j22.8
	+10%σ	19.37	2.39	0.66	32.0-j22.4
	+20%σ	19.63	2.37	0.68	33.7-j21.6
	+5%ε	18.78	2.20	0.63	28.8-j20.1
	+10%ε	18.32	2.14	0.61	27.8-j17.0
	+20%ε	17.57	2.03	0.58	26.1-j11.2
	+5%σ&+5%ε	18.21	2.06	0.58	27.2-j11.4
	+10%σ&+10%ε	18.79	2.21	0.63	29.5-j16.4
	+20%σ&+20%ε	18.48	2.18	0.67	28.9-j10.2

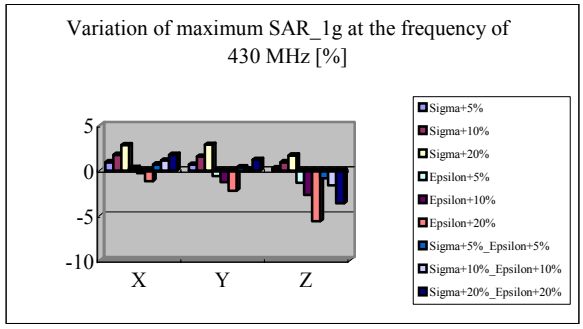

Figure 1.

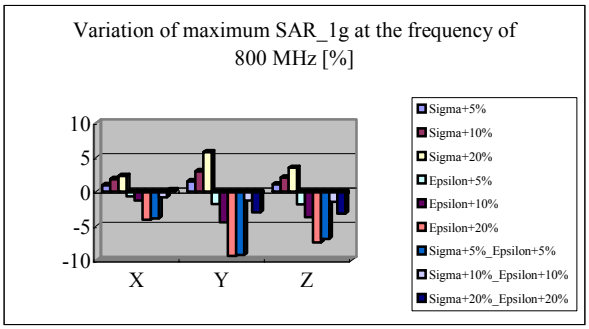

Figure 2. (a)

(b)

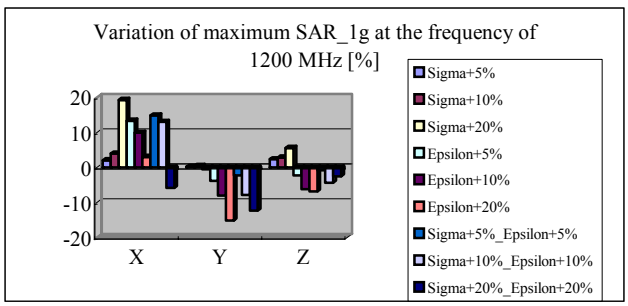

Figure 3.

Figure 4. (c)

Figure 5. Fig. 4. Variations of the maximum of averaged-1g SAR in the female body model with different dielectric properties. (a) at the operation frequency of 430 *MHz*; (b) 800 *MHz*; (c) 1200 *MHz*.

3. PUBLICATION AND AWARDS

[1] L.S. Xu, Max Q.-H. Meng and H.L. Ren, "Effect of Subject Size on Electromagnetic Radiation from Source in Human Body Following 2450MHz Radio Frequency Exposure," in *Proc. of the 2007 IEEE International Conference on Integration Technology*, pp. 326-329, March 20-23, 2007.

[2] L.S. Xu, Max Q.-H. Meng and H.L. Ren, "Variation of Radiation Effects and Signal Efficiency with Distance between Electromagnetic Source and Trunk Model," in *Proc. of the 29th International Conference of the IEEE Engineering in Medicine and Biology Society*, pp. 1184-1187, August 22-26, 2007.

[3] H.L. Ren, Max Q.-H. Meng, L.S. Xu, and X. Chen, "Radio Efficiency Evaluation of a Body Sensor Platform," in *Proc. of the 2007 IEEE/ASME International Conference on Advanced Intelligent Mechatronics*, ETH Zrich, Switzerland, September 4-7, 2007.

[4] L.S. Xu, Max Q.-H. Meng and H.L. Ren, "Electromagnetic Radiation from Ingested Sources in the Human Intestine at the Frequency of 2.4GHz," in *Proc. of the 23rd Progress In Electromagnetics Research Symposium*, pp 893-897, Hangzhou China, March 24-28, 2008.

[5] L.S. Xu, Max Q.-H. Meng and H.L. Ren, "Applicability of Homogeneous Human Trunk Phantom in Estimating the Radiation Characteristics of Body-worn Devices," *International Journal of Information Acquisition*., 5(1): 65-82, March 2008.

[6] L.S. Xu, Max Q.-H. Meng Y.W. Chan, C. Hu and H.B. Wang, "Influence of Anesthetic and Dead Animal Bodies on Ingested Wireless Device," in *Proc. of IEEE/ASME International Conference on Advanced Intelligent Mechatronics*, Xi'an China, pp. 176-180, July 2-5, 2008.

[7] L.S. Xu, Max Q.-H. Meng, H.L. Ren, Y.W. Chan, "Radiation Characteristics of Ingested Wireless Device at Frequencies from 430 MHz to 3 GHz," in *Proc. of the 30th Annual International Conference of the IEEE Engineering in Medicine and Biology Society*, Vancouver, Canada, pp. 1250-1253, August 20-24, 2008.

[8] L.S. Xu, Max Q.-H. Meng, H.L Ren, and Y.W. Chan, "Radiation Characteristics of Ingestible Wireless Devices in Human Intestine at Frequencies of 430 MHz, 800 MHz, 1.2 GHz and 2.4 GHz," *IEEE Transactions on Antennas and Propagation*, 2008, In Minor Revision.

[9] L.S. Xu, Max Q.-H. Meng and H.L. Ren, "Radiation Characteristics of 2.4 GHz Ingestible Wireless Devices in Human Intestine," Submitted to *International Journal of Medical Systems*.

[10] L.S. Xu, Max Q.-H. Meng and H.L. Ren, "Effects of Dielectric Parameters of Human Body on Radiation Characteristics of Ingestible Wireless Device at Operating Frequency of 430 MHz," Submitted to *IEEE Transactions on Biomedical Engineering*.

[11] L.S. Xu, and Max Q.-H. Meng, "Effects of Dielectric Parameters of Human Body on SAR for Ingestible Wireless Device at Operating Frequency of 430 MHz," Submitted to *2009 IEEE International Conference on Robotics and Automation*, May 12-17, 2009, Kobe, Japan

[12] L.S. Xu, and Max Q.-H. Meng, "Effects of Increase in Dielectric Values of Human Body on Specific Absorption Rate (SAR) Following 430, 800 and 1200 MHz radio Frequency Exposure to Ingestible Wireless Device," Submitted to *IEEE Transactions on Information Technology in Biomedicine*, 2008

PHOTONIC BIOSENSOR MICRO-ARRAYS FOR MOLECULAR DIAGNOSTICS APPLICATIONS

Principal Investigator: Prof. Aaron Ho-pui HO [(1)]
Co-Investigator: Prof. Siu-kai Kong [(2)]

Research Team Members: Chi-lok Wong , Research Assistant [(1)]
Shu-yuen Wu, Research Assistant [(1)]
Wing-wai Wong, Research Assistant [(1)]
Wu Yuen, Research Student [(1)]
Rebecca K.Y. Li, Research Student [(2)]

[(1)] Department of Electronic Engineering, CUHK
[(2)] Department of Biochemistry, CUHK

Project Start Date: 1st May 2006
Completion Date: 30th April 2008

ABSTRACT

This project aims to develop a novel surface plasmon resonance (SPR) photonic biosensor array platform that offers parallel detection of a range of biomolecular species without the use of any labeling procedures, thus drastically reducing the cost of performing such tests in a clinical environment. The project involves first experimentally demonstrating the feasibility of the new approach, then followed by the development of high detection resolution biosensor arrays for biomarkers and DNAs through analyzing the phase-signals associated with the pixels within a SPR image. Within this work we have also explored working on developing DNA detection capability. Within this work, we have also explored a new cross-polarization detection approach for further improvement of sensing resolution.

1. OBJECTIVES AND SIGNIFICANCE

The objectives of this project are:

- To develop a photonic biosensor platform in which micro-arrays of sensor sites can provide parallel identification for a range of molecular species that are of relevance to diagnostics applications.
- To establish this micro-array platform as an enabling technology for other photon-based or molecular techniques, through which important multi-lateral information on the immobilized target biomolecules may be collected.

The significance of this project is in field of biochips for diagnostics applications. Common biochips containing arrays of protein or DNA markers are being used as diagnostic devices for screening a variety of health-related molecular properties. The detection strategy has been based on chemiluminescence, i.e. emission of light upon detecting the presence of the target protein. However, this technique requires a proprietary process of inserting florescent label tags to the protein molecules. The reagents are extremely costly. In addition, the amount of chemiluminescence rapidly deteriorates as the detection process continues, thus making it difficulty for this technique to provide quantitative information. In this project, we propose to use the SPR technique for detecting the target biomolecules without having to use any florescence. The advantages are two-fold. First, removing the need of chemiluminescence will bypass any need of expensive proprietary biomolecule species. Second, SPR is a real-time quantitative technique that provides accurate measurement on the concentration of the target biomolecules. Despite these important attributes, chemiluminescence has

been generally preferred by the market because it offers relatively better detection sensitivity, which is a more important factor with regard to diagnostics products.

2. RESEARCH METHODOLOGY

2.1. Novel Optical Interferometer Design for High Resolution Optical Phase Detection

Surface plasmon resonance (SPR) is a phenomenon whereby a beam of light impinging at a glass-metal (typically gold) interface may induce oscillatory motion from the free electrons in the metal. This effect is extremely sensitive to refractive index changes, such as those caused by immobilization of biomolecular species on the gold surface. Hence, SPR has been under intense investigation as a sensing technique for biomolecular interactions.

This project involves the implementation of a SPR imaging system that can perform SPR phase analysis on a 2-dimensional scale, thus achieving arrayed biosensing detection. The optical instrumentation is built from the two differential phase SPR biosensor setups previously reported by the project PI for achieving high resolution refractive index measurements (see Figures 1 and 2).

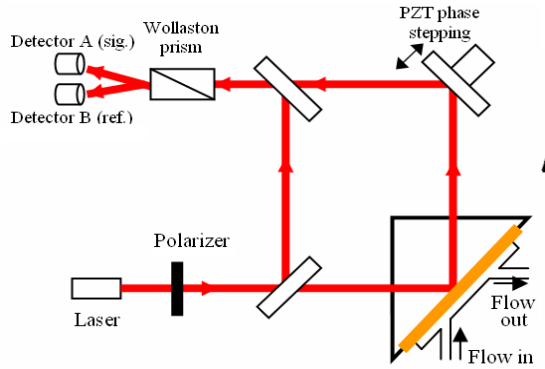

Figure 1. Self-balanced Mach-Zehnder differential phase SPR sensor

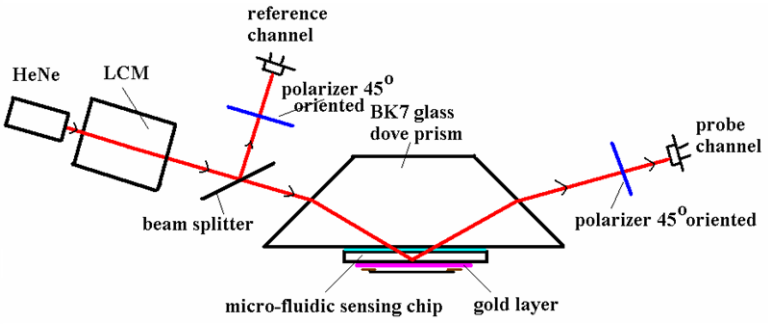

Figure 2. Single-beam self-referenced differential phase SPR sensor

The basis of our so-called “differential phase” technique hinges on the fact that when we operate two interferometers in the same optical system for the s- and p-polarizations, the SPR phase can be extracted by direct comparison of the phase readings produced by the two interferometers. The self-balancing or noise cancellation benefit comes from the fact that since all signals come from a single optical source and the interferometers traverse identical paths, phase subtraction between the two interferometers will result in zero fluctuations except for those generated from the SPR effect.

2.2. Development of Imaging SPR Capability for Biosensor Arrays Applications

The second important element of the proposed setup is the image analysis algorithm for extracting the SPR phase value for each pixel within the inteferograms. As depicted in Figure 3, the image analysis procedures involve first capturing a long sequence of video frames while the reference interference path is being periodically shifted, then followed by frame averaging, Fast-Fourier-Transform, narrow-band filtering for noise removal, and finally phase extraction through monitoring the time evolution of the signal intensity for each pixel.

2.3. Development of Biosensor Arrays

The biosensor arrays will be manufactured using standard spotting techniques through which small circular spots of the buffer solution containing the conjugate of the target antigen will be allowed to dry on the gold-coated. In this way, one can readily achieve having a variety of antigen species spotted on a single SPR biosensing surface. For the present project, we shall use biomarkers extracted by our collaborating partners from CUHK's medical school. Upon flowing the analyte sample into the detection chamber, the target antigen molecules, if they are present, will be immobilized to the sensor surface and result in a change in SPR phase.

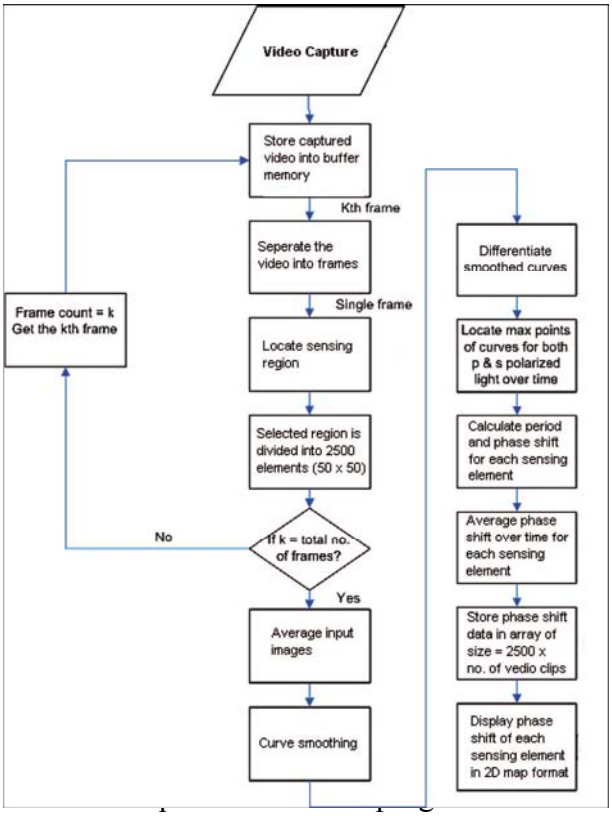

3. RESULTS ACHIEVED

3.1. SPR Phase Imaging with High Detection Resolution

During the first phase of this project a software programme has been developed for accurate phase extraction from SPR images, and we have successfully demonstrated its operation on biosensor arrays based on SPR phase imaging. Based on results obtained from using salt solution samples in a 10-element array setup, the experimental detection resolution was first found to be 4×10^{-5} refractive index unit (RIU). We used a Mach-Zehnder interfermeter setup as shown in Figure 1. Subsequently the system had been used for performing arrayed detection of BSA antigen-antibody binding reactions. Moreover, as the system underwent continuous improvement through extensive experimental efforts and better software signal processing, we have also significantly improved the detection threshold during the course of this project.

As the main aim of this project is to detect practical biomolecular species, among which the DNA molecules are of the highest importance. However, because of their low molecular weight, non-labeled detection of DNA using SPR has been a well-known major challenge within the SPR instrumentation community. To this end, our effort has been concentrated on developing image analysis algorithms for obtaining SPR phase distribution on a 2-dimensional scale. We have also tested the importance of using different imaging devices.

As shown in Figure 4, experimental results indicate that when we use a large number of pixels within the SPR phase image for calculating each phase data point, the measurement standard deviation (SD) decreases accordingly. In our case, a best result of SD = 0.019 degree has been achieved by using 50×50 pixels, which corresponds to a sensing resolution of $\sim 10^{-7}$ RIU. We believe that such a resolution should be sufficient for detecting DNA binding activities.

Figure 5 shows the effect of phase imaging frame rate on the measurement accuracy of the SPR phase. Higher frame rate will substantially improve the SPR phase accuracy. This is due to the fact that a more smooth sine wave extrapolation can be obtained if we use more dense data points within the intensity waveform generated during phase-stepping.

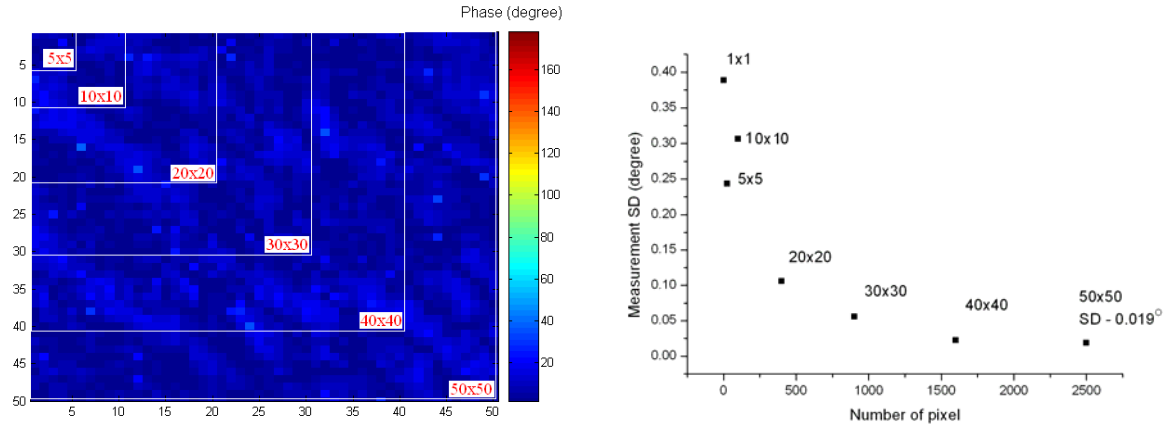

(a) (b)

Figure 4. Measurement of SPR phase standard deviation (SD) from a 2-dimensional sensor surface in contact with water over a period of 40 minutes. The SPR phase SD decreases with increasing number of pixel included in the SPR phase extraction region.

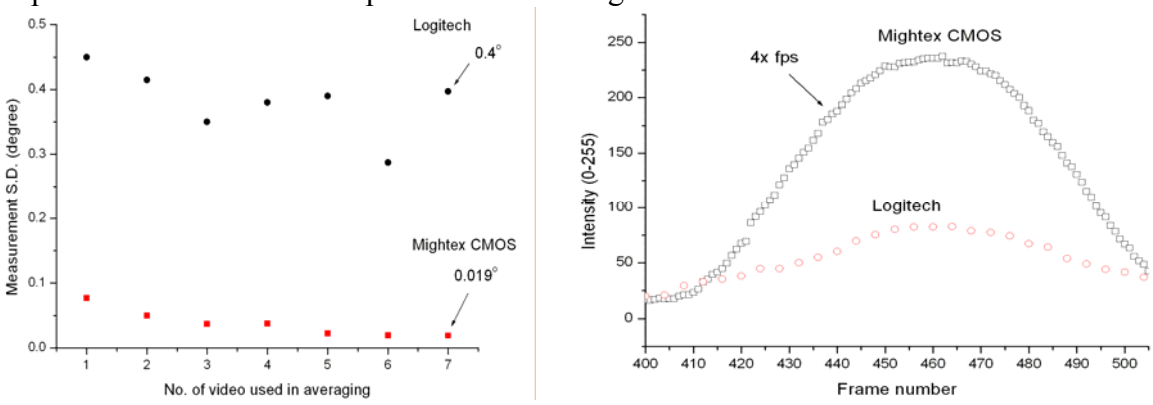

(a) (b)

Figure 5. SPR phase SD comparison between Mightex (120fps) and Logitech (30fps) cameras. Mightex provides >20 times improvement in SD from 0.4 to 0.019 degree.

3.2. Antigen-antibody Detection using SPR Sensor Arrays

The system built for this project has been shown to be capable of performing real-time SPR phase monitoring of biosensor arrays. The system was subsequently used for arrayed biosensing of BSA antigen-antibody binding reactions with various concentrations. Results of a typical arrayed biosensing experiment are depicted in Figure 6.

In order to further demonstrate its capability for real-time detection of real clinical samples, the biosensor array system was tested using clinical biomarker (Osteo-pontine) obtained from the Prince of Wale Hospital. An array of Osteo-pontine and control (BSA) samples was spotted on the gold-coated SPR sensor surface for measurement. Specific antibody binding interaction was observed only in the Osteo-pontine sites, while relatively low and non-specific signals were observed in the BSA antigen control sites. As a positive control experiment, BSA antibodies was allowed to run across the biosensor array and only a small amount of non-specific binding interaction was observed in the biomarker sites.

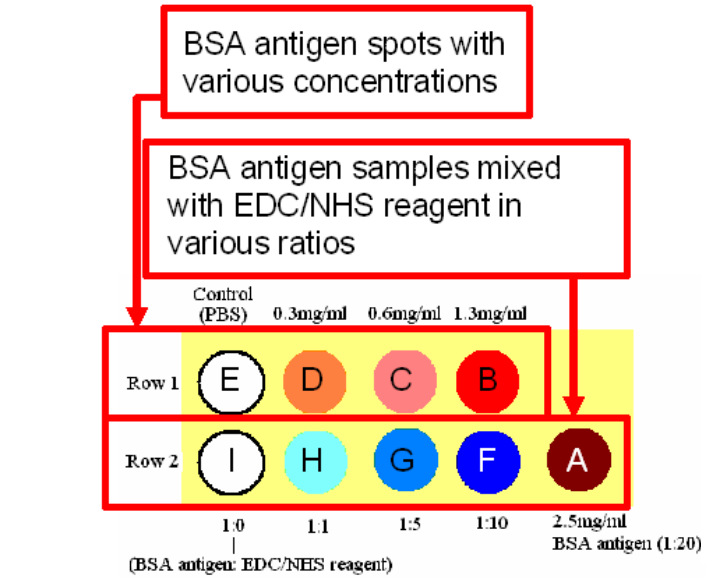

(a)

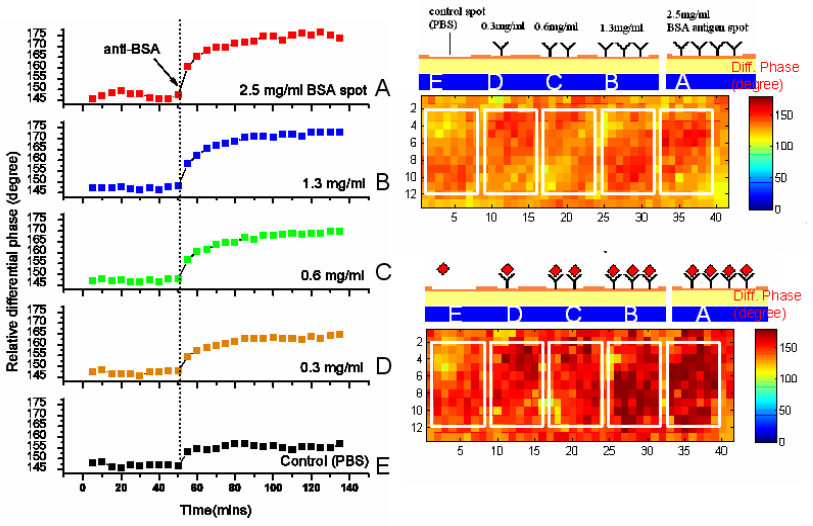

(b)

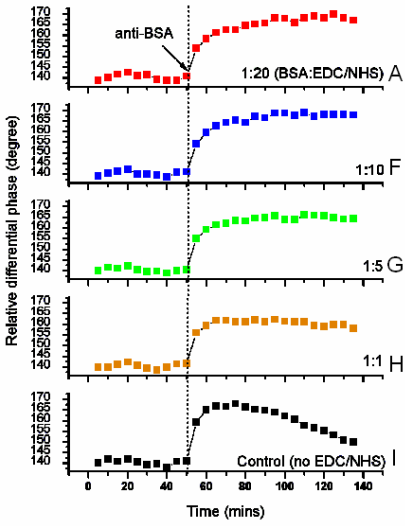

(c)

Figure 6.
(a) 9-element SPR biosensor array for detection BSA antigen-antibody binding reaction with various concentrations and EDC/NHS ratios;
(b) real-time SPR phase measurement plot and corresponding SPR phase map showing gradual increase of SPR phase caused by binding reaction, larger phase change with higher concentration of BSA antigen;
(c) effect of using various EDC/NHS ratio showing that a ratio of at least 1:10 should be used in order to obtain reliable results.

3.3. Detection of Herpes Virus DNA

While the SPR phase imaging work is ongoing, we conducted parallel experiments using a single-beam liquid crystal modulator (as shown in Figure 2) based SPR phase system that has a proven record of providing high sensing resolution in order to demonstrate the possibility of our SPR phase technique for label-free DNA detection because the requirement for extremely high resolution. The detection procedures first involve preparing the gold sensor surface for DNA detection using immobilized Avidin and then followed by series of surface activation steps not listed here. The corresponding SPR phase response curve is shown in Figure 7. We have successfully demonstrated that our SPR-based system can perform label-free detection of Herpes DNA, thus opening the possibility for low-cost molecular diagnostics application of this technique. As an extension of this project, we are now in the process of combining the LCM technique with the image analysis system developed in the earlier part of this project for arrayed biosensing of practical biomolecular species in a clinical environment.

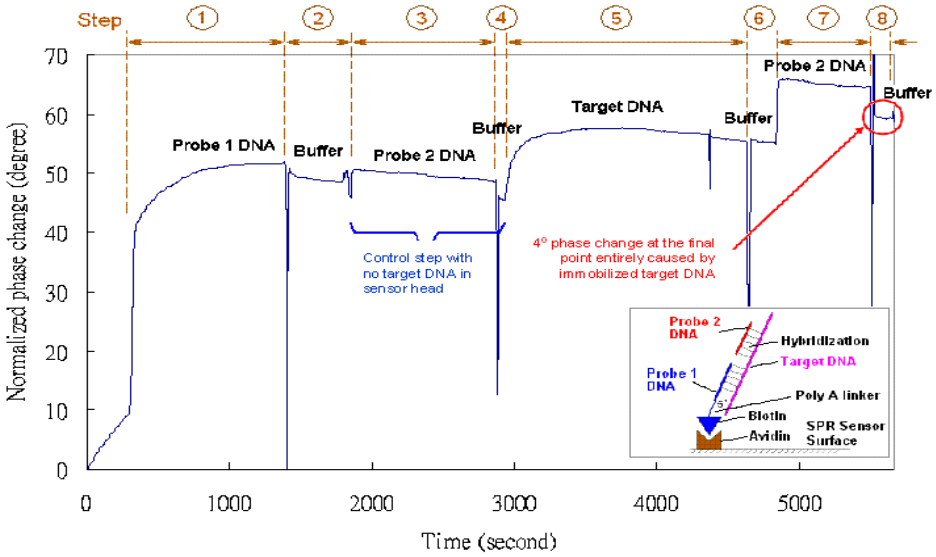

Figure 7: SPR phase plot showing the detection of Herpes DNA using complementary sequences Probe 1 and Probe 2. A net SPR phase change of 4 degrees caused by the immobilization of the target DNA has been observed.

4. PUBLICATION AND AWARDS

[1] C.L. Wong, H.P. Ho, Y.K. Suen, S.K. Kong, Q.L. Chen, W. Yuan, S.Y. Wu, "Real-time protein biosensor arrays based on surface plasmon resonance differential phase imaging," Biosensors and Bioelectronics 24, pp. 606-612, 2008.

[2] W. Yuan, H.P. Ho, Y.K. Suen, S.K. Kong, Chinlon Lin, "Improving sensitivity limit of surface plasmon resonance biosensors by detecting mixed interference signals", Applied Optics, 46, pp. 8068-8073, 2007.

[3] C.L. Wong, H.P. Ho, T. T. Yu, Y.K. Suen, W. Y. Chow, S.Y. Wu, W.C. Law, W Yuan, W.J. Li, S.K. Kong and Chinlon Lin, "Two-dimensional biosensor arrays based on surface plasmon resonance phase imaging," Applied Optics, 46, pp. 2325-2332, 2007.

[4] W. Yuan, H.P. Ho, C.L. Wong, S.K. Kong, Chinlon Lin, "Surface plasmon resonance biosensor incorporated in a Michelson interferometer with enhanced sensitivity", IEEE Sensors Journal, 7, pp. 70-73, 2007.

[5] S.Y. Wu and H.P. Ho, "Single-beam self-referenced phase-sensitive surface plasmon resonance sensor with high detection resolution," Chinese Optics Letters, 6, pp. 176-178, 2008.

[6] H.P. Ho, W. Yuan, C.L. Wong, S.Y. Wu, Y.K. Suen, S.K. Kong, Chinlon Lin, "Sensitivity enhancement based on application of multi-pass interferometry in phase-sensitive surface plasmon resonance biosensor," Optics Communications, 276, pp. 491-496, 2007.

[7] C.L. Wong, H.P. Ho, K.S. Chan, P.L. Wong, S.Y. Wu and Chinlon Lin, "Application of 2-D spectral surface plasmon resonance imaging to studying elastohydrodynamic lubricant (EHL) films," Tribology International, 41, pp. 356-366, 2008.

[8] C.L. Wong, H.P. Ho, Y.K. Suen, S.Y. Wu, W. Yuan and S.K. Kong, "Two-dimensional phase surface plasmon resonance biosensor for protein array detection" (submitted to Biosensors and Bioelectronics)

[9] C.L. Wong, H.P. Ho, Y.K. Suen, C. W. Yin, W.J. Li, S.K. Kong and Chinlon Lim, "Biosensor arrays based on surface plasmon resonance phase imaging," International Symposium on Biophotonics, Nanophotonics and Metamaterials, Hangzhou, China, pp. 102-105, 16-18 October 2006. (Best student paper award)

[10] W. Yuan, - 2nd runner-up of YDC Entrepreneurs' Challenge (E-Challenge) 2007 Business Plan Competition organized by The Young Entrepreneurs Development Council (YDC), Project title: "Surface Plasmon Resonance Biosensors," 30 June 2007. (AWARD)